High Gradient Magnetic Repulsion for 1. Separation and 2. Focusing of Cells and Biomolecules for Applications in Medicine and Biology

A Thesis

Submitted to the Faculty

of

Drexel University

by

Siddharth Vyas

in partial fulfillment of the

requirements for the degree

of

Doctor of Philosophy

March 2017

COPYRIGHT

DEDICATIONS

This dissertation is dedicated to my parents.

ACKNOWLEDGEMENTS

First, I would like to express my deepest gratitude to my advisor Dr. Gary Friedman, for his constant guidance and support throughout this PhD at Drexel University.

He taught me to look at the big picture.

I would also like to express my deepest gratitude to my co-advisor Dr. Vladimir Genis, for his constant guidance and support throughout my research and teaching at Drexel University.

He always pushed me to do my best.

I am immensely thankful to the committee chair Dr. Timothy Kurzweg for always being very supportive and always guiding me in the right direction at the important junctures of this PhD.

I am immensely thankful to Dr. Alexander Fridman for always being available to meet me and for guiding me in organizing and presenting the idea behind my research in the most effective way possible.

ACKNOWLEDGEMENTS

I am immensely thankful to Dr. Allon Guez for always being helpful in regards to asking important questions about the models used in my research and suggesting ways to make them better.

I would also like to thank Dr. Akhil Vaidya, Director – Center for Molecular Parasitology at the Department of Microbiology and Immunology for showing interest in my malaria diagnostic device and providing important feedback on preparing blood samples for the device.

I would also like to thank Suyash Bhatnagar from the Malaria lab at the Queen Lane campus and Yang Gao for helping me with the handling of the malaria samples.

I would also like to thank my family and friends for their love and support!

Table of Contents

List of Tables

List of Figures

Abstract

High Gradient Magnetic Repulsion for Separation and Focusing of Cells and Biomolecules for Applications in Medicine and Biology

Siddharth Vyas

Dr. Gary Friedman and Dr. Vladimir Genis

The ability to separate and focus cells and biomolecules enables many biological studies and medical diagnosis. At present most of the commercially available methods of magnetic separation work in batch mode with very limited control over selectivity of separation. In order to improve the selectivity of magnetic separation some researchers have suggested designs that utilize the phenomenon of magnetic attraction in order to pull the magnetic particles that are present in a flow towards a channel wall that's closer to the external attracting magnet. However, such designs require larger channel lengths for improved selectivity of separation as the magnetic field gradients produced by the external magnet are small and cannot exert sufficient attractive forces on the magnetic particles in order to pull them towards the channel wall. In regards to focusing, at present, there are no exclusively magnet methods available to separate and focus magnetic particles. The few magnetic focusing methods that do exist utilize the phenomenon of magnetic attraction along with secondary sheath flows in order to focus and separate the magnetic particles. However, these methods suffer from poor performance as magnetic particles can only be focused at very low flow rates thereby reducing the number of magnetic particles that can be effectively focused per unit time. At the same time these

methods require excellent control over flow rates of analyte and sheath fluid which is difficult to achieve.

So far, the use of high gradient repulsive magnetic forces for separation and focusing of magnetic particles has largely been ignored by researchers that are working on magnetic focusing and separation methods. This dissertation investigates the feasibility of high gradient repulsive magnetic forces to separate and focus magnetic particles that are present in a flow. These feasibility studies are performed using simple focusing and separation designs that do not require any secondary sheath flows. Numerical methods are employed to determine the trajectories of magnetic particles in these designs. As an example application, the high gradient repulsive magnetic forces are utilized to separate, focus, and concentrate malaria-infected red blood cells in order to improve the microscopic diagnosis of malaria. In addition, in regards to the magnetic-stent assisted drug targeting systems, the low capture of drug carrying magnetic particles by magnetic stent wires is attributed to the repulsion of magnetic particles that were not captured by the first wire.

1. Introduction and Review

1.1. Cell and Biomolecule Separation: Introduction and Applications

The ability to sort cells/biomolecules into distinct populations from a heterogeneous starting population enables many biological studies and medical diagnosis. Research involving cell/biomolecule analysis requires separation of cell/biomolecule types or subtypes as a final objective or as a preparative tool for further assays [1]. Cell/biomolecule sorting is also used to enrich or purify cell/biomolecule samples into well-defined populations to enhance efficiency in research and development applications. The history of cell separation dates back to the 1960s. A major breakthrough occurred in 1968 when Boyum published his paper [2] on Ficoll-density gradients for the isolation of lymphocytes from blood, leading to the development of new methods based on antigen antibody reactions. The first commercial cell sorter, which exploits a technique broadly known as fluorescence-activated cell sorting (FACS), was invented in 1969 by Herzenberg et al [3].

Separating and organizing cells/biomolecules is an important and fundamental tool in modern biology and medicine today. The need to sort cells/biomolecules is rapidly expanding towards the isolation of rarer target cell populations, including the enrichment of circulating tumor cells (CTCs), hematopoietic stem cells (HSCs), and circulating fetal cells (CFCs) from blood [4-7]. Specifically, for example, diagnosis and treatment of HIV disease relies on the efficient separation of human T-lymphocytes (CD4+) from whole blood [8, 9]. Similarly, malaria diagnosis and treatment relies on the separation of parasite-infected red blood cells (RBCs) from uninfected cells [10, 11]. Separation of neuronal cells has gained interest for its potential applications in cell replacement therapy of

neurodegenerative disorders such as Parkinson's disease, multiple sclerosis, and Alzheimer's [12-14]. Nucleated RBCs (NRBCs) are required to be separated from the peripheral blood of pregnant women for monitoring maternal, fetal, and neonatal health [6, 15].

Meanwhile, the growing interest in theranostics and personalized medicine, in which treatments are tailored to the prognoses of patients, is further driving the demand for rapid and high performance cell/biomolecule separation [16]. The use of highly selective cell separation procedures in clinical cell-based treatments has the potential to improve the quality of repair and the subsequent clinical outcome. Because of this potential, there is an increasing usage of these methodologies in the fields of tissue engineering and regenerative medicine, which has resulted in an increasing number of researchers using, or wanting to use, cell/biomolecule separation technologies [17].

The following are a few potential applications that would benefit from advances in cell/biomolecule separation and also portray its indispensability [18-21]:

- preparing various organ transplants, both autologous and heterologous
- removal of specific cell types responsible for immune rejection following transplants and treatments for autoimmune diseases
- purification of cell mixtures for diagnostic tests
- umbilical cord blood processing/prenatal blood testing for genetic disorders
- tracking tumor cells in the body,
- preparing specialized cell packs for blood transfusion (e.g., removal of lymphocytes from the transfusion) and

- isolation and detection of pathogenic microorganisms and parasites in food, environment and clinical samples

1.2. Cell/Biomolecule Separation Techniques

A large variety of cell/biomolecule separation methods are currently commercially available, these are predominantly based on three methodologies: adherence, density, and antibody binding [17]. Presently, cell/biomolecule separation techniques used are mostly bulk sorters based on physical criteria and include filtration and centrifugation techniques such as cell filtration, elutriation, centrifugation, sedimentation to name a few. The second group comprises flow-cytometry and magnetic cell sorting techniques based on affinity and biochemical cell surface characteristics. New techniques are also being developed that utilize microfluidic technologies [17, 22-24].

1.2.1. Adherence

Techniques that utilize cellular adherence are some of the simplest methods used for cell separation. An example of simple cell separation by adherence is the isolation of dental pulp stromal cells from whole digested dental pulp. In this technique, enzymatically digested dental pulp is filtered and plated directly onto tissue culture plastic, and following a period of culture, the adherent stromal cells are passaged [25]. This technique benefits from being very simple and cheap, but it is not at all specific and relies on the cells of interest adhering and in some instances rapidly proliferating to outcompete other adherent cells in the suspension, such as neurons and monocytes. Recently, techniques based on cell adherence, such as differential binding of cells to polymer brushes of varying lengths, grafted to glass surfaces, have been developed and

these are currently being refined [26]. However, despite this progress, current uses of adherence sorting are mostly only applicable when cell purity is not of concern and isolation of various subpopulations is not required.

1.2.2. Density

Density-based techniques are now mostly based on the use of centrifugation, although historically sedimentation based methods have been employed [27]. The ability to sort large numbers of cells based on their density, relative to a graduated separation medium (usually sugar based), makes these techniques particularly applicable for separations involving the use of blood which contains 4×10^9 to 6.5×10^9 cells/mL. However, despite the large-scale use of density-based methods, there are still problems with specificity as the differing densities of different cell populations are, in some instances, not large enough to be able to separate out individual cell types. As such, centrifugation methods are generally used if specificity is not absolutely necessary, as in aphaeresis, or as a pre-enrichment stage to remove cells like red blood cells and platelets.

1.2.3. Antibody binding

Antibody-binding methods generally refer to the commonly used techniques of fluorescence-activated cell sorting (FACS) and magnetic-activated cell sorting (MACS) [28-30]. Both technologies utilise the same cellular properties for separation, namely, cell surface antigens against which antibodies are raised. FACS separation relies on the conjugation of fluorescent labels to these antibodies, whereas MACS uses conjugation to iron oxide containing microbeads. Antibody-based methods of separation are currently

the gold standard for the selection of individual cell populations, and both FACS and MACS can be used to isolate cell populations to high purity.

1.2.4. Microfluidics and Lab-on-a-chip

The contributions of current commercial cell sorting platforms are significant, however, they suffer from some important limitations [23]:

- use of high operating pressures that sometimes results in loss of cell/biomolecule function or viability,
- bulky instrumentation that occupies large bench footprints ,
- requirement of technical expertise for operating complex machinery, and
- increased risk of sample contamination and safety concerns due to the sorting of aerosolized samples.

These limitations, as well as high unit and sample processing costs, must be overcome to enable more efficient clinical application and commercialization. Consequently, the next generation of cell sorting devices must meet higher standards for performance, versatility, and convenience, including [23]:

(i) faster sorting rates,

(ii) equal or improved accuracies,

(iii) ability to process native biological fluids,

(iv) ability to process diverse cell types,

(v) enhanced capabilities for multiplexed sorting,

(vi) simpler operating procedures enabling fully automated systems,

(vii) reduced biohazard risk by eliminating aerosols,

(viii) reduced cost, and

(ix) reduced size for operational convenience and portability.

To address these needs, researchers are actively looking toward microfluidic devices as the platform for the next generation translatable cell sorter. Microchip devices are a proven technology for cellular handling as they can offer precise spatial and temporal control in a greatly miniaturized platform [31, 32]. Microfluidics can be used to detect, focus, mix, count, lyse, and analyze individual cells on an integrated platform for complete lab-on-a-chip applications [33-36].

1.3. Microfluidic Cell/Biomolecule Separation Techniques: Active and Passive

Microfluidic cell/biomolecule separation techniques have usually been classified based on separation principles as active or passive. Simply put, active techniques rely on an external force field (e.g., acoustic, electric, magnetic, and optical) for functionality, while passive techniques rely on inertial forces, filters, and adhesion mechanisms (e.g., channel geometry and inherent hydrodynamic forces) for functionality [22, 23, 37].

1.3.1. Microfluidic Cell/Biomolecule Active Separation Techniques

1.3.1.1. Fluoroscent-Label Based Cell Sorting

Fluorescent label-based cell sorting relies on fluorescent probes or stains to identify cells by type. In traditional FACS, fluorescently-labeled cells organized in a laminar flow stream encounter a focused laser beam that scatters into a detector. The fluorescent signal is then analyzed to assign each cell a type for discrete sorting, whereby in the case of FACS, each cell is encapsulated into an aerosol droplet that is charged and electrostatically sorted [28]. To circumvent the need to form of aerosol droplets, many research groups have used fluorescent labels to identify cells in the microfluidic regime

for sorting by a variety of mechanisms as described in detail in this section. Similar to FACS devices, these technologies generally operate by ordering cells in flow streams for:

(i) serial interrogation by laser light,

(ii) real-time classification, and

(iii) rapid, command-driven sorting.

Since each cell is processed discretely, fluorescent label-based approaches are often associated with high efficiencies.

1.3.1.2. Electrokinetic methods

Electrokinetics describes a family of effects stemming from an applied electric field that results in the migration of cells and biomolecules. Electrokinetic forces can be used to directly displace cells, or cell-containing droplets, in fluids. For the purposes of this review, electrokinetic manipulations are divided into three categories: electrophoresis, dielectrophoresis, and electroosmotic flow. While these mechanisms are phenomenologically distinct, the forces they exert on cells are well-suited for sorting within the length scales of microfluidic devices.

1.3.1.2.1. Electrophoresis

Electrophoresis refers to the movement of suspended particles toward an oppositely charged electrode in direct current (DC). Since most cells possess a slight negative charge due to a locus of chemical groups on their surface, they migrate toward the positive electrode during electrophoresis, and the electrophoretic force exerted on that cell is proportional to its charge [38].

1.3.1.2.2. Dielectrophoresis

In contrast to electrophoresis, where cells move in a uniform electric field due to their surface charge, dielectrophoresis (DEP) refers to the movement of cells in a non-uniform electric field due to their polarizability. For movement in response to a dielectrophoretic force, cells do not need to possess a surface charge because, unlike a DC field, an alternating current (AC) is capable of polarizing the cell (i.e., inducing a dipole moment across the cell). Once exposed to an AC field, cells migrate either toward or away from the region of strongest field intensity depending on the electrical permeability of the cell and the fluid [38]. Cells with a higher permeability than the fluid are attracted toward the field maxima, which is known as positive DEP (pDEP) [39]. The opposite is true for negative DEP (nDEP), which is often preferable to minimize deleterious effects on cell function or viability that might occur due to high field strengths. The magnitude of the dielectrophoretic force is dependent on the size and properties of the cell/biomolecule, fluid, and the parameters of the electric field, which is useful for sorting cells/biomolecules by size and dielectric properties.

1.3.1.2.3. Electroosmotic flow

Unlike the electrically driven migration of cells within a stationary fluid (such as in electrophoresis and DEP), electroosmotic flow refers to the movement of a fluid due to the electrically induced migration of solvated ions, thereby transporting cells suspended within the fluid [40]. This principle was applied to sort fluorescent from non-fluorescent cells in microfabricated FACS devices using DC electroosmosis [41, 42]. While effective, a major disadvantage of DC electric fields for sorting cells is that Faradaic reactions (e.g., electrolysis of water) generally occur at the anode and cathode to maintain

a constant electric field, which can generate bubbles and harmful compounds, such as hydrogen peroxide, that may adversely affect cellular viability and solution pH if not carefully monitored and regulated [43]. As such, Puttaswamy *et al*. coupled nDEP with AC electroosmosis to mitigate these effects while retaining the ability to focus, transport, and sort cells [44].

1.3.1.3. Magnetic Separation

In magnetic cell/biomolecule sorting, sample cells are first incubated with magnetic beads with the recognition molecule (antibodies), for ''magnetic labeling'' instead of fluorescence. Then, a magnetic field gradient is used to isolate the magnetic beads, which in turn picks out the cells. This is often also termed as Magnetically Actuated Cell Sorter (MACS©), which is a trademark of Miltenyi Biotech, Bergisch-Gladbach, Germany, a company that provides commercial solutions for magnetic cell sorting. In contrast to FACS, which is serial in nature, magnetic cell sorting can be operated in either a serial or a parallel manner, resulting in higher throughput. Up to 10^{11} cells can be processed in 30 min [45]. One clear advantage of using a magnetic field is that the magnetic field is largely permeable to biological tissues and cells and less likely to interfere with cell function or immunochemistry necessary for magnetic labeling. The entire process can be done in solution phase, thereby minimizing any physical damage to the cells. It was shown that the magnetic particles do not influence viability or function of the labeled cells and do not affect the results of FACS later [45, 46]. Magnetic separation techniques for cell/biomolecule separation will be covered in detail in later sections of this dissertation.

1.3.2. Microfluidic Cell/Biomolecule Passive Separation Techniques

The technologies described thus far involve active methods for cell separation; however, the remaining systems involve passive approaches to separate, isolate, or enrich cell populations. Passive systems consist of a variety of methods that do not rely on fluorescent labels or beads. Instead, these methods rely on the inherent differences in cellular morphology between cell groups (e.g., size, shape, compressibility, and density) and can sort cells using inertial forces, hydrodynamic spreading, deterministic lateral displacement, filtration, transient cellular adhesion, and cellular immobilization [47].

1.4. Performance Criteria for Separation Techniques

Several parameters are used to evaluate the performance of a separation technique for cell/biomolecule separation, namely [17, 48-50]:

Efficiency(also termed as the recovery rate or yield) is the ratio between the number of isolated cells/biomolecules at the exit of the device over the number of known targeted cells/biomolecules introduced at the inlet. Another common measure of efficiency is enrichment, which is the ratio of the volumetric concentration of the isolated cells/biomolecules in the device with respect to the original supplied sample.

Purity is the ratio of isolated target cells/biomolecules with respect to the total number of captured cells/biomolecules.

Viability is the percentage of cells/biomolecules surviving the isolation process with respect to the total number of target cells/biomolecules.

Throughput is the time needed to separate a required number of cells/biomolecules.

Selectivity is defined as the ability of a separation technique to separate cells/biomolecules of more than one type from a heterogenous mixture.

Each separation technique has its advantages and disadvantages. In general, the choice of a separation technique depends on the type of cell/biomolecule to be separated and the required separation performance.

1.5. Cell and Biomolecule Focusing: Introduction and Applications

Focusing particles (both biological and synthetic) into a tight stream is usually a necessary step prior to counting, detecting, and sorting them. The various particle focusing approaches in microfluidic devices may be conveniently classified as sheath flow focusing and sheathless focusing. Sheath flow focusers use one or more sheath fluids to pinch the particle suspension and thus focus the suspended particles. Sheathless focusers typically rely on a force to manipulate particles laterally to their equilibrium positions. This force can be either externally applied or internally induced by channel topology. Therefore, the sheathless particle focusing methods can also be classified as active or passive by the nature of the forces involved.

As traditionally defined, particles can be focused in either two-dimensions (2D) or three-dimensions (3D). A 2D focusing normally indicates the horizontal focusing of particles to the center plane of a microchannel, where particles still scatter over the channel depth. This focusing is usually sufficient for continuous-flow particle sorters.

1.5.1. Sheath Flow Focusing

Among the diverse particle focusing methods, sheath flow focusing may be the most common one that has been adopted in microfluidic devices. This type of focusing has been realized by using either pressure-driven [51-53] or electric field driven [54-56] particle-free sheath flows to pinch the particle suspension flow and thus focus particles

into a single file. In general, one or more sheath fluids are generally used in order to obtain a 2D or 3D particle focusing.

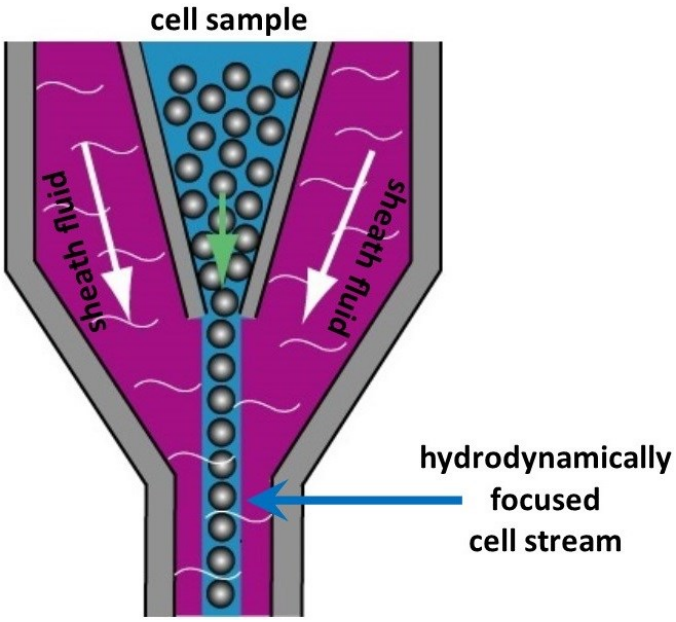

Figure 1. Sheath flow focusing. Once the sample is injected into a stream of sheath fluid within the flow chamber, the sample is force into the center of the stream forming a single file by the principle of hydrodynamic focusing.

Compared to other force-based sheathless focusing approaches whose focusing capability normally varies with the particle size, sheath flow focusing is mostly determined by the flow-rate ratio between the sheath fluid and the particle suspension and is therefore able to focus very small particles and even molecules. Moreover, both the location and the dimension of the focused particle stream are readily tunable, which can be achieved by adjusting the flow rate of each of the sheath fluids such as the devices developed by Howell et al. [57] and Lee et al. [58]. However, the requirement of sheath flow(s) also has some significant drawbacks, for example, it complicates the device

control, increases the device operation cost (due to, for example, the consumption of sheath fluids), and dilutes the particle concentration as well.

1.5.2. Sheathless focusing

Sheathless particle focusers typically rely on a force to manipulate the suspended particles laterally to their equilibrium positions. This force can be either externally applied such as acoustic [59], dielectrophoretic [60], magnetic [61], and optical [62], or internally induced by channel topology including hydrophoretic [63] and inertial [64], etc. Therefore, the sheathless particle focusing approaches can also be classified as active or passive by the nature of the forces involved. These two sub-categories of microfluidic sheathless particle focusers have been reviewed extensively by Xuan et. al. [65].

1.5.3. Review of Existing Focusing Methods

There are several active focusing methods and some of them utilize a secondary sheath flow. However, all of these methods suffer from the problem of low throughput because they are able to focus the particles at only very low flow rates.

Table 1. Comparison of Various Particle Focusing Methods.

Researchers	Method	Channel Dimensions	Particle Size	Flow Rate
Kyongtae Kim et. al. Microfluid Nanofluid. 2014. [66]	Slanted microstructure array	Length: 23.91 mm Width: 50 µm Height: 30 µm	Spherical particles of 10 µm diameter.	1 µL/min
Taotao Zhu et. al. Microfluid Nanofluid. 2011. [67]	Ferrofluids with 10 nm magnetic particles.	Length: 40 mm Width: 1.6 mm Height: 28 µm	Spherical particles of 4.8, 5.8, and 7.3 µm diameter.	8 µL/min
Afshar et. al. Analytical Chemistry. 2011. [68]	Magnetic attraction and secondary sheath flow.	Length: 10 mm Width: 200 µm Height: 100 µm	Spherical particles of 1.05, and 2.83 µm diameter.	0.36 µL/min
Jinjie Shi et. al. Lab Chip. 2008. [69]	Acoustophoresis	Length: 13 mm Width: 50 µm Height: 50 µm	Spherical particles of 1.9 µm diameter.	10 µL/min
Che-Hsin Lin et. al. Microelectromechanical System. 2004. [70]	Dielectrophoresis and secondary sheath flow.	Length: NA Width: 80 µm Height: 25 µm	Spherical particles of 10 and 20 µm diameter.	0.05 µL/min

From the above table it is clear that all of these particle focusing methods suffer from the problem of low throughput because of the very low values of flow-rates used for focusing.

1.6. Magnetic Separation and Focusing

1.6.1. Introduction

For a long time, magnetism has stood out as an interesting and important driving force to separate the magnetic components from non-magnetic components in a mixture. The idea of using magnetic separation techniques in cell/biomolecule separation has enjoyed a resurgence of interest over the last decade. This has primarily been brought

about by the development of new magnetic particles with improved properties for various cell/biomolecule separation procedures. Magnetic separation of cells has several advantages in comparison with other techniques used for the same purpose [71]:

- Given the non-magnetic behavior of the vast majority of biological samples, it permits the target cells/biomolecules to be isolated directly from crude samples such as blood, bone marrow, tissue homogenates, stool, cultivation media, food, water, soil etc.
- Compared to other more conventional methods of cell separation, magnetic separation is relatively simple and fast and in a way may be considered a sample enrichment step for further chromatographic and other analysis.
- The static magnetic field does not interfere with the movement of ions and charged solutes in aqueous solutions as does the electric field.
- The large differences between magnetic permeabilities of the magnetic and non-magnetic materials can be exploited in developing highly selective separation methods.
- The shear forces associated with binding and elution are minimal compared to centrifugation or filtration increasing the yield of active cells.

In general, the magnetic separation procedure is gentle, facilitating the rapid handling of delicate cells in an unfriendly environment. The cells isolated by magnetic separation process are usually pure, viable and unaltered.

Magnetism and microfluidics; neither of these two concepts are new, yet it has only been in recent years that they have been combined. Today we can see magnetic forces being combined with microfluidics in an amazing variety of ways. Magnetic forces have

now been successfully employed to manipulate magnetic objects such as magnetic particles, magnetically labelled cells/biomolecules or plugs of ferrofluids inside a microchannel.

1.6.2. Natural and Synthetic Magnetic Particles

Generally speaking, there are two types of magnetic separations when working with cells/biomolecules. In the first type, cells to be separated demonstrate sufficient intrinsic magnetic moment so that magnetic separations can be performed without any modification. At present only two types of such cells are known in the nature, namely red blood cells (erythrocytes) containing high concentrations of paramagnetic hemoglobin, and magnetotactic bacteria containing small magnetic particles within their cells. In the second type, one or more non-magnetic components of a mixture have to be tagged by a magnetic label to achieve the required contrast in magnetic susceptibility between the cell and the medium. The attachment of magnetic labels (mainly particles) is usually mediated by affinity ligands of various nature, which can interact with target structures on the cell surface. In the most often used approach antibodies against specific cell surface epitopes are used, but other specific ligands can be employed, too. The newly-formed complexes have magnetic properties and can be manipulated using an appropriate magnetic separator.

Magnetic particles for use in cell/biomolecule separation should fulfil some important criteria:

- they should be chemically stable and should not aggregate in the media used in cell/biomolecule separation,

- they should show very little magnetic remanence after having been subjected to the magnetic field,
- they should not bind to cells/biomolecules non-specifically,
- there should be very little leakage of the immobilized affinity ligand (Ab, antigen, lectin, carbohydrate) from the particles during storage,
- they should allow a fast and complete magnetic separation of the cells/biomolecules labelled with particles and of excess particles from the unlabeled cells/biomolecules, and
- they should be of a size which minimizes phagocytosis.

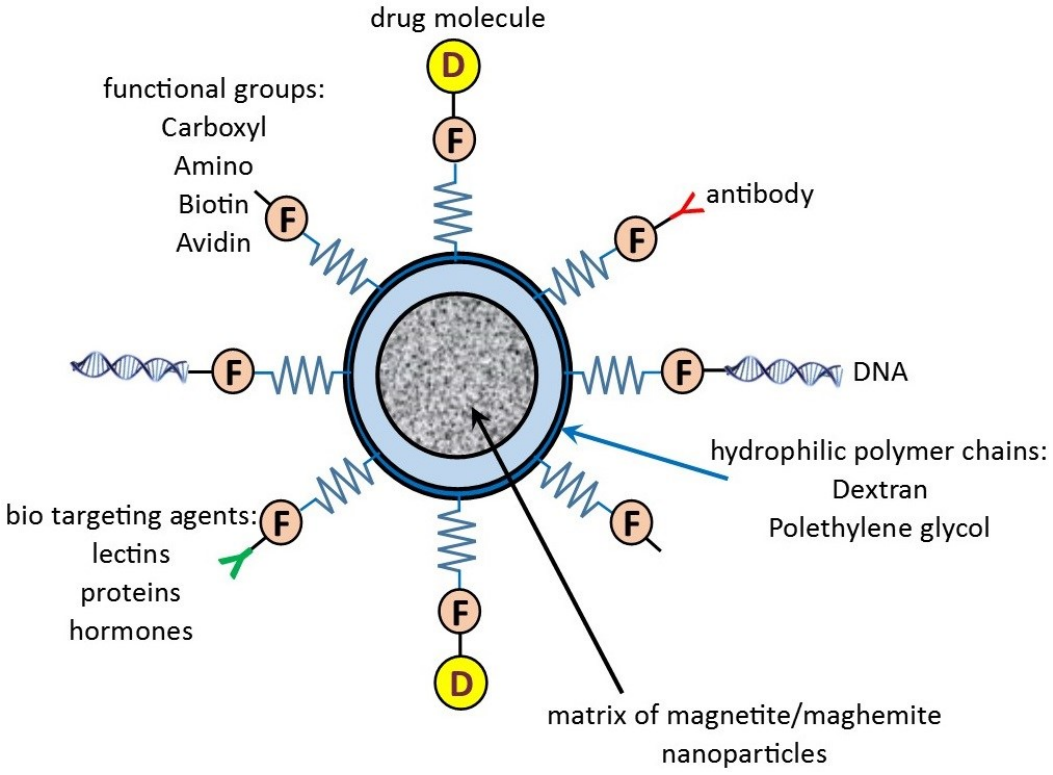

Figure 2. A functionalized magnetic particle.

1.6.3. Superparamagnetism

For most cell/biomolecule separation applications, superparamagnetic particles with a high magnetic saturation are used. Superparamagnetism can be viewed as the combination of paramagnetic and ferrimagnetic behaviour. Like paramagnets, superparamagnetic materials exhibit zero remanence, i.e. in the absence of an applied external magnetic field their average magnetization is zero. As a result, these particles disperse better in solutions as they do not tend to magnetically interact with each other to form aggregates. However, their magnetic susceptibility is much higher than paramagnets and like ferrimagnets they reach magnetic saturation but without exhibiting a magnetic hysteresis loop. Highly magnetizable particles are preferred as they generate greater magnetic flux densities when submitted to an applied external magnetic field. Therefore, less intense fields can be used for an efficient concentration/separation process and better process dynamics are achievable.

1.6.4. Synthesis of Magnetic Labels/Beads

The vast majority of the magnetic particles used are based on the iron oxides, magnetite (Fe_3O_4) and maghemite (γ-Fe_2O_3). Maghemite is isostructural to magnetite with a cation deficient site and it is generally produced by oxidating the latter with ferric nitrate [72] or by exposing it to air [73]. Although in bulk, both materials have a high saturation magnetization (magnetite 92–100 $Am^2\ kg^{-1}$, maghemite 60–80 $Am^2\ kg^{-1}$) (Cornell and Schwertmann, 2003) they do not have zero remanence. In fact, for ferrimagnetic materials in the bulk state, superparamagnetism is only observed in small crystallites ranging from 1 to 30 nm which in the case of superparamagnetic iron oxide nanoparticles (SPIONs)

typically show a 20–50% decrease in the saturation magnetization [74]. Several other ferrites composed by Co, Cu, Ni and Mn exhibit higher magnetization but are more prone to oxidation and unlike the aforementioned iron oxides are not biocompatible.

1.6.5. Examples of Commercially available Magnetic Particles

During the last 30 years, magnetic particles have been well established as standard tools for the isolation of defined cell/biomolecule subsets in modern cell biology and immunology. In 1977, Molday et al. published the use of iron-containing polymeric microspheres conjugated to lectins for the separation of red blood cells and antibody-coated cells [75]. Today, magnetic cell sorting techniques are well established, and they come in different flavors. The magnetic particles used for labeling of the cells, can be roughly divided into micro- and nanobeads. Such beads are provided commercially, for example [76],

- Dynal®- (microbeads 1–3 μm; Invitrogen, Carlsbad, USA),
- MACS®- (nanobeads 20–100 nm; Miltenyi Biotec, Bergisch Gladbach, Germany),
- IMAG®- (nanobeads 100–500 nm; BD Biosciences, San Jose, USA),
- EasySep®- (nanobeads about 150 nm; Stem Cell Technologies1, Vancouver, Canada), or
- MagCellect®-beads (nanobeads abount 150 nm; R&D Systems (Techne), McKinley Place NE, USA).

1.6.6. Review of Existing Magnetic Separation Techniques

At present, the magnetic separation techniques for cell/biomolecule separation are attraction based where the magnetic field and the magnetic field gradients are used to pull the magnetic particles towards the magnet in order to separate them. The magnetic force depends on the gradient of the applied magnetic field and also on the volume and magnetization of the particle. Most of the commercially available magnetic separation systems for cell/biomolecule separation perform in batch mode. The basic principle of batch magnetic separation is very simple. Magnetic particles are mixed with the sample containing the target compound(s). Following an incubation period when the target compound(s) bind to the magnetic particles the whole magnetic complex is easily and rapidly removed from the sample using an appropriate magnetic separator. After washing out the contaminants, the isolated target compound(s) can be eluted and used for further work [77]. Test tube magnetic separators enable separation of magnetic particles from volumes ranging between about 5 µL and 50 mL. It is also possible to separate cells from the wells of standard microtitration plates. Magnetic complexes from larger volumes of suspensions (up to approximately 500 - 1000 mL) can be separated using flat magnetic separators [71].

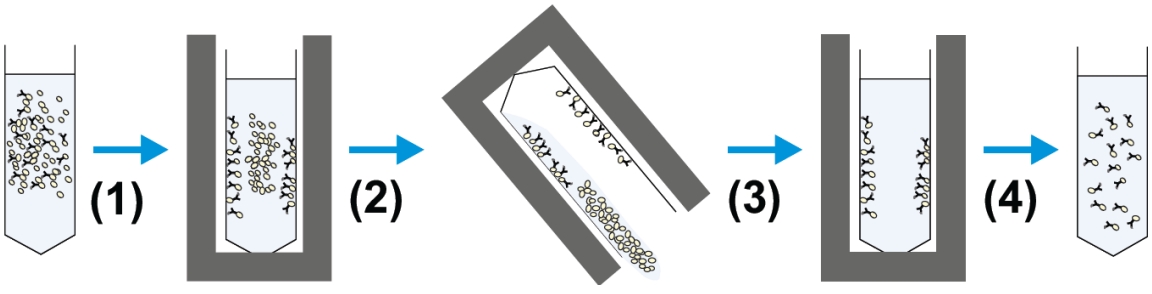

Figure 3. A batch-mode magnetic separation system [17].

On the other hand the development of microfluidic systems for cell/biomolecule separation has led to the burgeoning of various microscale magnetic separation techniques over the past two decades. Researchers are now increasingly showing interest in microfluidics based continuous flow magnetic separation systems. Such systems are characterized by the flow of the liquid and suspended cells/biomolecules through the separation system. Continuous flow separators feature either two outlets or multiple outlets. The design with two outlets is sometimes termed as split flow thin fractionation, whereas the design with multiple outlets is often termed as free-flow magnetophoresis, in analogy to free-flow electrophoresis. Through the use of continuous flow separators, it is possible to separate particles of different sizes and/or different magnetizations. The particle trajectory is the sum of two flow vectors: the hydrodynamic velocity arising from pumping the liquid through the microfluidic system and the magnetically induced velocity. Balancing of these two flow vectors is required to generate sufficient deflection. These systems are usually more expensive and more complicated in comparison with the batch separators.

So far, continuous separation of magnetic particles in microfluidic channels has been demonstrated by manually placing a permanent magnet or electromagnet beside a microchannel that contains multiple outlets [78-80]. For example, in the design by Pamme et. al., magnetic particles of 2.0 and 4.5 μm diameter with magnetic susceptibilities of 1.12×10^{-4} and 1.6×10^{-4} m^3 kg^{-1}, were introduced in continuous flow in a microfabricated channel. Permanent magnets were used to apply a magnetic field perpendicular to the laminar flow. The magnetic particles were deflected from the direction of laminar flow depending on their magnetic susceptibility, size, and flow rate. It was found that the 4.5-

μm diameter particles with the larger susceptibility deflected more from the direction of laminar flow in comparison to the 2.0-μm magnetic particles. The non-magnetic 6-μm polystyrene beads, however, were not deflected at all.

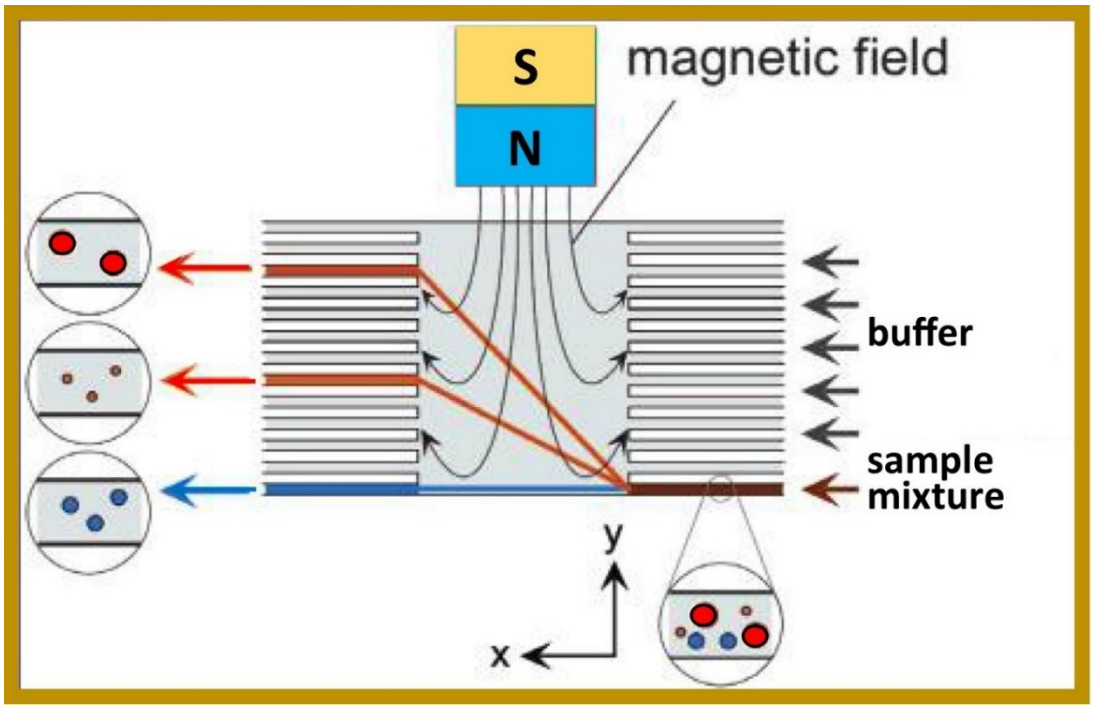

Figure 4. Concept of free-flow magnetophoresis in the design by Pamme et. al. [80].

Magnetic particles of different sizes and magnetic susceptibility are pumped into a laminar flow chamber; a magnetic field is applied perpendicular to the direction of flow using permanent magnets. Particles deviate from the direction of laminar flow according to their size and magnetic susceptibility and are separated from each other and from nonmagnetic material.

The biggest drawback of this design is that the magnetic particles to be separated begin far away from the permanent magnet in the region where magnetic field gradients are weak. The gradients produced by permanent magnets decay rapidly with the distance from the magnet. Therefore, a large magnet is required to effectively separate the magnetic particles, this in turn increases the length of the separation chamber.

High-gradient magnetic separation (HGMS) systems can generate a large magnetic force with simple device structures. With the development of microfabrication technologies, it has become possible to microfabricate HGMS systems along with microfluidic channels on a single chip. Several on-chip HGMS system microfluidic designs for continuous magnetic separation have been reported. For example, the design by Inglis et. al. used microfabricated magnetic stripes aligned on the bottom of the fluid chamber to horizontally separate magnetically tagged leukocytes trapped on the magnetic stripes away from red blood cells (RBCs) flowing through the chamber [81]. In another design, a microfabricated magnetic wire was placed in the middle of the flow stream along the length of a single microfluidic channel, and used to separate deoxyhemoglobin RBCs from white blood cells based on the difference in their relative magnetic susceptibilities [82]. However, both of these designs were used to separate magnetic particles of only one kind from a non-magnetic mixture and the selectivity of separation was not studied.

1.6.7. Review of Existing Magnetic Focusing Techniques

Flow focusing is an important factor in the manipulation of particles and cells in continuous flow, forcing them into narrow, well-defined streams to allow their processing and sorting with high precision and reproducibility. Perhaps the most common and

crucial application of flow focusing is in flow cytometry and fluorescence activated cell sorting (FACS) for the detection, counting and separation of cells. The advent of microfluidic technology has seen a great deal of interest in the miniaturization of FACS procedures in conjunction with magnetic methods to focus particles [68, 83-85].

Afshar et. al. have claimed to be the first group of researchers to have achieved magnetic focusing of micro-sized magnetic particles in microfluidic systems via the use of an external magnet and one external sheath flow. The principle behind their design is simple. First, the high-gradient magnetic field generated by means of a micro-machined field concentrator is used to retain the magnetic particles flowing through the buffer in a dense plug. Then the magnetic retention force is slowly reduced in the presence of an external one-dimensional sheath flow, this results in controlled release of the particles into a fine streamline with regular longitudinal interparticle spacing (see Figure 5.). However, Afshar et. al. mention that this design is capable of focusing only ≈ 500-1000 particles. Another drawback of this design is that many particles are lost during the initial plug formation step.

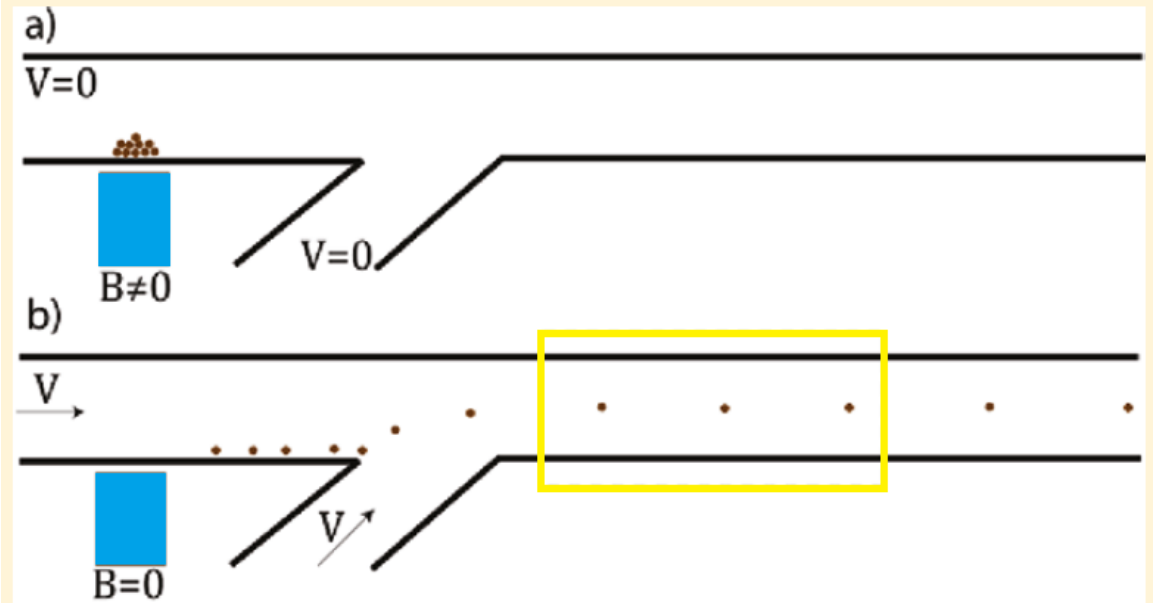

Figure 5. Magnetic focusing design of Afshar et. al. using one magnetic field concentrator and one external sheath flow [68].

As far as we know at present, there are no exclusively magnetic methods of focusing magnetic particles.

1.7. Motivation for this work

Fluorescence measurement of dye-labeled cells is a commonly adopted method for flow cytometry where focusing of cells is required. Light emitted from or scattered by the cells provides the necessary information regarding their individual size, shape and chemical composition. However, the conventional flow cytometer systems tend to be bulky and expensive. Fluid handling systems which are an integral part of flow cytometry systems incorporate the management of flow rates of analyte and sheath fluids through the system. Fluid handling systems are part of the reason that these systems tend to be

bulky. There is a need to design more compact cell/biomolecule focusing and separation devices. Over the past decade, microfluidic devices have been increasingly used to manipulate particles and cells owing to their reduced sample consumption, low-cost, small footprints, and other advantages [24, 47, 48, 86].

Microelectromechanical systems (MEMS) are typically generated using planar lithography and etching process, which results in a 2-D planar structure in nature. A major drawback of such structures is that they do not readily support the use of neighboring sheath flows to focus the cells in the center of the sample flow, and, at present most of the focusing methods rely on the use of secondary sheath flows. Typically, a multilayer structure is more suitable while using sheath flows to achieve 3-D sample focusing. However, such devices tend to be extremely complex. At the same time, the introduction of sheath flows brings the potential of dilution and contamination of cell/biomolecule sample. Researchers are therefore looking at sheathless means of focusing microsized particles.

Some of the active microfluidic techniques that have been developed include dielectrophoresis, acoustophoresis, and magnetophoresis. In general, these techniques rely on the low-Reynolds-number nature of a fluid flow to allow the focusing technique to occur in a more or less predictable fashion. Although these active microfluidic techniques have proven successful to some extent for some biological applications, their typically low throughput has been a principal impediment to their widespread use and application. The typical flow rates in such systems continue to be less than 10 μL/min. For example, Shi et al. proposed a novel on-chip particle focusing technique using standing surface acoustic waves [69]. In their experiment, 1.9 μm diameter polystyrene beads were observed to focus into a narrow stream in the center of a 50×50 μm channel. The reported

fluid flow velocity was 6.7 cm/s, yielding a flow rate of around 10 μl/min in the microchannel. Afshar et. al. claim to be the first group of researchers to utilize magnetic forces for microparticles manipulation and focusing. However, similar to other methods of focusing, their method is dependent on the use of a complicated secondary sheath flow. In addition, they were able to focus magnetic beads (1.05 μm diameter and 2.83 μm diameter) only at very small flow rates of 0.36 μL/min where the beads had an average flow velocity of 0.3 mm/sec.

As far as we know, at present, there are no exclusively magnetic methods available for focusing and separation of magnetic particles. In addition, the other active methods of focusing that have been suggested by other researchers continue to suffer from the problem of low-throughput.

1.8. Scope of this thesis

This thesis presents novel high gradient magnetic repulsion based methods of focusing and separation of magnetic particles that are present in flow. These methods does not require any secondary sheath flows. Specifically, chapter 2 presents the model that provides rough estimates and general guidelines for employing high gradient repulsive magnetic forces in focusing and separation of micrometer-sized spherical magnetic particles in microfluidic systems with low Reynold's number flows. A magnetic particle focusing and separation design is presented and the trajectories of magnetic particles (with different sizes and different magnetic contents) are computationally determined using the solutions of first order ordinary differential equations that are solved numerically using MATLAB. The throughput of this magnetic repulsion based focusing design is also compared with other active microfluidic methods of focusing. Chapter 3

utilizes this magnetic repulsion based focusing design to focus and concentrate malaria-infected red blood cells in order to improve the diagnosis of malaria. Chapter 4 studies the kinematics of capture of drug carrying magnetic particles by magnetic wires in regards to magnetic stent assisted drug targeting systems. Such designs have traditionally suffered from very small captures (< 10%) for practical blood flow velocities in arteries where the stent could potentially be placed, this low capture is attributed to the fact that the particles that are not captured by the first wire are repelled towards the center of the channel when compared to their starting position.

2. Mathematical Model of Magnetic Particle Motion in Low Reynold's Number Flows

Models described in this chapter are intended to provide rough estimates and general guidelines for separation and focusing of micrometer-sized spherical magnetic particles in microfluidic systems with low Reynold's number flows. General guidelines are determined from studying the interplay of competing forces in the system. Specifically, magnetic forces will be evaluated against the effects of Stoke's drag that typically occur in such systems. The results can be used to determine which specific parameters, such as particle size and its magnetic content, position of the separating/focusing magnets, direction of magnetization of the magnets, and average flow velocity, best contribute towards separation/focusing. While general modeling principles will be described in this chapter, their application to specific situations will be described in Chapters 3 and 4, wherein computational simulations are used to study magnetic separation and magnetic focusing in relation to magnetic-stent assisted drug targeting and magnetic diagnosis of malaria respectively.

2.1. Key Magnetic Terms and Concepts

2.1.1. Magnetic dipole

The "dipole" is a mathematical construct used to describe the field produced by two opposing charges spaced infinitesimally apart. When a dipole is placed in a spatially ***uniform*** field, the two poles experience equal force but in opposing directions, leading to rotation but zero net force on the dipole. The rotation continues until the dipole moment

points in the direction of the applied field in order to minimize its potential energy. This is illustrated in Figure 6.

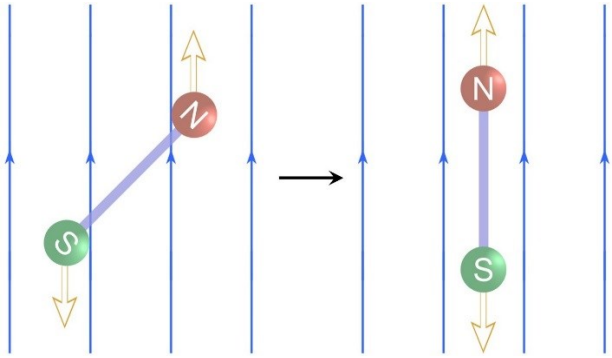

Figure 6. Rotation of a magnetic-dipole in a spatially uniform field. There is no translational motion of the dipole

In a spatially varying magnetic field, on the other hand, the two poles of the dipole experiences opposing forces but with a net difference in magnitude, leading to a net force on the dipole in the direction of the magnetic field gradient. This net force on the dipole causes the translational motion of the dipole. The physical basis for the interaction of a dipole with a magnetic field gradient is illustrated in Figure 7.

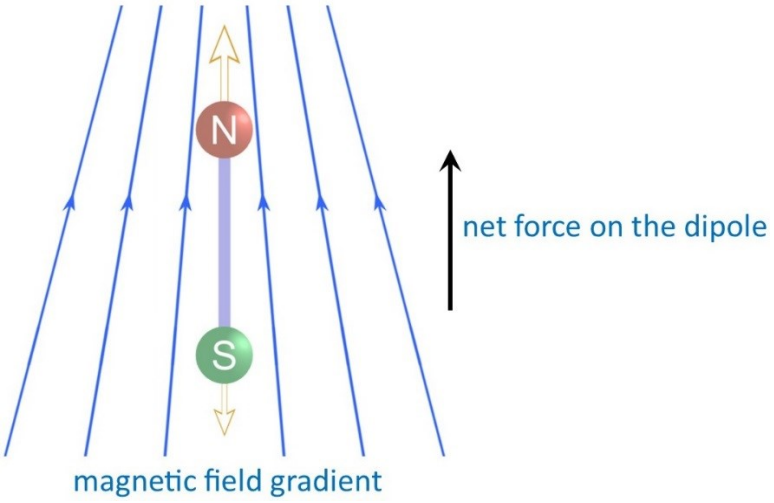

Figure 7. Translational motion of a magnetic-dipole in presence of a magnetic field gradient.

The strength of the magnetic field is proportional to the density of magnetic field lines at each position in space. Magnetic field lines of constant density across space, as shown in Figure 6, is consistent with that of uniform fields, and in this case magnetic dipoles will experience only rotation until its magnetic moment is aligned with the direction of the external field. When the density of magnetic field lines is spatially non-uniform, as depicted in Figure 7, the magnetic bead will experience both rotation and net force in the direction of the strongest magnetic field.

2.1.2. Magnetic moment

Leslie-Pelecky et. al. (1996), Pankhurst et. al. (2003), and Gijs (2004) have extensively examined the magnetic properties of nano-sized and micro-sized magnetic particles for applications in medicine and biology [87-89]. Typically, magnetic particles (1-5 μm diameter) consist of a large number of single-domain (10-50 nm) magnetic

particles embedded inside a polymer or glass matrix. Single-domain magnetic particles exhibit superparamagnetic behavior. The magnetization of single-domain magnetic particles is experimentally determined and expressed in the units of magnetization per unit mass (emu/g). The magnetization per unit volume is obtained by multiplying magnetization per unit mass and the density of the magnetic material.

When the external field is strong enough, the particles reach magnetic saturation, a point at which the magnetic domain is completely aligned with the external field. When exposed to fields stronger than the saturation field, the particle magnetization is constant and independent of the field strength. The average saturation magnetization (per unit volume) of magnetite particles is ≈ 350 kA/m [90, 91]. Typically magnetite particles reach their saturation magnetization for field strengths ≈ 0.4-0.6 T.

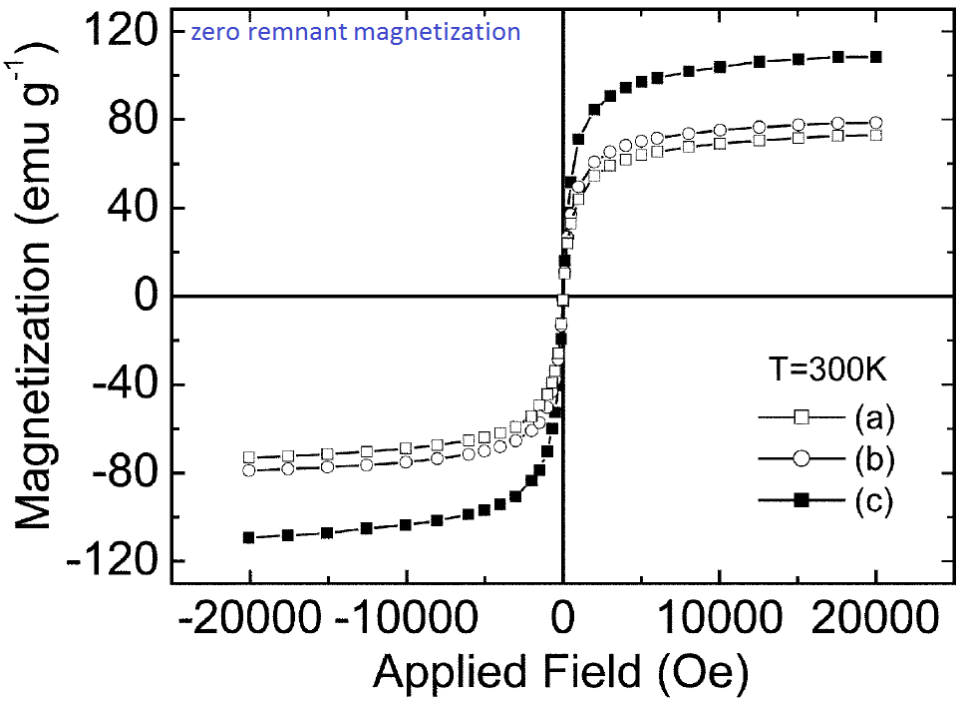

Figure 8. Magnetization curve for three different types of single-domain magnetite particles in the study by Hou. et. al. [90].

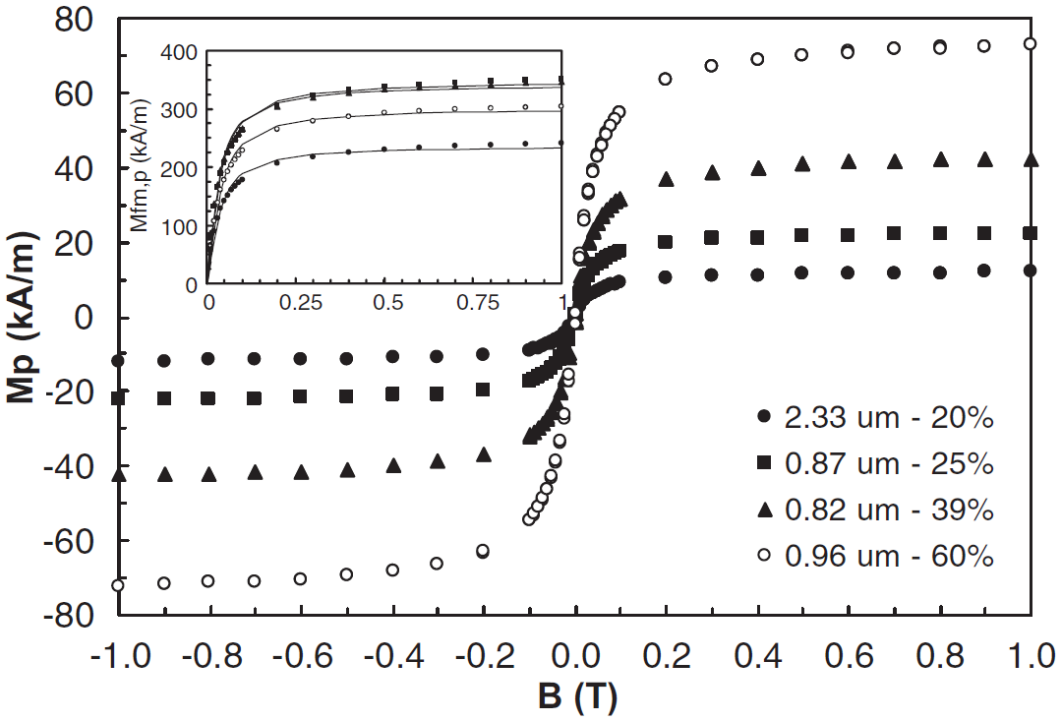

Figure 9. Magnetization saturation of particles with different sizes and different magnetic content in the study by Aviles et. al. [92].

The magnetic moment of a magnetic particle is obtained by multiplying the magnetization (per unit volume) and the volume of its magnetic material. The percentage volume content of magnetic material in a magnetic particle is related to its percentage weight content in the magnetic particle by the formula [92-94]:

$$\%Volume_{magnetite} = \frac{\%Weight_{magnetite}}{\%Weight_{magnetite} + (1 - \%Weight_{magnetite})\frac{\rho_{magnetite}}{\rho_{polymer}}} \quad (2.1)$$

where,

$\rho_{magnetite}$= density of magnetite and ≈ 5×10^3 kg/m^3

$\rho_{polymer}$= density of polymer ≈ 1×10^3 kg/m^3

2.1.3. Magnetic force

For the purpose of reducing the burden on modeling efforts, the particles in this dissertation are assumed to be uniformly magnetized to saturation. In this scenario, spherical particles can be modeled as point dipoles, because the field due to a uniformly magnetized sphere behaves exactly like the field due to a point dipole at the center of the sphere. The magnetic force acting on a point-like magnetic dipole moment of magnitude $\vec{m}$ in a magnetic field gradient $\nabla\vec{B}$ is given by [87, 95-97]:

$$\vec{F}_{mag} = (\vec{m}.)\nabla\vec{B} \tag{2.2}$$

The total magnetic moment of the particle can be written as:

$$\vec{m} = Volume_{MP}\vec{M} \tag{2.3}$$

Where, $Volume_{MP}$ is the volume of the particle and $\vec{M}$ is its volumetric magnetization, which in turn is given by,

$$\vec{M} = \Delta\chi\vec{H} \tag{2.4}$$

Where,

$$\Delta\chi = \chi_{MP} - \chi_w \tag{2.5}$$

is the effective susceptibility of the magnetic particle relative to water. For the case of a dilute suspension of magnetic particles in pure water, we can approximate the overall response of the particles plus water system by $\boldsymbol{B} = \mu_0\boldsymbol{H}$, this yields:

$$\vec{F}_{mag} = \frac{V_{MP}\Delta\chi}{\mu_0}\left(\vec{B}.\right)\nabla\vec{B} \tag{2.6}$$

2.1.4. Principle of High Gradient Magnetic Separation (HGMS)

As was mentioned in the previous section, for particles that have reached magnetic saturation, the magnetic force depends only on the magnetic field gradient.

$$\vec{F}_{mag} = (\vec{m}.)\nabla\vec{B} \tag{2.7}$$

It is important to note that the strength of the magnetic field and the magnetic field gradients decrease rapidly with distance from the surface of the magnet. For example, for a cylindrical magnet, the magnetic field along the axis of magnetization is given by [98]:

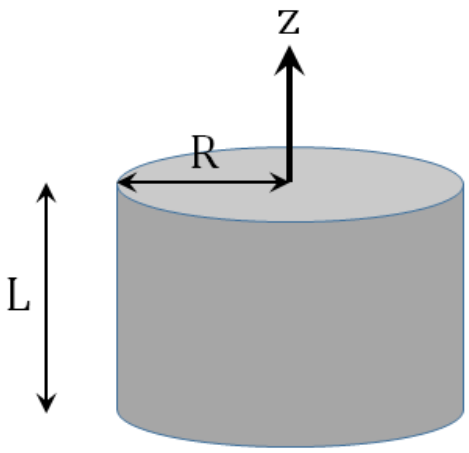

Figure 10. Permanent cylindrical magnet.

$$\vec{B}(z) = \frac{\mu_0 M}{2}\left[\frac{z}{\sqrt{z^2+R^2}} - \frac{z-L}{\sqrt{(z-L)^2+R^2}}\right] \tag{2.8}$$

$$\frac{\partial}{\partial z}\vec{B}(z) = \frac{\mu_0 M}{2}\left[\frac{1}{\sqrt{z^2+R^2}} + \frac{1}{\sqrt{(z-L)^2+R^2}} - \frac{z^2}{(z^2+R^2)^{\frac{3}{2}}} - \frac{(z-L)^2}{[(z-L)^2+R^2]^{\frac{3}{2}}}\right] \tag{2.9}$$

The decay of the magnetic field and the magnetic field gradients for the permanent cylindrical magnet is plotted in Figures 11 and 12 respectively. The remnant field Br is 1.48 T.

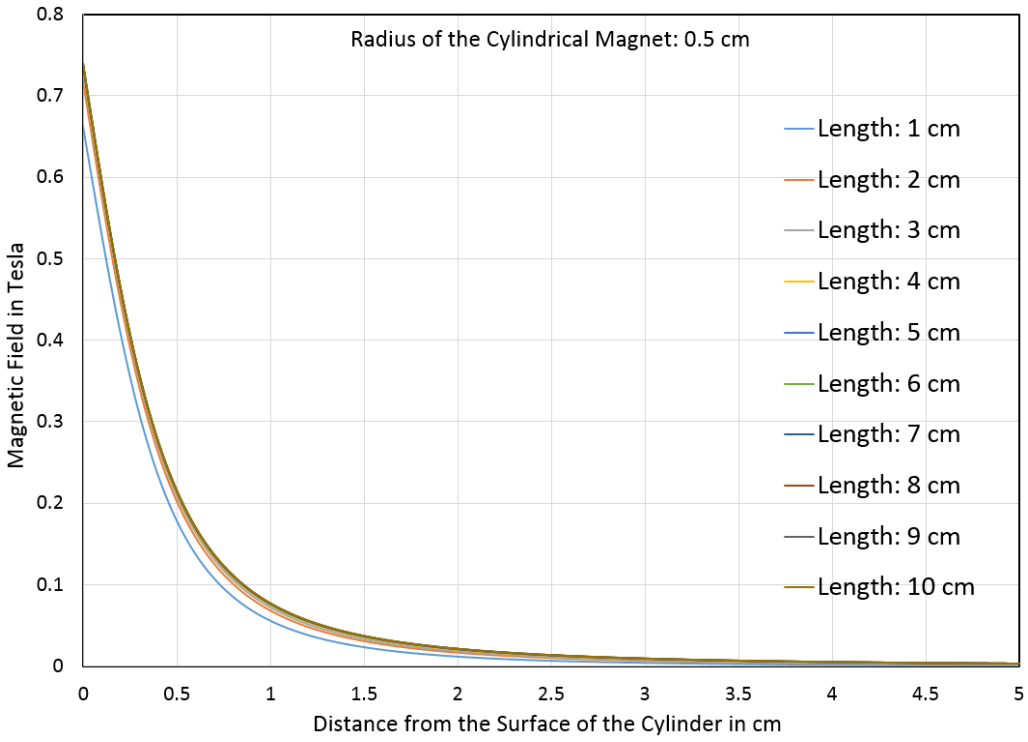

Figure 11. Decay of magnetic field from the surface of the magnet.

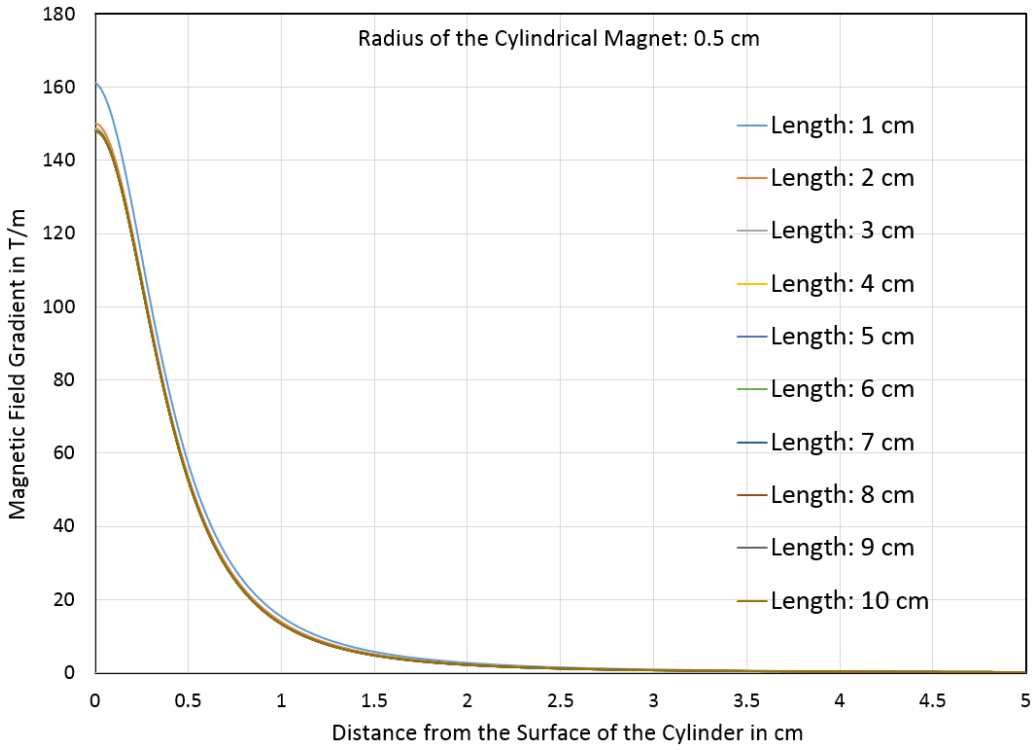

Figure 12. Decay of magnetic field gradients from the surface of the magnet.

Figures 11 and 12 suggest that it's practically impossible to exert sufficient magnetic force on a magnetic particle that is more than a few centimeters away from the surface of the magnet (for example: magnetic drug targeting inside the body).

To overcome this limitation, researchers have suggested positioning of small and easily magnetizable ferromagnetic elements (wires, seeds etc.) near the target separation volume. The role of these elements (local magnets) is to locally produce high magnetic field gradients (of the order ~ 10^6 T/m), these gradients allow the appearance of very strong magnetic forces with short-range action. Such a system, where a large external magnet is used to magnetize the magnetic particles and the local magnets (that produce

strong gradients locally) is generally referred to as a High Gradient Magnetic Separation system.

2.2. Magnetic Field of a Ferromagnetic Wire Magnetized by an External Field

Ferromagnetic wires (Fe, Stainless Steel Grade 304, Stainless Steel Grade 430, Nickel etc.) have been commonly employed as local magnets in HGMS systems. In order to determine the value of magnetic field gradients produced by the local magnets, it is important to know the expression for the magnetic field produced by the local magnets. The magnetic field of an infinite cylindrical wire of radius R_{wire} magnetized perpendicular to its axis by a uniform external field B_0 is given by [99-103]:

$$\vec{B}\,(x,z) = \frac{\mu_0 M}{2} R_{wire}^2 (B_x(x,z).\hat{x} + B_z(x,z).\hat{z}) + B_0.\hat{z} \tag{2.10}$$

Where,

$M = saturation\ magnetization\ of\ the\ wire\ material\ in\ A/m$

$$B_x(x,z) = \frac{2xz}{(x^2+z^2)^2} \tag{2.11}$$

$$B_z(x,z) = \frac{z^2-x^2}{(x^2+z^2)^2} \tag{2.12}$$

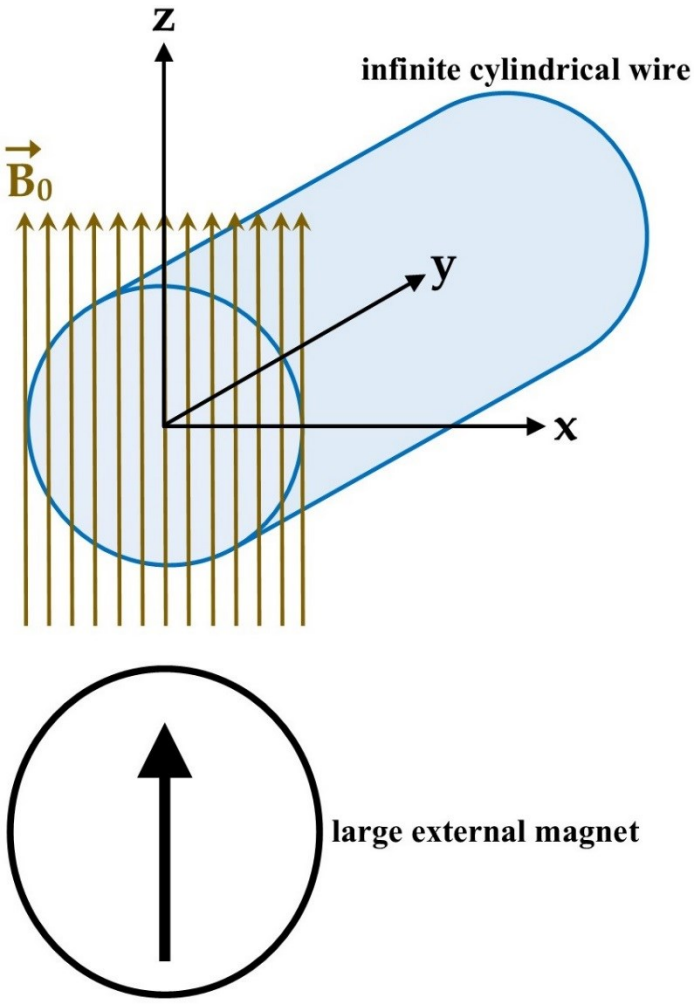

Figure 13. Infinite cylindrical wire magnetized by a uniform external field.

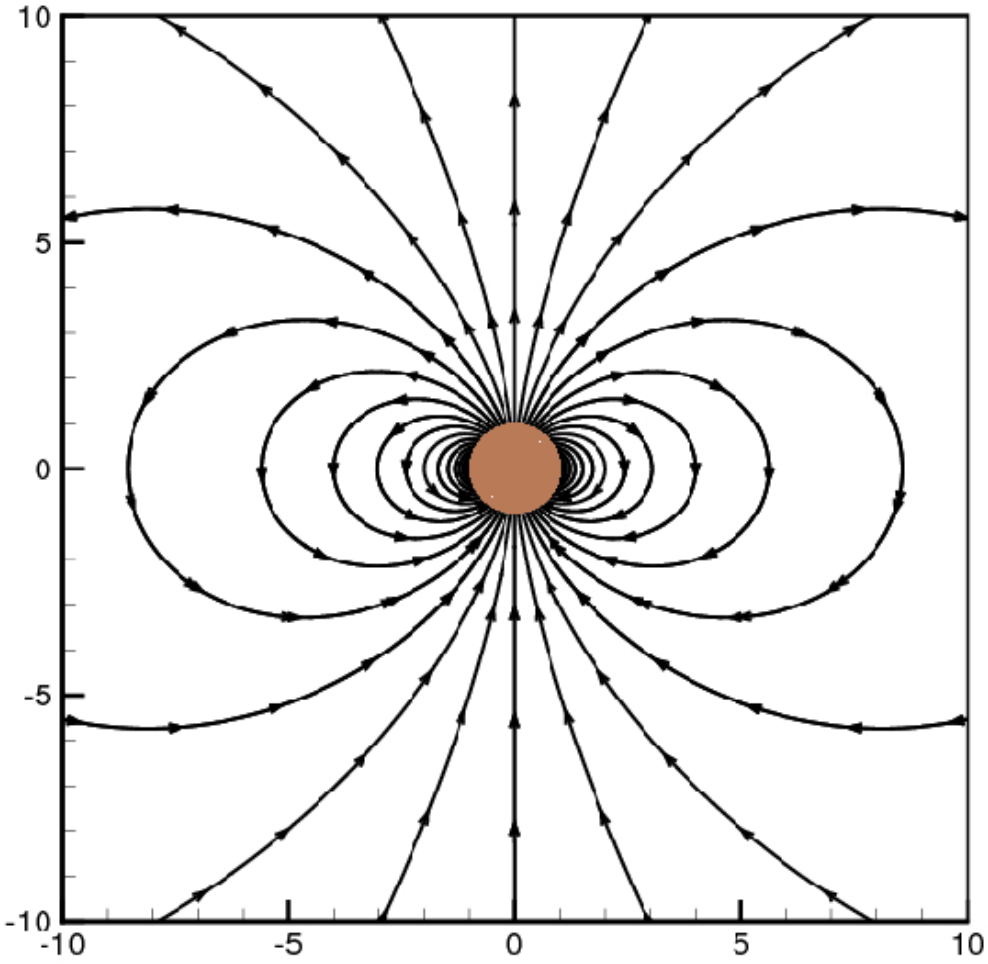

Figure 14. Magnetic Field of a Wire.

2.3. Regions of Attraction and Repulsion around a Magnetic Wire.

After the magnetic moment of a magnetic particle is found by a suitable method, the force on the particle (magnetic dipole) can be computed using Equation (2.2). The matrix notation for this equation in Cartesian coordinates is given by Equation (2.13). In this equation, the spatial derivatives, B_x, B_y, B_z, are the orthogonal magnetic field vectors [87].

$$\vec{F}_{mag} = \begin{bmatrix} F_{mag\_x} \\ F_{mag\_y} \\ F_{mag\_z} \end{bmatrix} = \begin{bmatrix} \frac{\partial}{\partial x}B_x & \frac{\partial}{\partial y}B_x & \frac{\partial}{\partial z}B_x \\ \frac{\partial}{\partial x}B_y & \frac{\partial}{\partial y}B_y & \frac{\partial}{\partial z}B_y \\ \frac{\partial}{\partial x}B_z & \frac{\partial}{\partial y}B_z & \frac{\partial}{\partial z}B_z \end{bmatrix} \begin{bmatrix} m_x \\ m_y \\ m_z \end{bmatrix} \tag{2.13}$$

If the magnetic particle is magnetized to saturation in the z-direction by a powerful external magnetic field [87], then

$$m = (0, 0, m_z) \tag{2.14}$$

This yields,

$$\vec{F}_{mag} = \begin{bmatrix} F_{mag\_x} \\ F_{mag\_y} \\ F_{mag\_z} \end{bmatrix} = \begin{bmatrix} \frac{\partial}{\partial x}B_x & \frac{\partial}{\partial y}B_x & \frac{\partial}{\partial z}B_x \\ \frac{\partial}{\partial x}B_y & \frac{\partial}{\partial y}B_y & \frac{\partial}{\partial z}B_y \\ \frac{\partial}{\partial x}B_z & \frac{\partial}{\partial y}B_z & \frac{\partial}{\partial z}B_z \end{bmatrix} \begin{bmatrix} 0 \\ 0 \\ m_z \end{bmatrix} \tag{2.15}$$

and,

$$\vec{F}_{mag\_x} = m_z \frac{\partial}{\partial z}B_x \tag{2.16}$$

$$\vec{F}_{mag\_y} = m_z \frac{\partial}{\partial z}B_y \tag{2.17}$$

$$\vec{F}_{mag\_z} = m_z \frac{\partial}{\partial z}B_z \tag{2.18}$$

It is important to note that regions of attraction and repulsion exist around a magnetic wire that has been magnetized perpendicular to its axis by an external magnet. The regions of magnetic attraction and magnetic repulsion can be obtained from the equation of magnetic field of the wire (equation 2.10) and the corresponding magnetic field gradients.

$$B_x(x,z) = \frac{2xz}{(x^2+z^2)^2} \tag{2.19}$$

$$\frac{\partial}{\partial x}B_x(x,z) = \frac{-2z(3x^2-z^2)}{(x^2+z^2)^3} \tag{2.20}$$

$$\frac{\partial}{\partial z}B_x(x,z) = \frac{2x(x^2-3z^2)}{(x^2+z^2)^3} \tag{2.21}$$

$$B_z(x,z) = \frac{z^2-x^2}{(x^2+z^2)^2} \tag{2.22}$$

$$\frac{\partial}{\partial x}B_z(x,z) = \frac{2x(x^2-3z^2)}{(x^2+z^2)^3} \tag{2.23}$$

$$\frac{\partial}{\partial z}B_z(x,z) = \frac{2z(3x^2-z^2)}{(x^2+z^2)^3} \tag{2.24}$$

The region of magnetic attraction in the z-direction can be obtained as:

$$\vec{F}_{mag\_z} < 0, or\ m_z\frac{\partial}{\partial z}B_z < 0 \tag{2.25}$$

This implies,

$\frac{2z(3x^2-z^2)}{(x^2+z^2)^3} < 0, or\ 3x^2 < z^2, or\ \frac{x}{z} < \frac{1}{\sqrt{3}}, or\ \theta < 30°$

(2.26)

Similarly, the region of magnetic repulsion in the x-direction can be obtained as:

$$\vec{F}_{mag\_x} > 0, or\ m_z \frac{\partial}{\partial z} B_x > 0 \quad (2.27)$$

This implies,

$$\frac{2x(x^2 - 3z^2)}{(x^2 + z^2)^3} > 0, or\ x^2 > 3z^2, or\ \frac{z}{x} < \frac{1}{\sqrt{3}}, or\ \theta < 30°$$

The direction of magnetic force experienced by a magnetic dipole in the vicinity of such a magnetic wire can be represented by the schematic depicted in Figure 15.

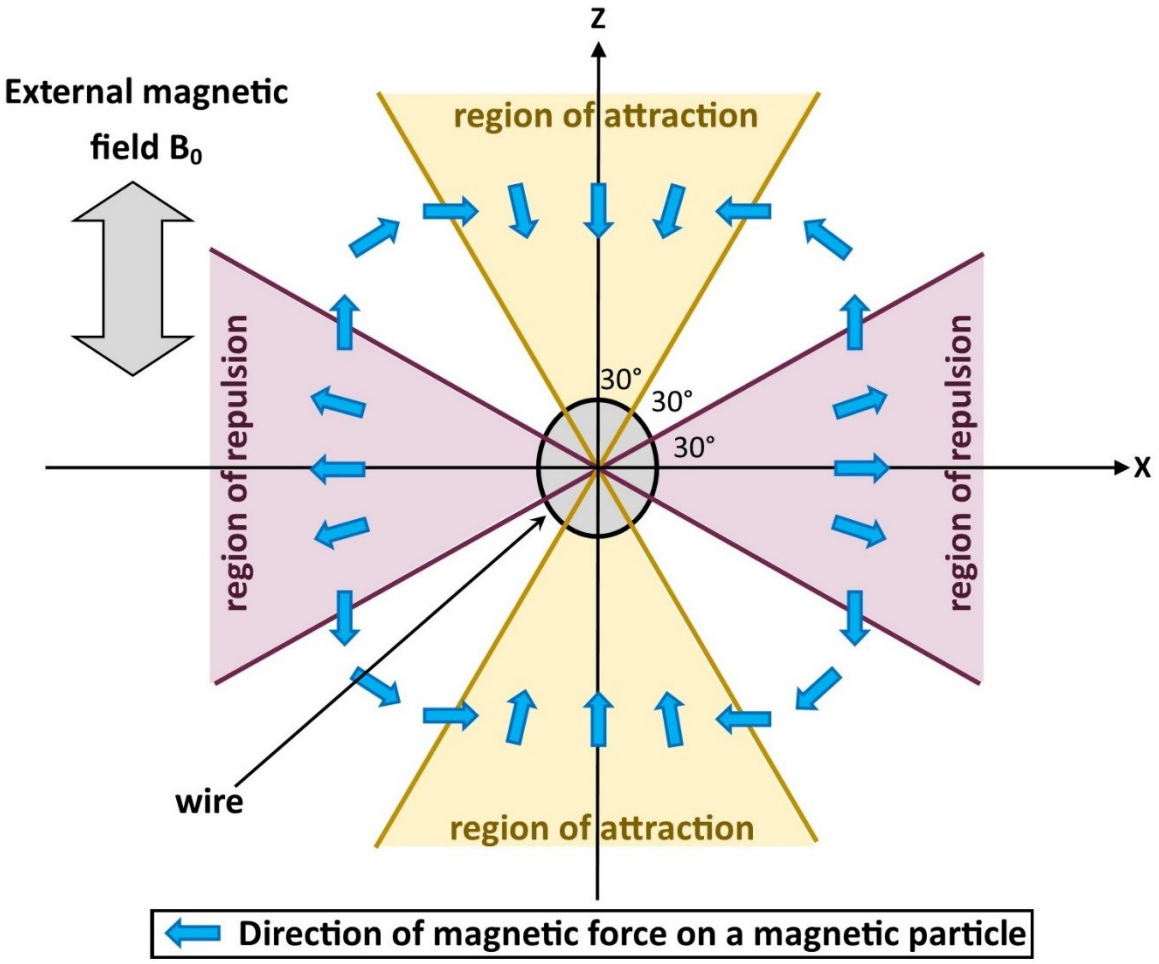

Figure 15. Direction of magnetic force experienced by a magnetic dipole in the vicinity of a magnetic wire that has been magnetized by an external magnetic field.

Frazier and Han [104] have presented the same phenomenon to represent the direction of magnetic force that will be experienced by a red blood cell if it was in the vicinity of such a wire.

It is therefore possible to focus a magnetic particle along the height of a channel if one magnetic wire is positioned on top of the channel and the other magnetic wire is positioned underneath the channel. This repulsion of magnetic particle is depicted in the schematic of Figure. 16.

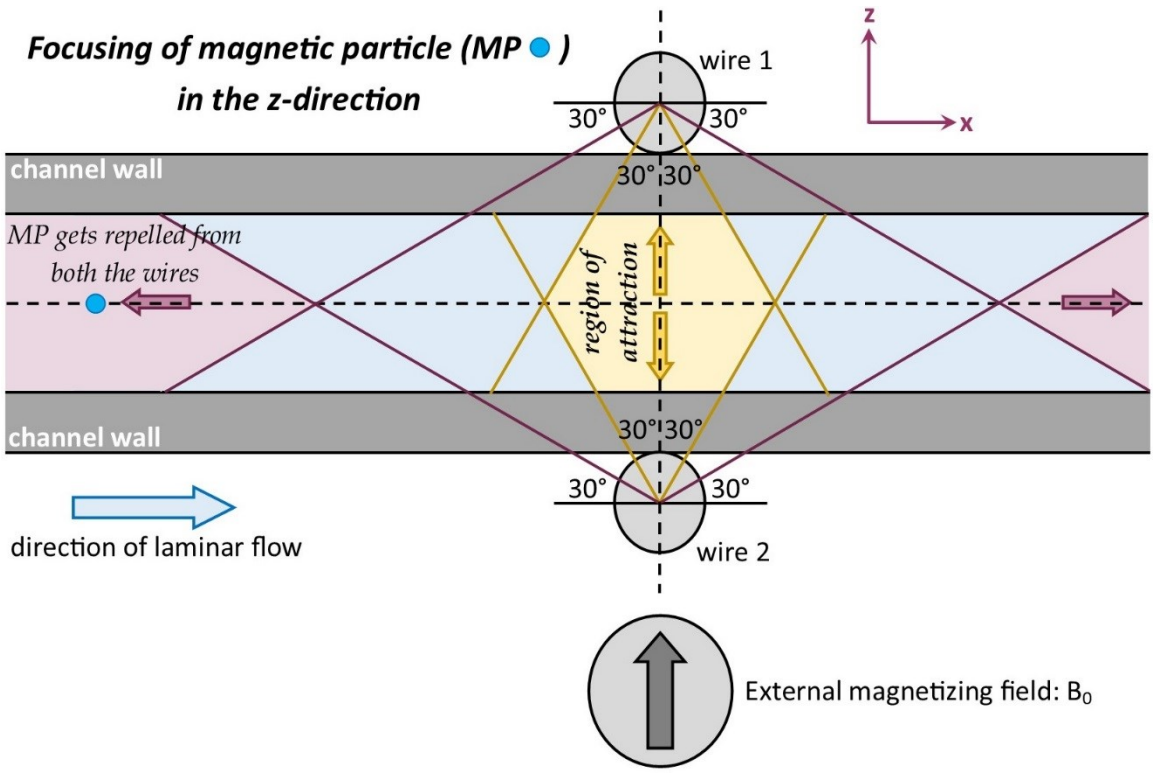

Figure 16. Focusing of the magnetic particle towards the center of the channel height by the two magnetic wires. As long as the particle stays in the region of repulsion of the magnetic wires (the purple colored region), it will be continuously repelled towards the center of the channel.

2.4. Conceptual Review of Existing HGMS Systems

At present HGMS systems for cell/biomolecule separation in microfluidic systems can be broadly classified into two categories:

- One local magnet (for example, a magnetic wire that is magnetized perpendicular to its axis) is positioned along the length of the separation chamber and along the direction of flow.
- Several local magnets (wires, seeds, etc.) are positioned perpendicular to the length of the separation chamber and perpendicular to the direction of flow.

The first category of HGMS systems where a local magnet (usually a wire) is positioned along the length of the separation chamber and along the direction of flow in a microfluidic systems has been studied both theoretically and experimentally by several researchers [11, 104-106].

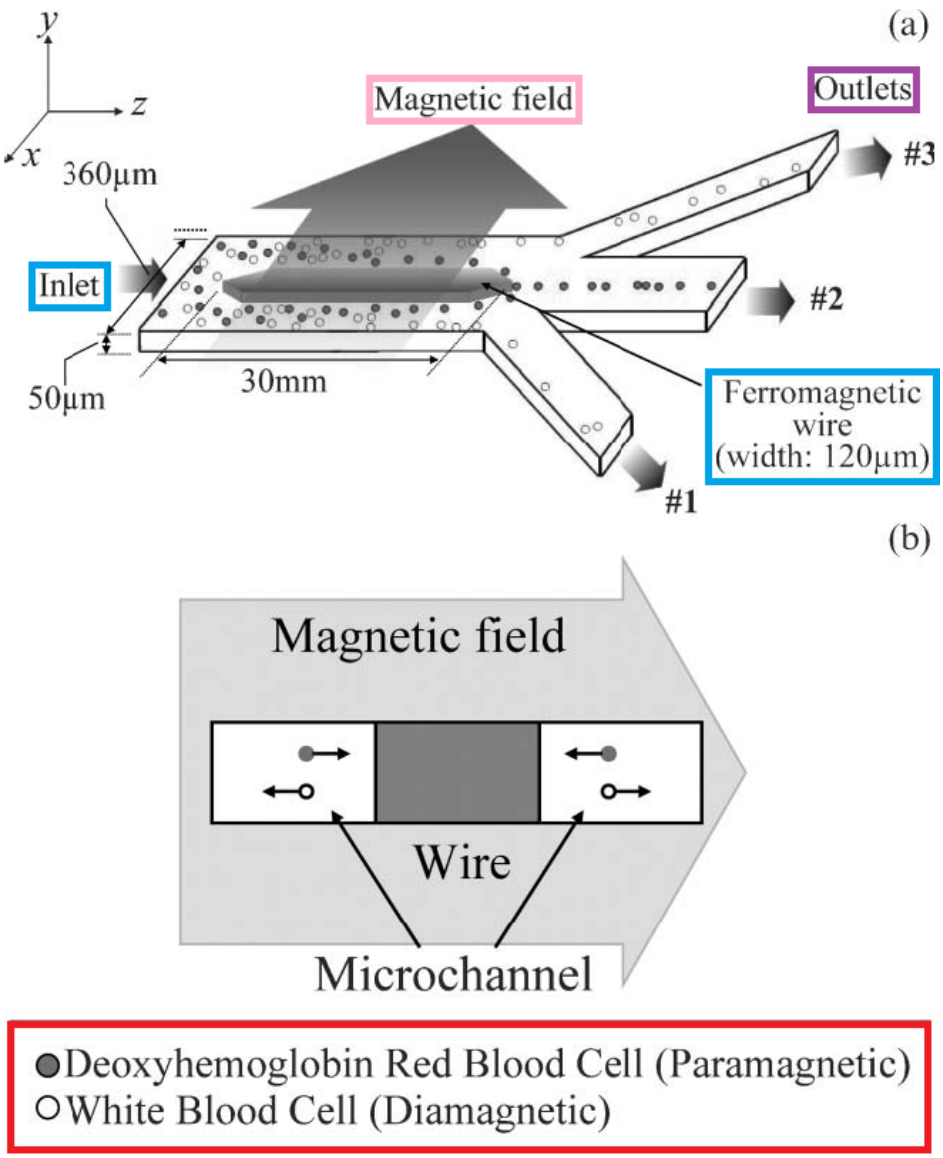

Figure 17. HGMS system for red blood cell separation by Frazier and Han [106].

For example, Frazier and Han positioned a 120 µm wide nickel wire (magnetized perpendicular to its axis by a Nd-Fe-B permanent magnet) along the direction of flow and in the center of their microfluidic separation chamber in order to locally produce strong magnetic field gradients in order to attract locally present red blood cells by exerting sufficiently strong attractive magnetic forces on the them. So far, all such designs and

systems, in theory and in practice, have utilized the phenomenon of magnetic attraction to pull the magnetic particles of interest towards the local magnet. It was also found that such systems were able to attract more particles as the length of the high-gradients producing wire increased.

The second category of HGMS systems where several magnetic wires are positioned perpendicular to the length of the separation chamber and perpendicular to the direction of flow have also been studied by several researchers primarily in reference to magnetic-drug targeting systems to solve the problem of in-stent restenosis [92, 95, 107-109]. However, in all of these studies, neither the experimental work nor the computational models were set up to test any particular hypothesis regarding the mechanism of capture of magnetic particles by magnetic wires. Hence we do not gather any useful information that we can employ towards the improvement of such HGMS systems.

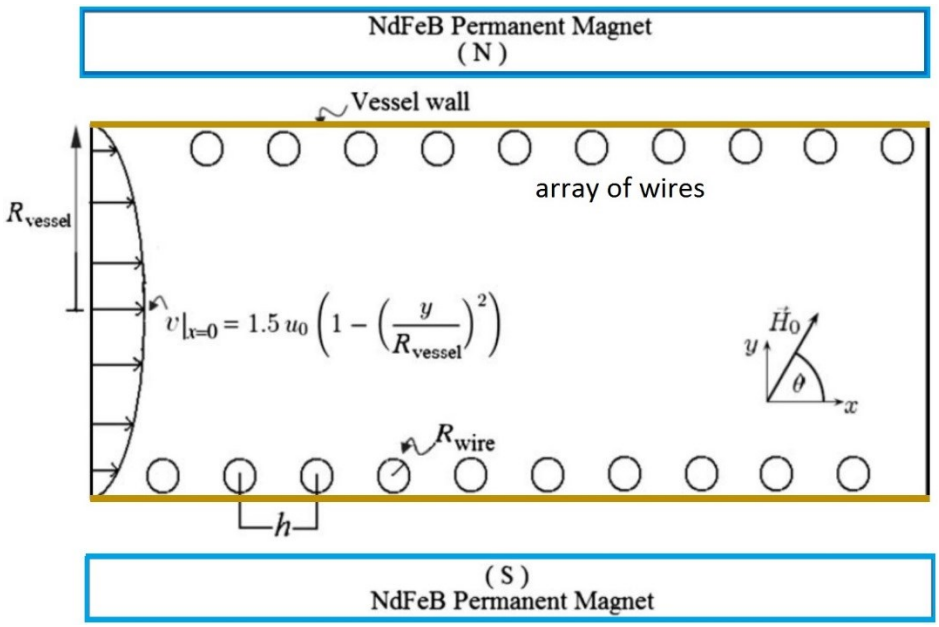

Figure 18. 2D design of the HGMS system for computational study of capture of magnetic particles by Cregg et. al. [107].

2.5. Summary of Model Assumptions

This section describes the assumptions that are usually made when the motion of micro-sized magnetic particles is studied in a microfluidic HGMS system. Magnetic particle transport in HGMS systems (Figure 18) is dependent on several factors such as inertia, gravity, magnetic force, viscous drag, particle/blood-cell interaction, particle/fluid interaction, interparticle effects such as magnetic dipole-dipole interactions, etc. The magnetic particle motion can be expressed using Newton's second law as [92, 93, 110]:

$$mass_{MP}\frac{dv_{MP}}{dt} = \vec{F}_{mag} + \vec{F}_{drag} + inertia + gravity + interaction\ forces \qquad (2.13)$$

Where $mass_{MP}$ is the mass of the magnetic particle, and v_{MP} is the velocity of the magnetic particle.

2.5.1. Gravitational Force on Magnetic Particle

The gravitational force on a magnetic particle present in a fluid is given by:

$$\vec{F}_{gravity+buoyancy} = Volume_{MP}(\rho_{MP} - \rho_{fluid})gravity \quad (2.14)$$

Where,

ρ_{MP}= density of the magnetic particle, and

ρ_{fluid} = density of the fluid

Table 1 Magnetic force and gravitational force experienced by a 1 μm diameter magnetic particle for different magnetite weight content values. The value of magnetic field gradient is 100 T/m. The magnetic particle is present in water and is assumed to have reached its saturation magnetization for all the cases listed in the table.

Table 2. Magnetic force and gravity for a 1μm diameter magnetic particle.

% weight magnetite	Mass of the MP (kg)	Density of the MP (kg/m3)	Gravitational force (N)	Magnetic force (N)
10	$5.69 \times (10^{-16})$	$1.09 \times (10^{3})$	$4.46 \times (10^{-16})$	$4.55 \times (10^{-13})$
20	$6.23 \times (10^{-16})$	$1.19 \times (10^{3})$	$9.77 \times (10^{-16})$	$9.97 \times (10^{-13})$
30	$6.89 \times (10^{-16})$	$1.31 \times (10^{3})$	$1.62 \times (10^{-15})$	$1.65 \times (10^{-12})$
40	$7.70 \times (10^{-16})$	$1.47 \times (10^{3})$	$2.41 \times (10^{-15})$	$2.46 \times (10^{-12})$
50	$8.73 \times (10^{-16})$	$1.67 \times (10^{3})$	$3.42 \times (10^{-15})$	$3.49 \times (10^{-12})$
60	$1.01 \times (10^{-15})$	$1.92 \times (10^{3})$	$4.74 \times (10^{-15})$	$4.83 \times (10^{-12})$
70	$1.19 \times (10^{-15})$	$2.27 \times (10^{3})$	$6.53 \times (10^{-15})$	$6.66 \times (10^{-12})$
80	$1.45 \times (10^{-15})$	$2.78 \times (10^{3})$	$9.12 \times (10^{-15})$	$9.31 \times (10^{-12})$
90	$1.87 \times (10^{-15})$	$3.57 \times (10^{3})$	$1.32 \times (10^{-14})$	$1.35 \times (10^{-11})$
100	$2.62 \times (10^{-15})$	$5.00 \times (10^{3})$	$2.05 \times (10^{-14})$	$2.10 \times (10^{-11})$

Table 1. shows that the gravitational force is approximately three orders smaller than the magnetic force. Therefore, gravitational force is ignored in this study. In general gravitational force is always ignored when analyzing magnetophoretic motion of micro-sized particles, as it is very weak when compared to the magnetic force.

2.5.2. Laminar Flow in the Channel

Throughout this work, and in microfluidics work in general, the concept of low Reynolds number flow is important. The Reynolds number is often used by scientists and

engineers to communicate whether flow is turbulent or not. The Reynolds number is essentially the ratio of inertial effects to viscous effects and can be written as:

$$Reynold's\ Number\ Re = \frac{\rho_{fluid} v_{avg} L}{\eta_{fluid}} \quad (2.15)$$

Where L is the characteristic length scale of the channel such as channel diameter.

In a typical microfluidic device the Reynolds number is less than 1, (for example, for, ρ_{fluid} = 1000 kg/m^3, v_{avg} = 0.01 m/s, L = 1×10^{-5} m and η_{fluid} = 0.001 kg/m/s). This implies that inertia is quickly damped or absorbed by the viscosity and that there is no turbulence. Low Reynold's number flow is time independent.

2.5.3. Magnetic Particle's Reynolds Number and Stoke's Drag

Similarly, whether it is inertial or viscous effects that dominate the particle's motion in the channel can be determined by evaluating the particle's Reynold's number as:

$$Particle's\ Reynold's\ Number\ Re_{MP} = \frac{D_{MP} \rho_{fluid}}{\eta_{fluid}} v_{avg} \quad (2.16)$$

where,

D_{MP}= diameter of the magnetic particle = 1 μm

ρ_{fluid}= density of the fluid = 10^3 kg/m^3

η_{fluid}= viscosity of the fluid = 8.9 × 10^{-4} kg/m-sec

v_{avg}= average flow velocity in the channel = 10 cm/sec

This yields,

$Re_{MP} \ll 1$

Therefore, particle's inertia is ignored.

For particle Reynold's number, Re_p«1, and under a fully developed laminar flow, the drag force on a spherical particle with diameter D_{MP} is given by the Stokes drag as:

$$\vec{F}_{drag} = 6\pi\eta r_{MP} v_{avg} \tag{2.17}$$

2.5.4. Interparticle Magnetic Dipole-Dipole Interactions

The force between two magnetic dipoles is given by [111]:

$$\vec{F}_{m_a m_b} = \frac{3\mu_0}{4\pi r^4}[\{(\hat{r} \times \vec{m}_a) \times \vec{m}_b + (\hat{r} \times \vec{m}_b) \times \vec{m}_a\} - 2\hat{r}(\vec{m}_a . \vec{m}_b) + \{5\hat{r}(\hat{r} \times \vec{m}_a).(\hat{r} \times \vec{m}_b)\}] \tag{2.18}$$

Assuming that both the magnetic dipoles are magnetized along the axis of the external magnetic field, the above equation reduces to:

$$\vec{F}_{m_a m_b} = \frac{3\mu_0 |\vec{m}|^2}{4\pi r^4}[\{2(\hat{r} \times \vec{m}) \times \vec{m}\} - 2\hat{r} + \{5\hat{r}|\hat{r} \times \vec{m}|^2\}] \tag{2.19}$$

This study assumes the presence of dilute particle suspensions in which the particle volume concentration (total volume occupied by the particles per unit volume of the fluid) is small. In such situations, interparticle magnetic dipole-dipole interactions can be neglected [112, 113].

2.5.5. Brownian Diffusion – Stoke's Einstein Equation

The diffusion coefficient, *D*, for the free diffusion of a single particle in a liquid, far away from other particles or a wall, is given by the Einstein's equation:

$$D = \frac{kT}{f}\ m^2/s \tag{2.20}$$

where kT is the thermal energy, k is the Boltzmann constant (1.38×10^{-23} $m^2 kg\ s^{-2} K^{-1}$), and f is the friction coefficient of the particle. For a spherical particle with radius r_{MP} in a

Newtonian liquid with viscosity η, the friction coefficient for translational motion equals the Stokes friction factor,

$$f = 6\pi\eta r_{MP} \tag{2.21}$$

The combined result is called the Stokes-Einstein (SE) diffusion coefficient for translational sphere diffusion. Brownian motion can influence particle capture when the particle diameter D_{MP} is sufficiently small. Gerber et al. have developed the following criterion to estimate this diameter:

$$|F|D_{MP} \leq kT \tag{2.22}$$

Where $|F|$ is the magnitude of the total force acting on the particle. Gerber et al. have studied the capture of Fe_3O_4 particles in water using a single magnetic wire, and have estimated the critical particle diameter for this application to be:

$$D_{c,p} \equiv \frac{kT}{|F|} = 40\ nm, where\ |F| = 0.1\ pN$$

Therefore, Brownian diffusion is ignored in this study.

2.5.6. Magnetic Particle's Relaxation Time and Stoke's Number

The magnetic particle's equation of motion can now be written as:

$$mass_{MP}\frac{dv_{MP}}{dt} = \vec{F}_{mag} + \vec{F}_{drag} \tag{2.23}$$

$$mass_{MP}\frac{dv_{MP}}{dt} = 6\pi\eta r_{MP}(v_{MP} - v_{avg}) + \vec{F}_{mag} \tag{2.24}$$

$$\frac{dv_{MP}}{dt} = \frac{6\pi\eta r_{MP}(v_{MP}-v_{avg})}{mass_{MP}} + \frac{\vec{F}_{mag}}{mass_{MP}} \tag{2.25}$$

$$\frac{dv_{MP}}{dt} = \frac{6\pi\eta r_{MP}(v_{MP}-v_{avg})}{\rho_{MP}\frac{4}{3}\pi r_{MP}^3} + \frac{\vec{F}_{mag}}{mass_{MP}} \tag{2.26}$$

$$\frac{dv_{MP}}{dt} = \frac{6\eta(v_{MP}-v_{avg})}{\rho_{MP}\frac{4}{3}r_{MP}^2} + \frac{\vec{F}_{mag}}{mass_{MP}} = \frac{(v_{MP}-v_{avg})}{\tau} + \frac{\vec{F}_{mag}}{mass_{MP}} \tag{2.27}$$

$$\tau = particle\ relaxation\ time = \frac{\rho_{MP}\frac{4}{3}r_{MP}^2}{6\eta} = \frac{\rho_{MP}D_{MP}^2}{18\eta} \tag{2.28}$$

$$\tau < 100\ ns$$

The Stokes number is a dimensionless number that characterizes the behavior of particles suspended in a fluid flow. The particle Stokes number is defined as the ratio of the particle relaxation time to the characteristic flow time scale (based on the bulk velocity and tube diameter), or:

$$Stk = \tau\frac{v_{avg}}{Diameter_{channel}} \tag{2.29}$$

For a 1 mm channel diameter, the particle Stoke's number is ≈ 9×10^{-7}. This means the particles relax extremely quickly to the velocity of the flow around them. If the particles are moved by an external force, their surrounding fluid will move with them. Thus, it is reasonable to assume no relative motion between the fluid and particles.

2.5.7. Magnetic Particle's Acceleration

Magnetic particle's acceleration is often ignored in low Reynold's number flows. It can be shown that the time during which the particle changes its velocity is of the order of nanoseconds.

$$mass_{MP}\frac{d^2 r_{MP}}{dt} = \vec{F}_{drag} + \vec{F}_{mag} \tag{2.30}$$

$$\Delta v(t) \equiv v_{MP}(t) - v_{avg} \tag{2.31}$$

$$mass_{MP}\frac{d\Delta v(t)}{dt} = -6\pi\eta r_{MP}\left[v_{MP}(t) - v_{avg}\right] + \vec{F}_{mag} \tag{2.32}$$

The particle relaxation time is given by,

$$\tau = particle\ relaxation\ time = \frac{\rho_{MP} D_{MP}^2}{18\eta} = \frac{D_{MP} Re_{MP}}{18|v_{MP} - v_{avg}|} \tag{2.33}$$

This gives,

$$\frac{d\Delta v(t)}{dt} = -\frac{\Delta v(t)}{\tau} + \frac{\vec{F}_{mag}}{mass_{MP}} \tag{2.34}$$

$$\Delta v(t) = \Delta v(t)(t=0)e^{-\frac{t}{\tau}} + (1 - e^{-\frac{t}{\tau}})v_{MP} \tag{2.35}$$

Where,

$$v_{MP} = \frac{\vec{F}_{mag}}{6\pi\eta r_{MP}} \tag{2.36}$$

$$\tau = \frac{D_{MP} Re_{MP}}{18|v_{MP} - v_{avg}|} < 100\ nsec \tag{2.37}$$

The characteristic timescale over which the particle changes its velocity becomes for $Re_p << 1$ of the order of nanoseconds. Because we are not interested in this short-lived transient behavior we neglect the particle acceleration altogether.

This yields,

$$0 = \vec{F}_{drag} + \vec{F}_{mag} \tag{2.38}$$

2.6. Repulsion Based Magnetic Focusing

2.6.1. Specific Geometric Configuration for Fluid Flow and Magnetic Field Gradient Source

As far as we know, at present there are no exclusively magnetic methods for focusing of magnetic particles for cell and biomolecule focusing. This study utilizes the phenomenon of high gradient magnetic repulsion to focus magnetic particles in flow. Specifically, the design consists of a rectangular microfluidic channel with multiple magnetic wires positioned on top of and underneath it along the length of the channel at an angle theta with respect to the channel axis. Strong magnetic field gradients, produced by the wires, exert sufficient repulsive magnetic forces on the magnetic particles in order to focus them in a specific region in the channel.

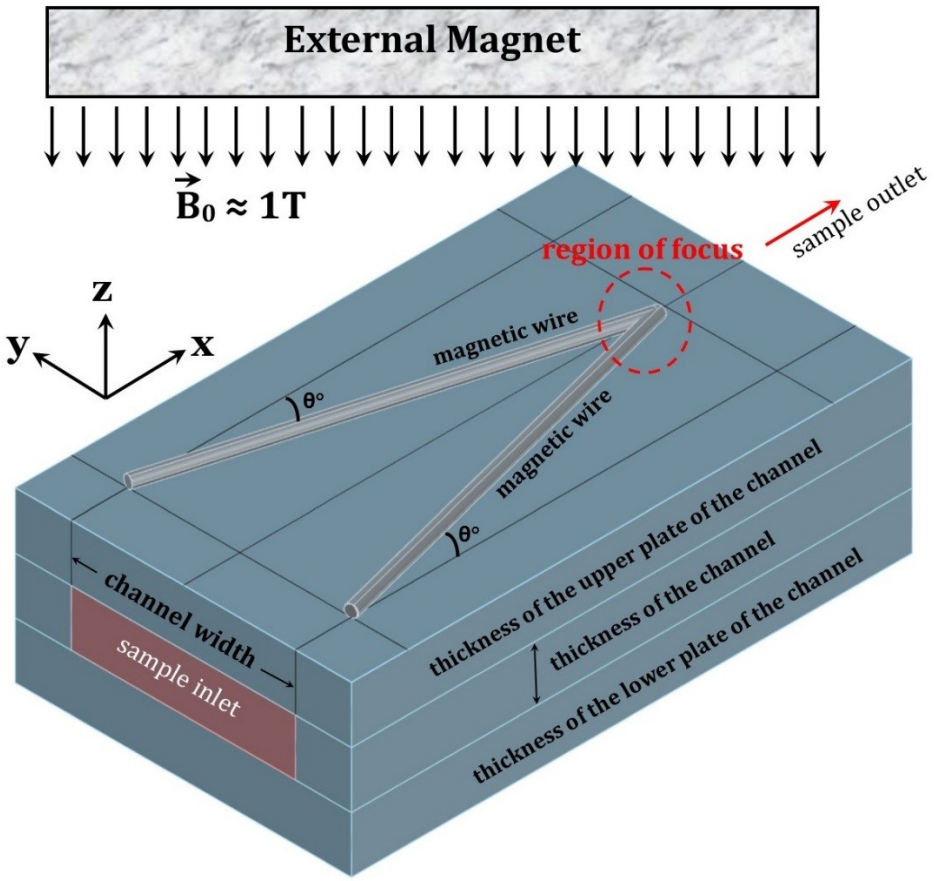

Figure 19. Magnetic focusing design.

2.6.2. Illustration of Magnetic Repulsion Principle in the Geometric Configuration

Magnetic repulsion is used to focus the magnetic particles. High gradient magnetic repulsion constrains the magnetic particles to move along the length of the wires in the x-y plane. Specifically, the component of magnetic force that is along y-direction and perpendicular to the flow repels the magnetic particles away from the wires causing their lateral movement in the x-y plane and focusing them towards the center of the channel where the wires meet (see Figure. 20). Designs based on a similar principle where high magnetic field gradients provide forces at an angle to the flow of paramagnetic

micro/nano meter sized particles in an essentially 2D geometry in order to sort them have been used before by other researchers [28–30]. The aim of our design is to use the high magnetic field gradients (≈10,000 T/m) produced by the magnetic wires in order to exert sufficiently strong repulsive magnetic forces on the magnetic particles in order to focus them in a small region inside the channel.

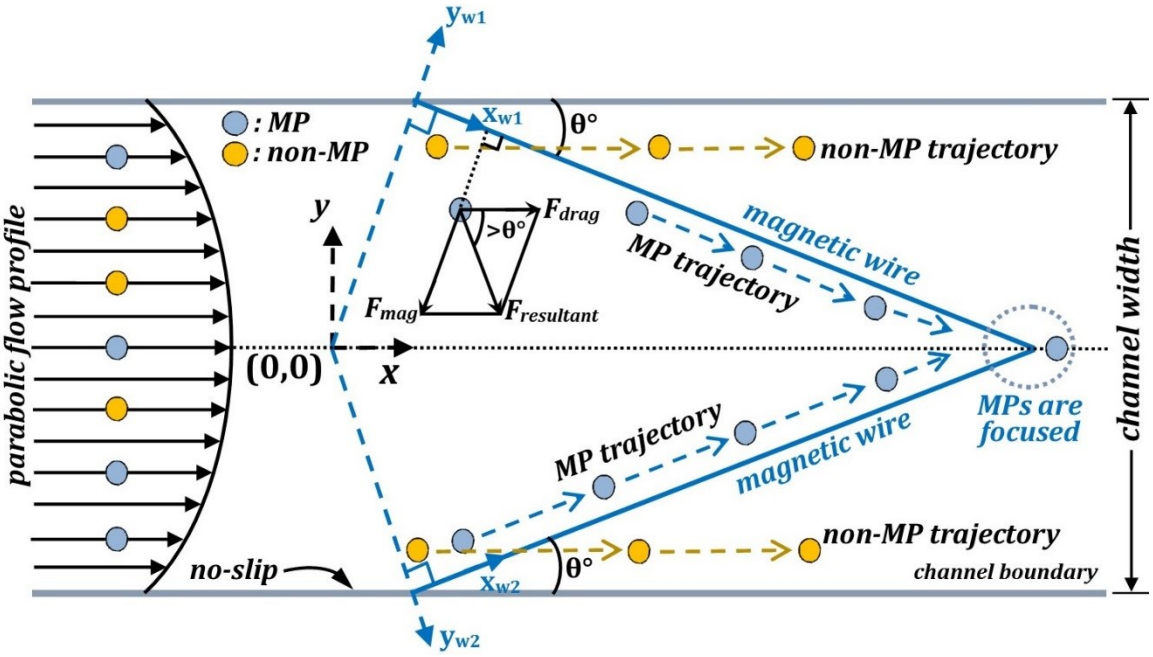

Figure 20. Top view of magnetic focusing design.

2.6.3. Specific Expressions for Magnetic Forces Used in the Mathematical Model

The derivations for the expressions of normal and axial components of magnetic force experienced by a spherical magnetic particle that has been magnetized to saturation in this repulsion based magnetic focusing design can be found in the appendices of this dissertation.

The magnitude of the axial component of the magnetic force experienced by a magnetic particle by one magnetic wire in this design is given by:

$$F_{mx}(y_w, z).\hat{x} = |\vec{m}| \frac{\left[\frac{-2y_w(-B_0 y_w^2 + 3z^2 B_0 + k)}{(x^2+z^2)^3}\right]}{\sqrt{\left\{\frac{2y_w z}{(y_w^2+z^2)^2}\right\}^2 + \left\{\frac{z^2-y_w^2}{(y_w^2+z^2)^2} + \frac{B_0}{k}\right\}^2}} \sin\theta \tag{2.39}$$

The magnitude of the normal component of the magnetic force experienced by a magnetic particle by one magnetic wire in this design is given by:

$$F_{my}(y_w, z).\hat{y} = |\vec{m}| \frac{\left[\frac{-2y_w(-B_0 y_w^2 + 3z^2 B_0 + k)}{(x^2+z^2)^3}\right]}{\sqrt{\left\{\frac{2y_w z}{(y_w^2+z^2)^2}\right\}^2 + \left\{\frac{z^2-y_w^2}{(y_w^2+z^2)^2} + \frac{B_0}{k}\right\}^2}} \cos\theta \tag{2.40}$$

$$k = \frac{\mu_0 M}{2} R_{wire}^2 \tag{2.41}$$

Where M is the volumetric magnetization saturation of the magnetic wire, R_{wire} is the radius of the magnetic wire, $|\vec{m}|$is the magnitude of the magnetic moment of the particle, and B_0 is the strength of the external magnetizing field.

2.6.4. Effects of Wire diameter on Magnetic Force

The maximum magnetic force experienced by the magnetic particle depends on the diameter of the magnetic wire. The diameter of the magnetic wires to be used in the design is determined based on the channel height and the thickness of the channel wall. It is well known that the magnetic interactions exerted by a larger wire, although much weaker, are longer ranged, i.e., the magnetic particles can feel the magnetic effect of the wire at farther distances away from it [99].

$$F_{my_w}(y_w, z).\hat{y}_w = |\vec{m}| \frac{\left[\frac{-2y_w(-B_0 y_w^2 + 3z^2 B_0 + k)}{(x^2+z^2)^3}\right]}{\sqrt{\left\{\frac{2y_w z}{(y_w^2+z^2)^2}\right\}^2 + \left\{\frac{z^2 - y_w^2}{(y_w^2+z^2)^2} + \frac{B_0}{k}\right\}^2}} \quad (2.42)$$

The above equation is used to determine the force experienced by a 1 μm diameter magnetic particle with 10% magnetite by volume content. The height of the channel wall is fixed at 3 μm. The height of the channel is kept at only a few micrometers more than the particle size in order to limit the movement of the particle along the z-direction. The particle is assumed to be present at half the channel height. Figure 21 suggests that for a channel wall thickness of 100 μm, a 400 μm diameter wire shall be used because it will exert the maximum repulsive force on the particle. From Figure 22 it is clear that as the thickness of the channel wall increases the required diameter of the focusing wire also increases, this is in agreement with [99]. It is also important to note that as the diameter of the focusing wire increases the maximum repulsive magnetic force experienced by the particle decreases.

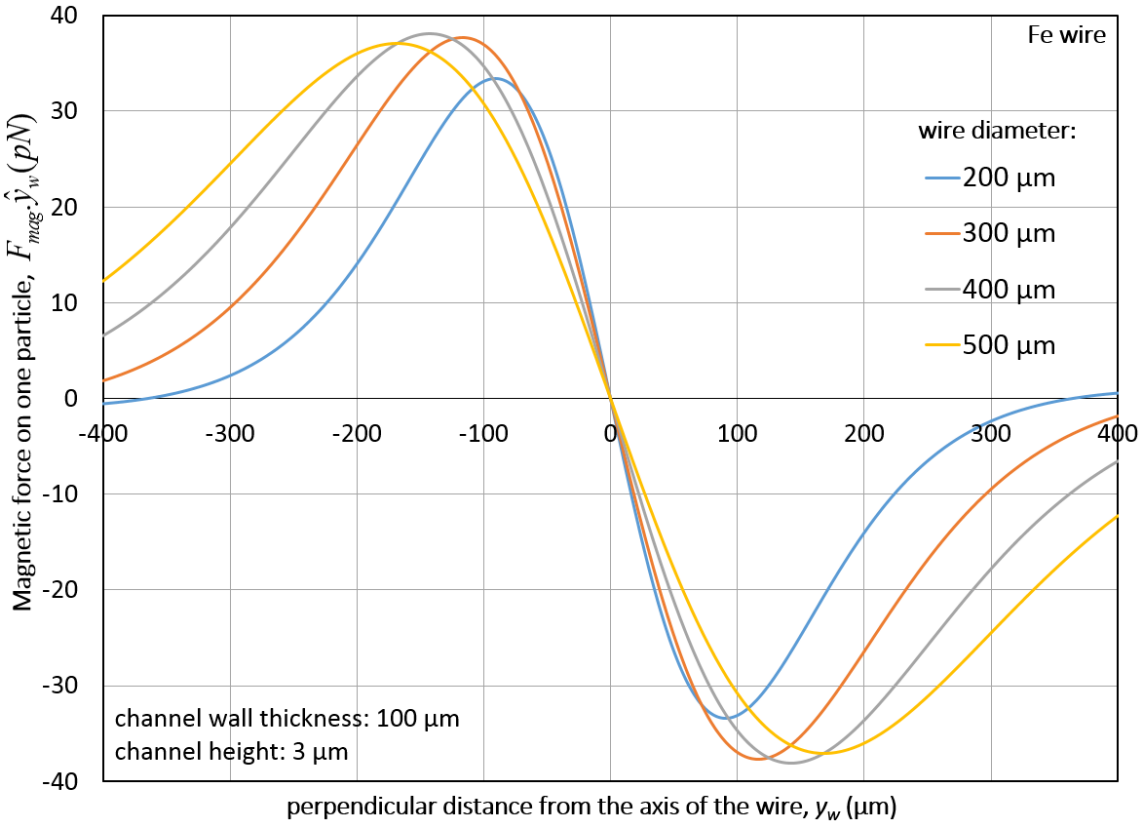

Figure 21. Repulsive magnetic force experienced by a particle of 1 um diameter because of wires of different diameters.

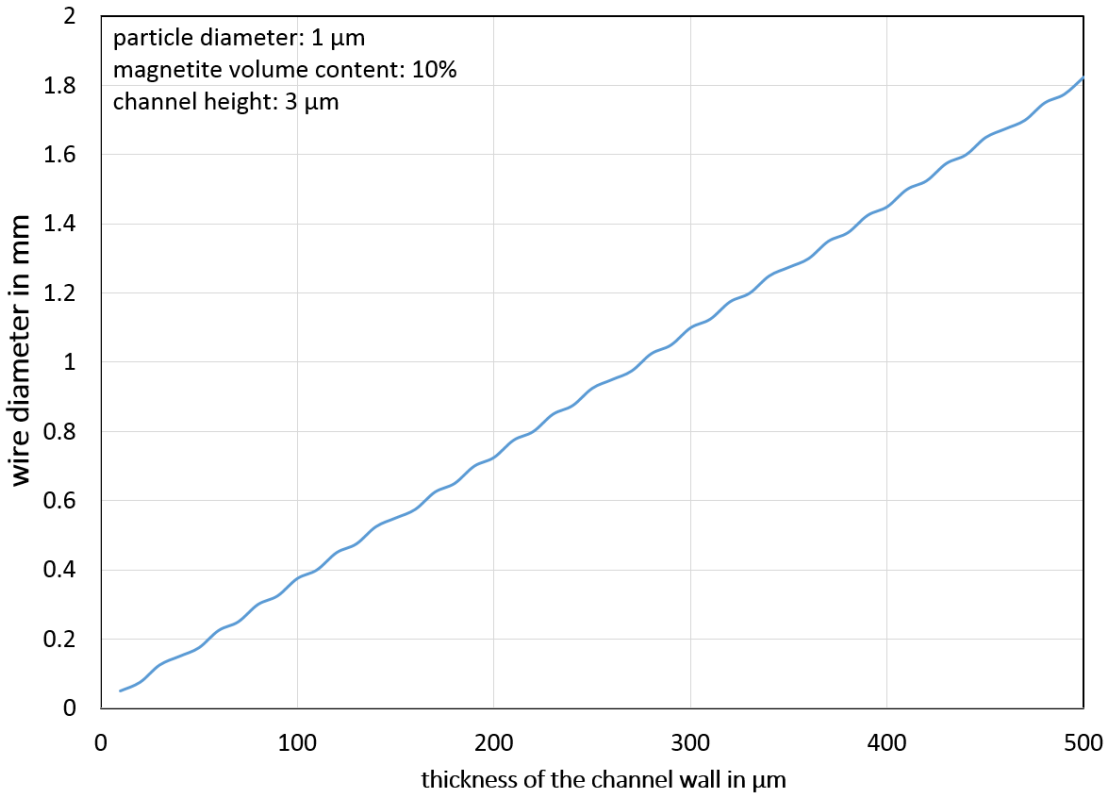

Figure 22. Required wire diameter for different values of channel wall thickness.

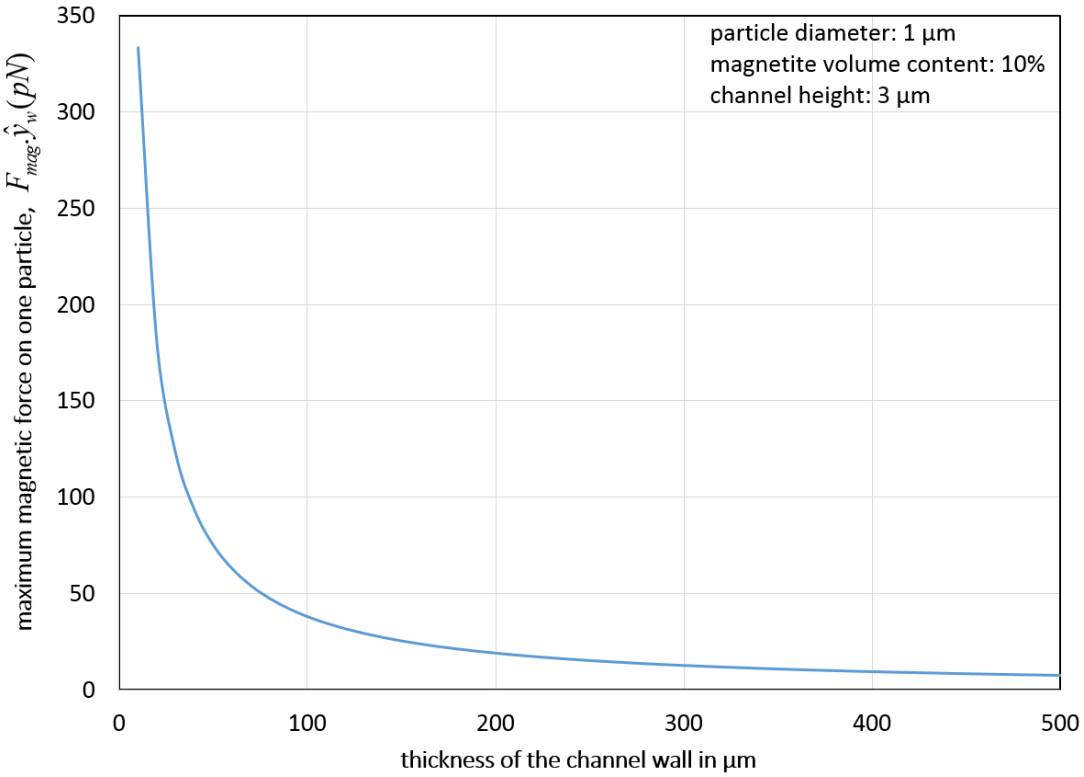

Figure 23. Drop in the maximum repulsive magnetic force experienced by the particle with the increase in the channel wall thickness.

2.6.5. Specific Expression for Drag Force in the Fluid Channel

The drag force experienced by the particle is given by:

$$F_{drag}(y).\hat{x} = 6\pi\eta R_{MP} v_{avg}\left[1 - \left(\frac{2y}{channel\ width}\right)^2\right] \tag{2.43}$$

Where, η is the viscosity of the fluid, R_{MP} is the radius of the magnetic particle, and v_{avg} is the average flow velocity in the channel.

2.6.6. Analytical Approximation of Average Flow Velocity in the Channel

The average flow velocity in the channel needed to focus the magnetic particles to the center of the channel can be approximated using the maximum magnetic force experienced by the particle.

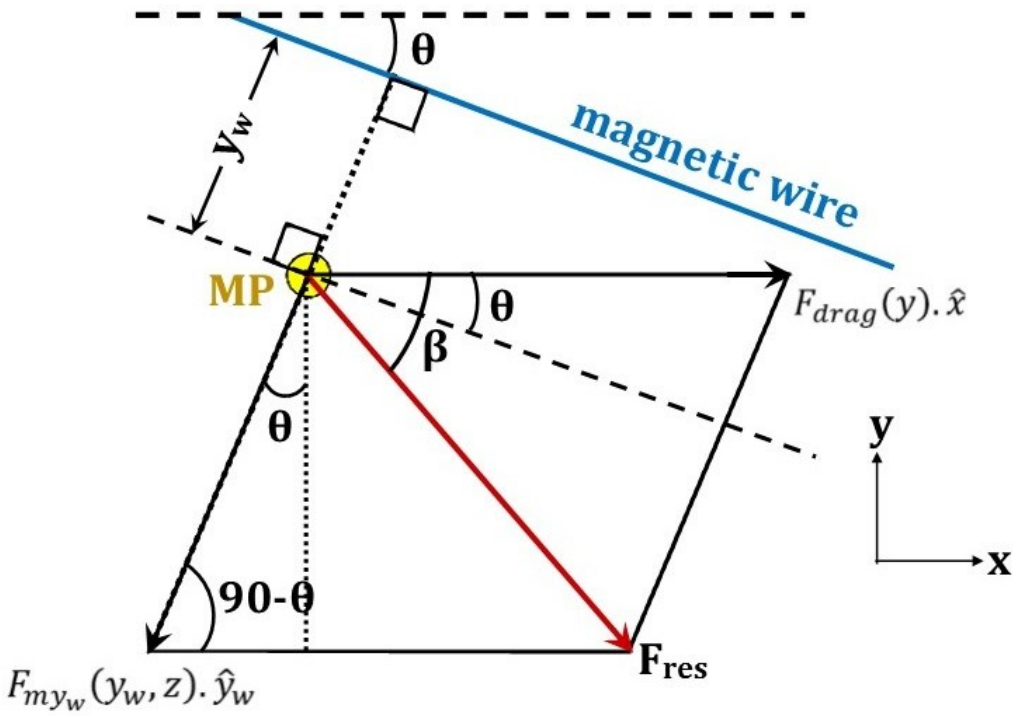

Figure 24. Analytical approximation of the maximum value of average flow velocity in the channel that can be used to focus the magnetic particles to the center of the channel.Magnetic force and drag force acting on the magnetic particle. The particle will get focused towards the center of the channel as long as β > θ.

The MP will continue to get focused towards the center of the channel as long β is greater than θ. The maximum value of average velocity in the channel needed to focus the MP can be approximated using the maximum value of magnetic force $F_{my_w}(y_w, z).\hat{y}_w$ acting on the particle.

$$v_{max} = \frac{\{tan(90-\beta)F_{max\_my_w}(y_w,z).\hat{y}_w.cos\theta\}+F_{max\_my_w}(y_w,z).\hat{y}_w sin\theta}{6\pi\eta r_{MP}} \quad (2.44)$$

$$v_{max\_avg} = \frac{2}{3} v_{max} \quad (2.45)$$

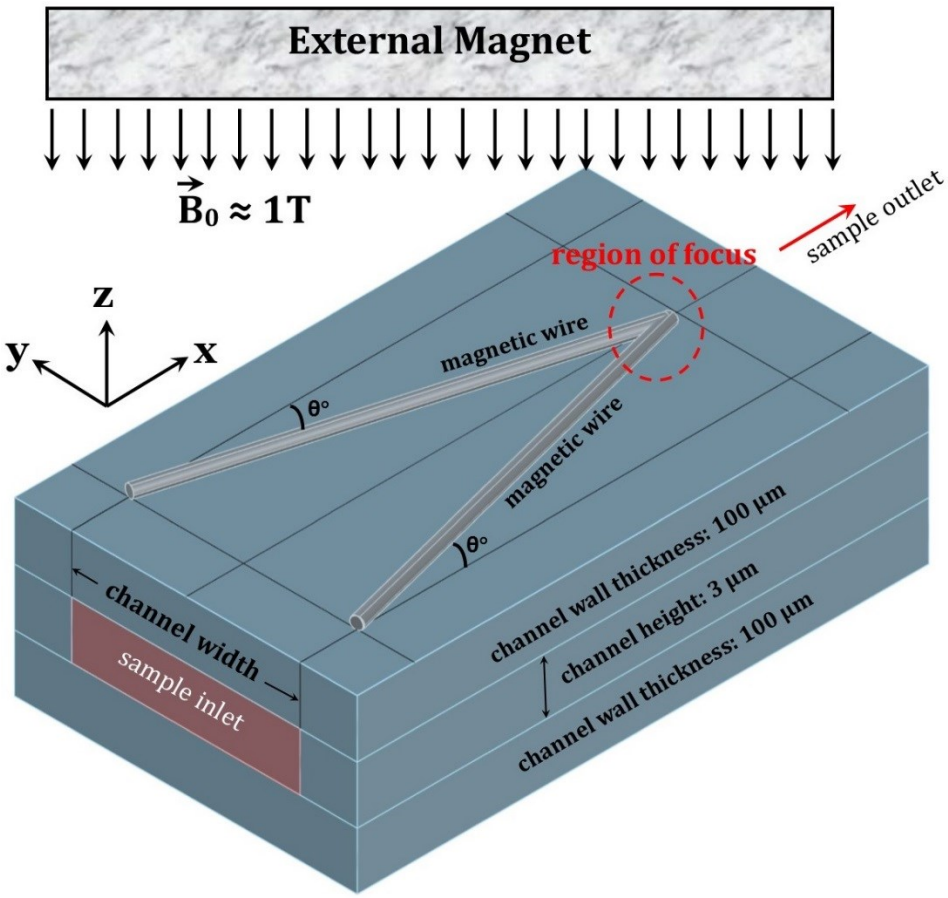

Figure 25. Magnetic focusing design that is used to analytically determine the maximum value of average flow velocity in the channel that can be used to focus the magnetic particles to the center of the channel.

The maximum value of average flow velocity in the channel needed to focus the MP is determined for the configuration presented in Figure 25. The required diameter of the magnetic wire for this design is 375 µm.

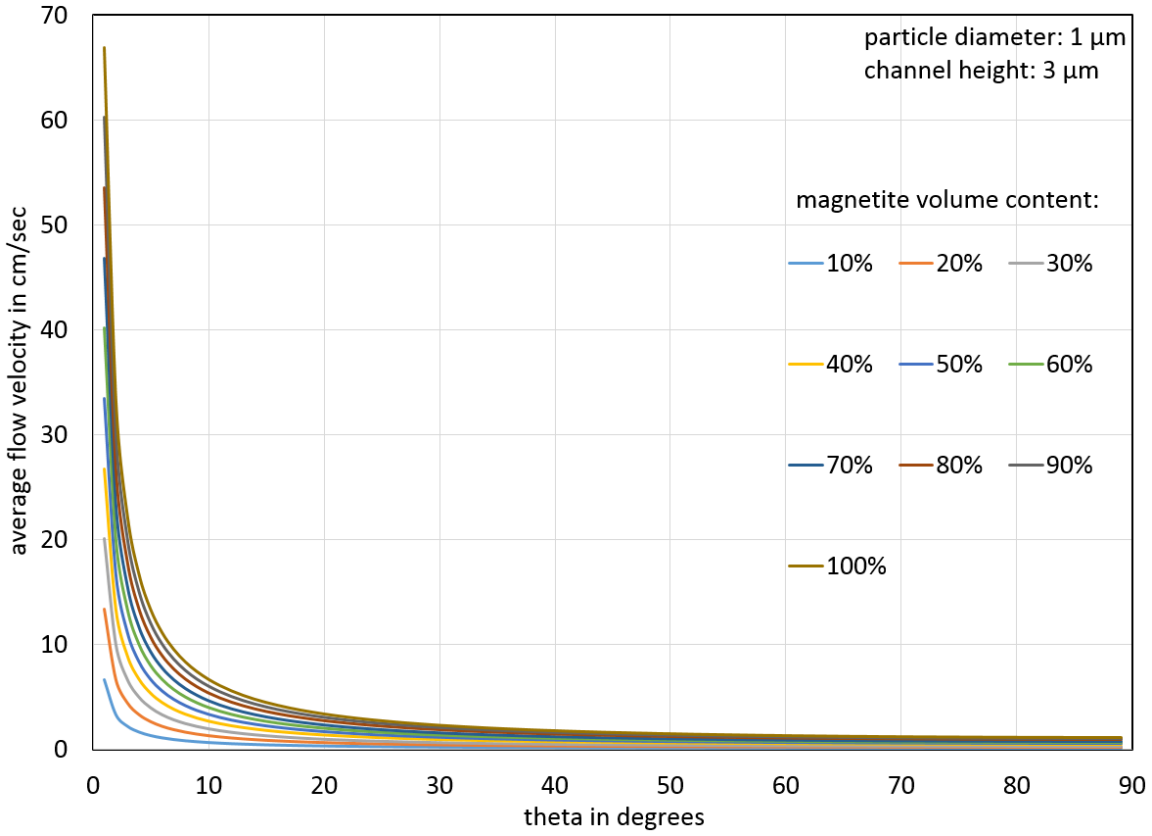

Figure 26. Plot showing maximum average flow velocity in the channel that can be used to focus the magnetic particle to the center of the channel as a function of θ.

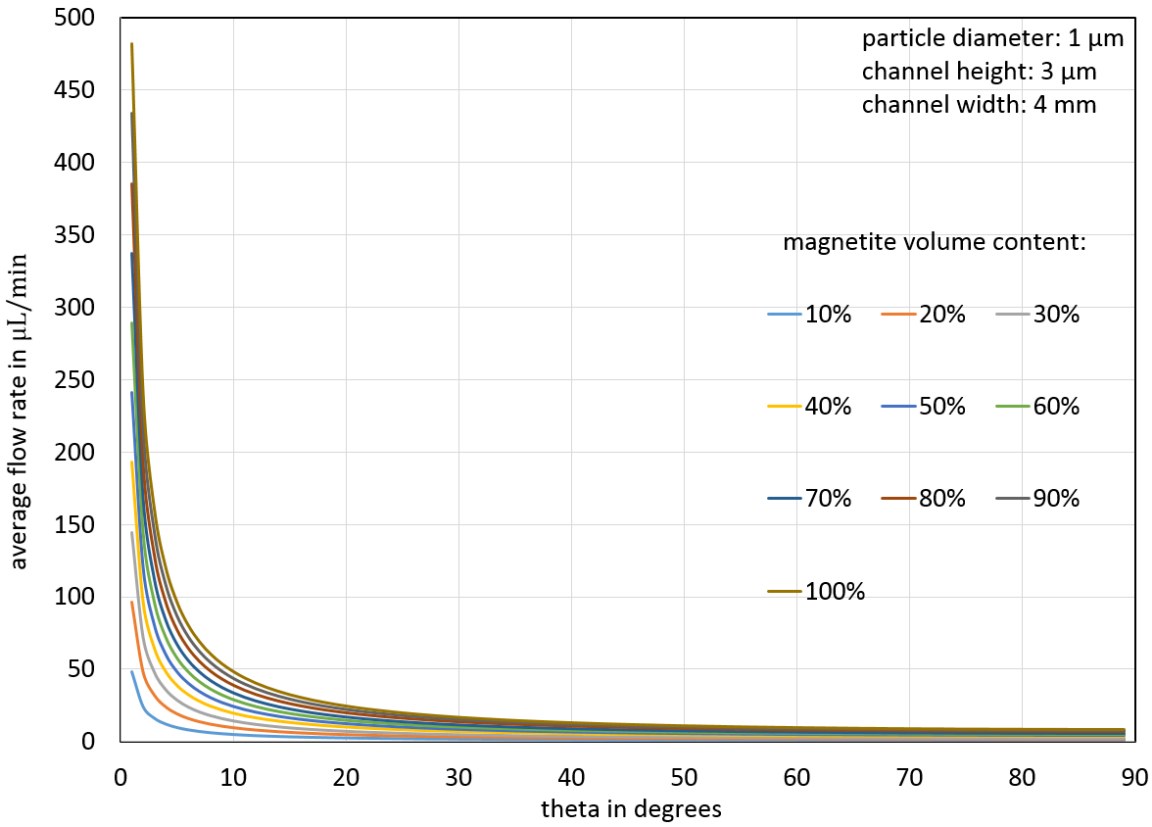

Figure 27. Plot showing maximum average flow rate in the 4 mm wide channel that can be used to focus the magnetic particle to the center of the channel as a function of θ.

2.6.7. Equation for the Trajectory of the Magnetic Particle in the Fluid Channel

The trajectory of the magnetic particle is determined by the solution of the following first order ordinary differential equation which is an initial value problem. The initial value represents the perpendicular starting position of the magnetic particle along the width of the channel.

$$\frac{\Delta y}{\Delta x} = \frac{F_{my}(y_w,z).\hat{y}}{F_{mx}(y_w,z).\hat{x}+F_{drag}(y).\hat{x}} \tag{2.46}$$

This is a non-separable, non-linear equation. Numerical methods are used to solve this equation.

2.6.8. Numerical Implementation of the Mathematical Model using MATLAB

The equation for the trajectory of the magnetic particles is a first order ordinary differential equation (ODE) that is solved numerically using MATLAB. MATLAB has several different functions for the numerical solution of ordinary differential equations. The MATLAB ode solvers are generally better than anything one would program themselves. They are able to estimate the error in the solution at each step size, and decide whether or not the step size is too large (error to high) or too small (inefficient).

Stiffness is a subtle, difficult, and important concept in the numerical solution of ordinary differential equations. It depends on the differential equation, the initial conditions, and the numerical method. A problem is stiff if the solution being sought varies slowly, but there are nearby solutions that vary rapidly, so the numerical method must take small steps to obtain satisfactory results. Stiffness is an efficiency issue. If we weren't concerned with how much time a computation takes, we wouldn't be concerned about stiffness. Nonstiff methods can solve stiff problems; they just take a long time to do it.

This study uses ODE45 and ODE15s to determine the trajectories of magnetic particles. They are explicit Runge–Kutta formulas for nonstiff initial-value problems and backward differentiation formulas for stiff initial-value problems, respectively. These methods are unquestionably among the most effective and widely used. MATLAB recommends that ODE45 should be the first solver one should try. The ODE45 solver (an

explicit Runge-Kutta method) is generally efficient, however, it can become unstable with stiff systems. This will manifest itself by the solver taking shorter and shorter time steps to compensate. The solution will either take a long time, or the time step will be reduced to the point where machine precision causes the routine to fail. In such situations the use of ODE15s solver is recommended. However, because it is an implicit scheme, it has to solve (possibly large) sets of equations at each time step.

All the Matlab solvers will vary the step size to produce a solution which is accurate to a given error. One can override this by setting a maximum step size (which can force the solver to take too small a step). It is generally best to let the solver choose the step size. Options are set by creating an options structure with the odeset command.

2.6.9. MATLAB Simulated Trajectories of the Magnetic Particle.

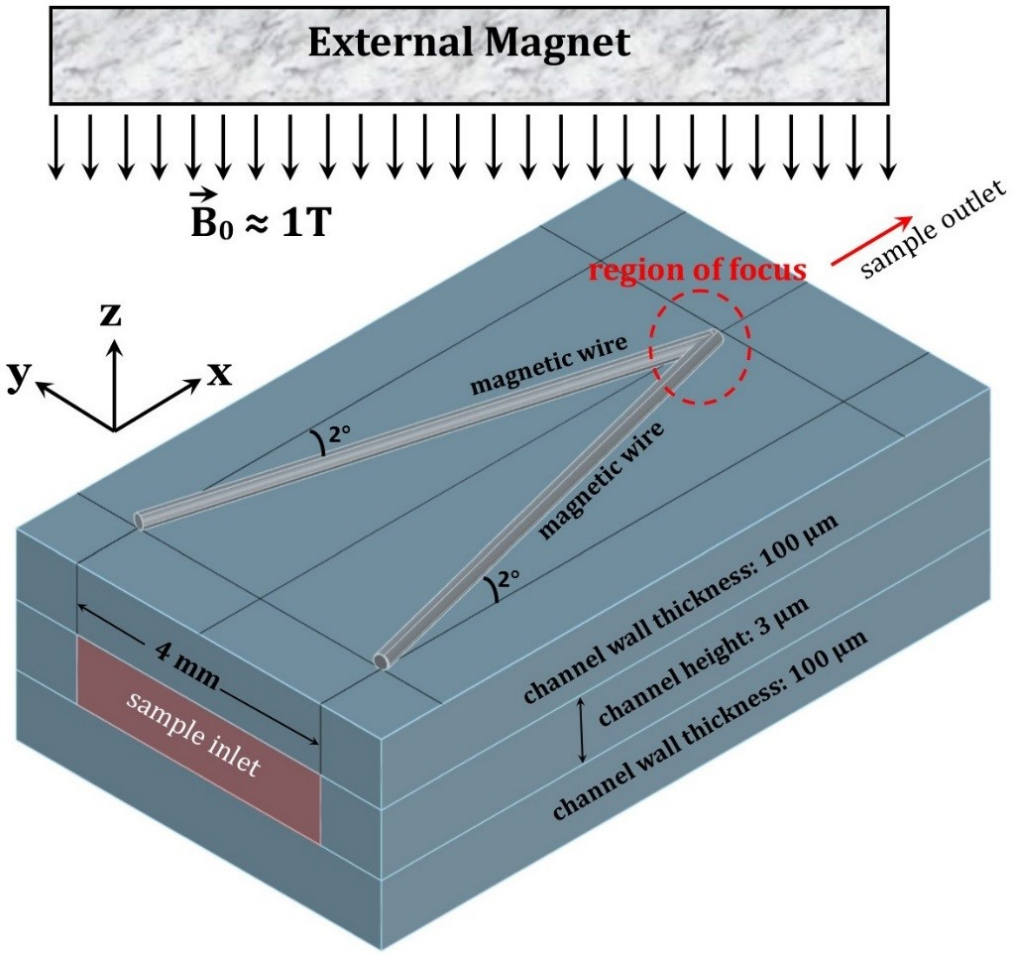

Figure 28. Magnetic focusing design for which the trajectories of the magnetic particle in the channel are numerically determined.

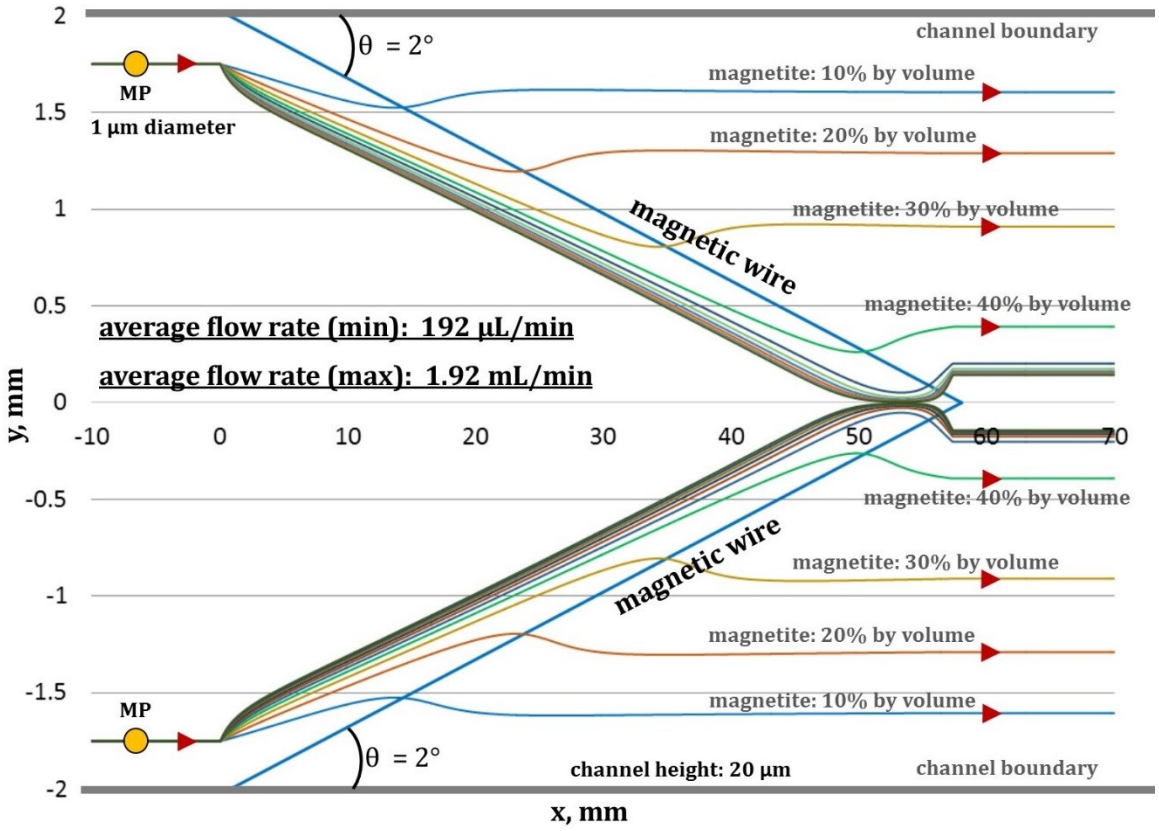

Figure 29. MATLAB simulated trajectory of the magnetic particles with different magnetite content for the same starting position in the 4 mm wide channel.

Figure 29 shows that for a given flow rate it is easier to focus those magnetic particles towards the center of the channel that have higher magnetite content. The magnetic force experienced by a magnetic particle is dependent on the volume content of magnetite in that particle and higher is the magnetite content in the particle, higher is the magnetic force experienced by the particle.

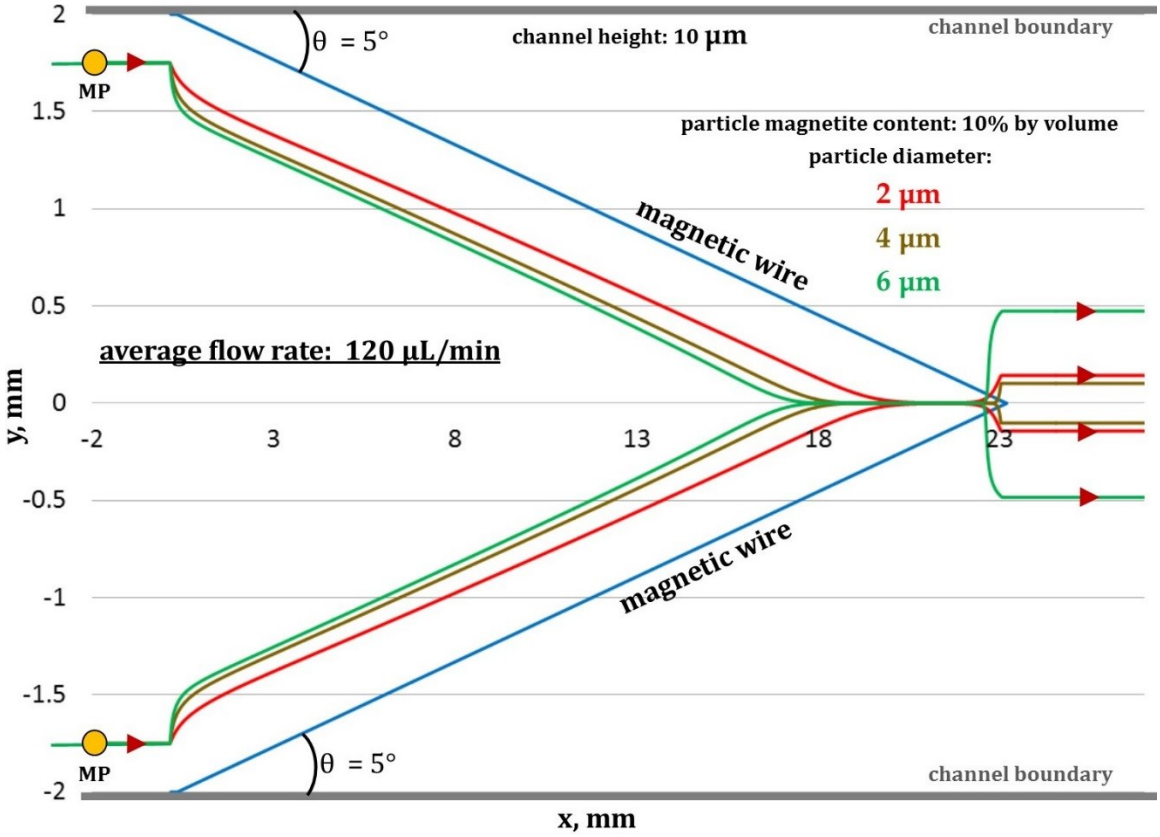

Figure 30. MATLAB simulated trajectories of magnetic particles of different size but same magnetic content for the same starting position in the 4 mm wide channel. All particles get focused to the center of the channel.

Figure 30 shows that for a flow rate of 120 µL/min in the channel, it is possible to focus magnetic particles of 2 µm, 4 µm, and 6 µm diameter to the center of the channel.

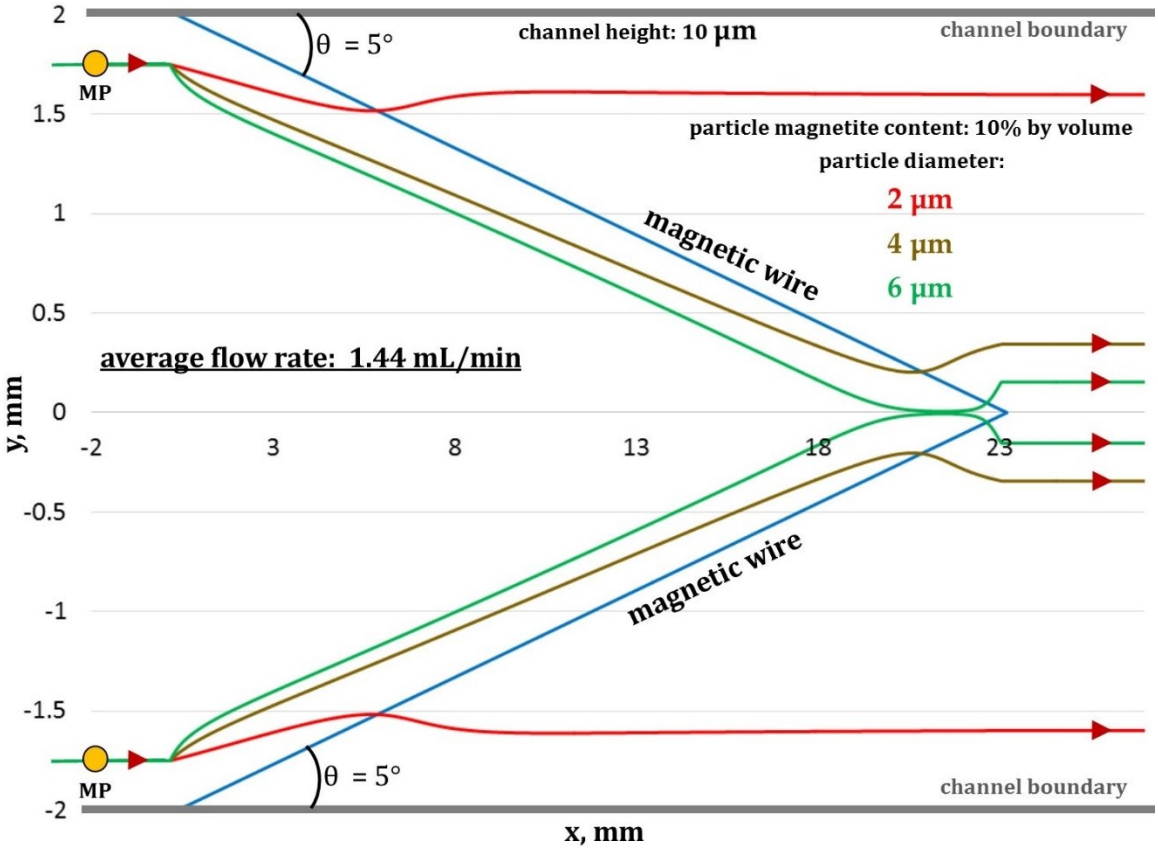

Figure 31. MATLAB simulated trajectories of magnetic particles of different sizes but same magnetic content in the fluid channel. Only particles with 6 um diameter are focused to the center of the channel.

Figure 31 shows that it is possible to separate magnetic particles of different sizes using flow rates that will focus only magnetic particles of a specific diameter and a specific magnetic content to the center of the channel, particles with overall smaller magnetic content do not get focused to the center of the channel and are separated.

2.7. Repulsion based Magnetic Separation

2.7.1. Review of Existing High Gradient Magnetic Separation Methods

Researchers have been trying to attract drug-carrying magnetic particles to magnetic stents for magnetic drug-targeting purposes since the early 2000s. Aviles et. al. have extensively examined the capture-efficiency of magnetic wires in capturing magnetic particles in such HGMS systems with the help of both experiments and computational models. It is important to note that in their design the magnetic wires are present inside the separation chamber against the channel walls and are obstructing the flow. Based on their experimental and computational results they made the following important observations which are quite consistent with the observations made by other researchers:

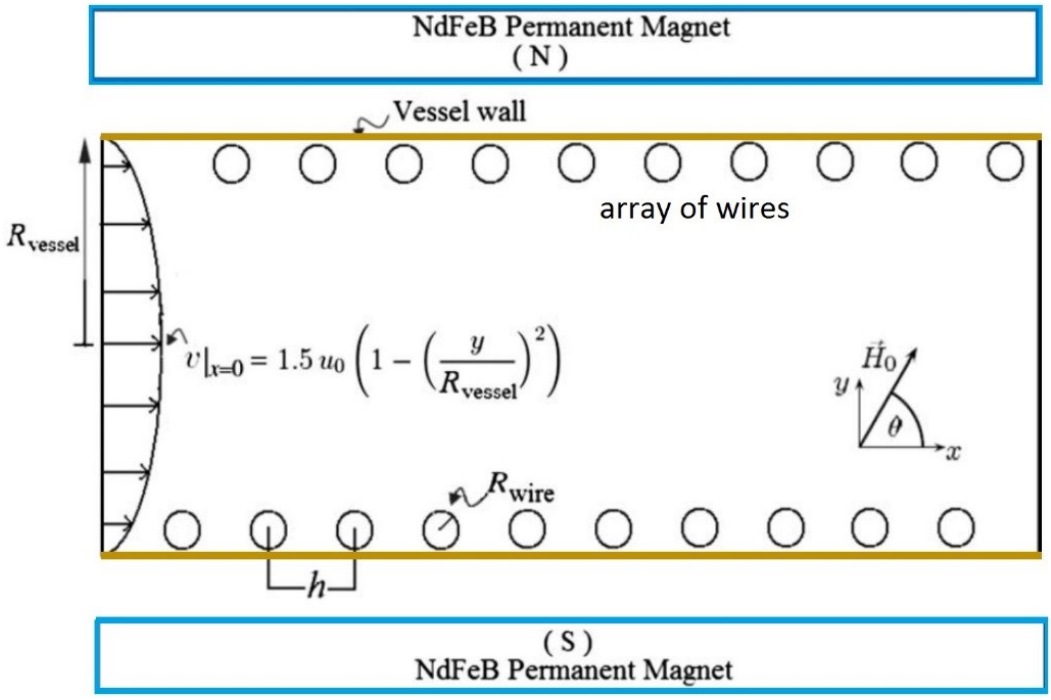

Figure 32. 2D design of the HGMS system for computational study of capture of magnetic particles by stent by Cregg et. al. [107].

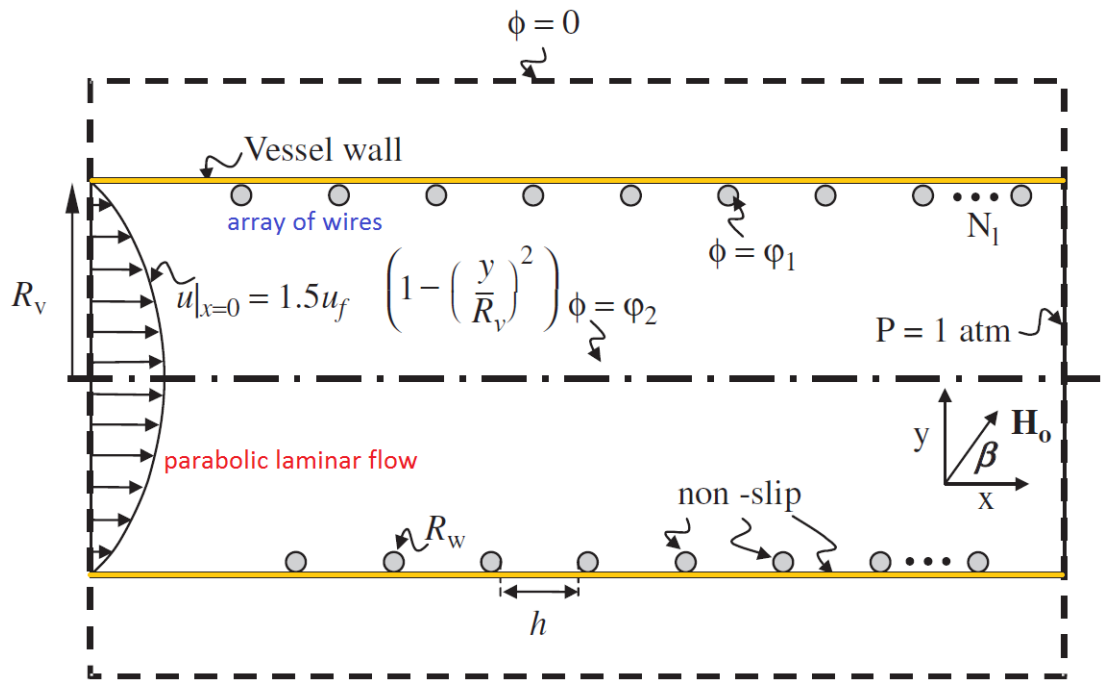

Figure 33. 2D design of the HGMS system for computational study of capture of magnetic particles by stent by Aviles et. al. [92].

- The capture efficiency of magnetic wires is very small (< 10%) for average flow velocities above 10 cm/sec.
- In experimental results, there is minimal increase (≈ 10%) in capture efficiency of magnetic wires with increase in the diameter of magnetic wires (from 50 μm diameter to 200 μm diameter).
- **In computational results, the first wire attracted essentially all of the magnetic particles that could be attracted. Subsequent wires hardly attracted any more magnetic particles.**
- In computational results, there is minimal increase (< 5%) in capture of magnetic particles with increase in the number of magnetic wires (10 to 18).

- Experimentally many wires showed capture, this was attributed to the fact that not all wires lay completely against the inner wall of the channel like they were supposed to, some of them penetrated more into the flow field than others. The distribution of capture was uneven.

It is important to note that none of these studies so far have focused on studying the kinematics of capture of magnetic particles by the array of magnetic wires. These studies primarily show the small capture efficiency of magnetic wires and minuscule increase in capture efficiency with the increase in the number of wires. While Aviles et. al. showed that it is the first wire that captures all the particles, they did not present data on or discuss what happens to the particles that were not captured by the first wire. It is important to know this information because it is the end position of the particles that were not captured that determines if it is the attraction or the repulsion phenomenon that dominates the movement of magnetic particles in such systems.

2.7.2. Possible Trajectories of a Magnetic Particle in the Fluid Channel

Figure 34 illustrates the three possible outcomes for the trajectory of a magnetic particle in a HGMS system where two magnetic wires are aligned perpendicular to the direction of flow. Trajectory 1 shows that the particle is captured by the first wire. Trajectory 2 shows that the particle was not captured and moved closer towards the wall of the channel suggesting that the magnetic particle was attracted towards the wires. Trajectory 3 shows that the particle was not captured and moved away from the wall of the channel suggesting that the magnetic particle was repelled by the wires.

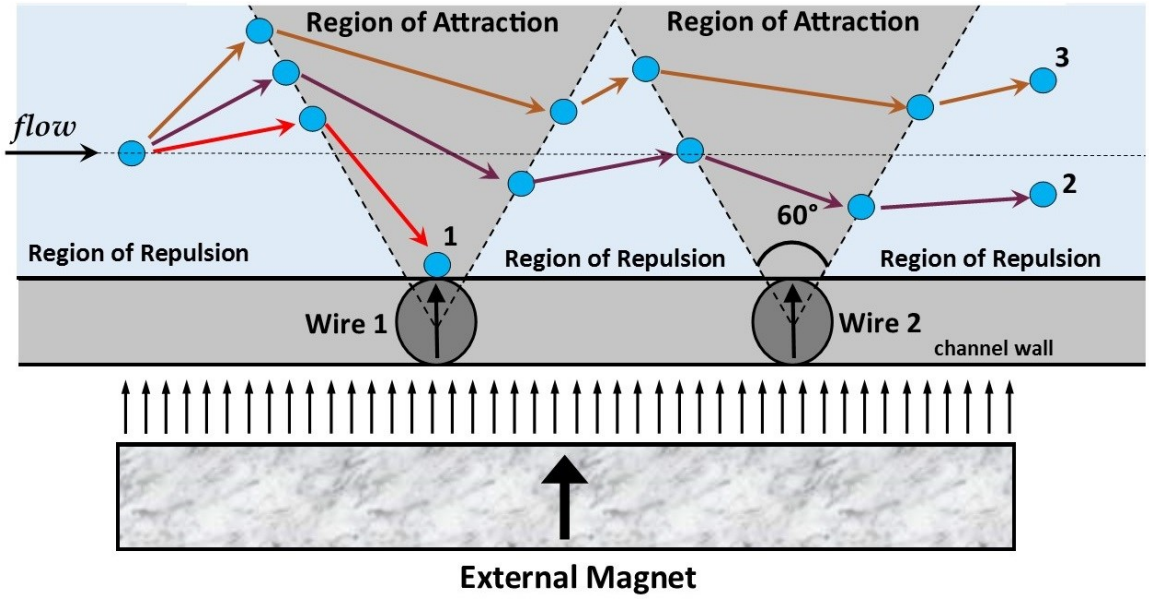

Figure 34. Possible trajectories of a magnetic particle in presence of an array of wires aligned perpendicular to the flow in a HGMS system.

2.7.3. Specific Geometric Configuration for Fluid Flow and Magnetic Field Gradient Sources

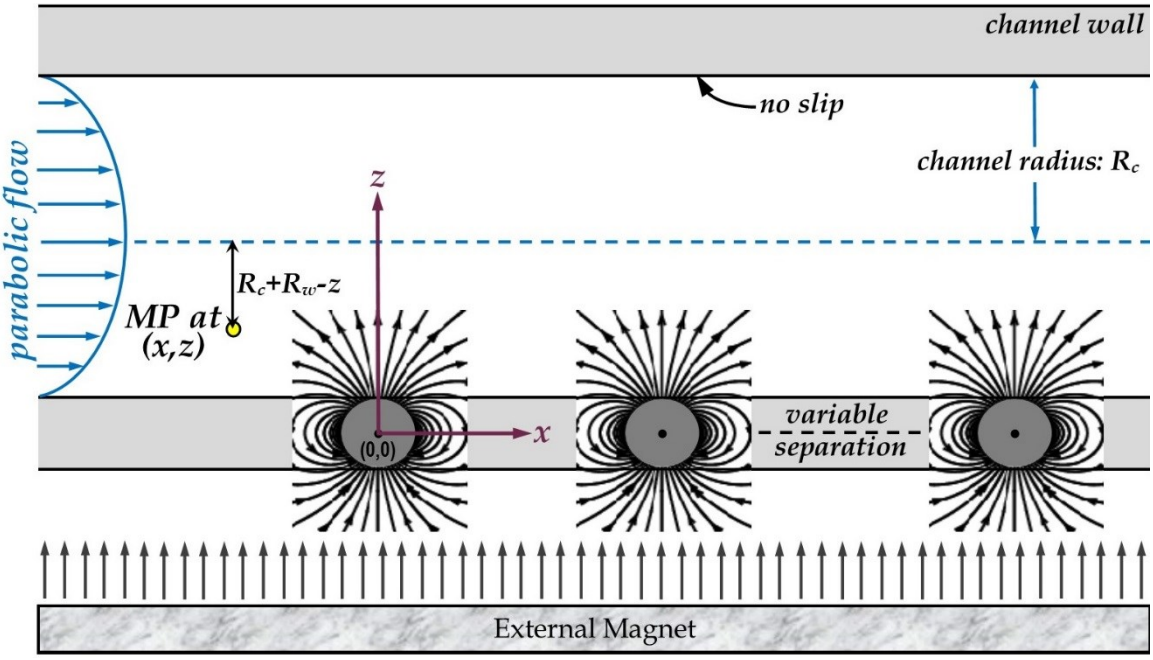

Figure 35. Repulsion based high gradient magnetic separation design.

2.7.4. Specific Expressions for Magnetic Forces Used in the Mathematical Model

The derivations for the expressions of normal and axial components of magnetic force experienced by a spherical magnetic particle that has been magnetized to saturation in a HGMS system can be found in the appendices of this dissertation. These expressions are missing from the available texts and literature.

The magnitude of the normal component of the magnetic force experienced by a magnetic particle is given by:

$$F_{mz}(x,z).\hat{z} = |\vec{m}| \frac{\left[\frac{-2z(-3B_0x^2+B_0z^2+k)}{(x^2+z^2)^3}\right]}{\sqrt{\left\{\frac{2xz}{(x^2+z^2)^2}\right\}^2+\left\{\frac{z^2-x^2}{(x^2+z^2)^2}+\frac{B_0}{k}\right\}^2}} \quad (2.47)$$

Similarly, the magnitude of the axial component of the magnetic force experienced by a magnetic particle is given by:

$$F_{mx}(x,z).\hat{x} = |\vec{m}| \frac{\left[\frac{-2x(-x^2B_0+3z^2B_0+k)}{(x^2+z^2)^3}\right]}{\sqrt{\left\{\frac{2xz}{(x^2+z^2)^2}\right\}^2+\left\{\frac{z^2-x^2}{(x^2+z^2)^2}+\frac{B_0}{k}\right\}^2}} \quad (2.48)$$

Where, $|\vec{m}|$ is the magnitude of the magnetic moment of the particles and B_0 is the strength of the external magnetizing field.

2.7.5. Equation for the Trajectory of the Magnetic Particle in the Fluid Channel

The trajectory of the magnetic particle is determined by the solution of the following first order ordinary differential equation which is an initial value problem. The initial value represents the perpendicular starting position of the magnetic particle along the width of the channel.

$$\frac{dz}{dx} = \frac{\sum F_{mag}.\hat{\boldsymbol{z}}}{F_{drag}.\hat{\boldsymbol{x}}+\sum F_{mag}.\hat{\boldsymbol{x}}} \quad (2.49)$$

This is a non-separable, non-linear equation. Numerical methods are used to solve this equation.

2.7.6. MATLAB Simulated Trajectory of the Magnetic Particle in the Fluid Channel

The trajectory of the magnetic particle in presence of an array of magnetic wires that are aligned and magnetized perpendicular to the flow is shown in Figure 36. The diameter of the particle is 1 μm, and the diameter of the wires is 127 μm.

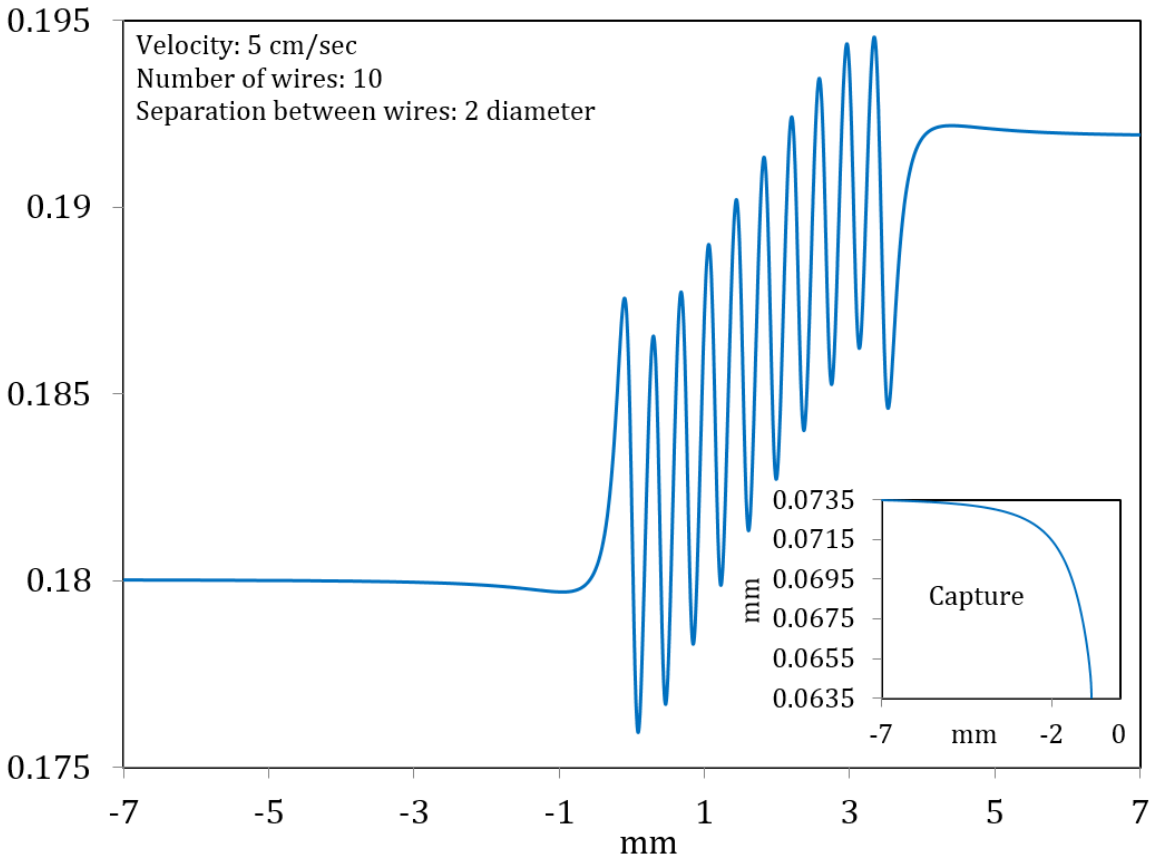

Figure 36. Repulsion of magnetic particle by an array of magnetic wires that are aligned and magnetized perpendicular to the flow. Inset shows capture by the first wire for a different starting position of the magnetic particle in the channel.

An example application of magnetic separation is described in chapter 4 of this dissertation in regards to magnetic stent assisted drug targeting systems.

3. Example Application I: Magnetic Diagnosis of Malaria

This chapter presents a repulsion based high gradient magnetic separation design that utilizes magnetic properties of hemozoin present in malaria-infected red blood cells (mRBCs) in order to separate and concentrate them inside a microfluidic channel for easier examination under the microscope. The design consists of a rectangular microfluidic channel with multiple magnetic wires strategically placed on top of and underneath it along the length of the channel. The strong magnetic field gradients produced by the wires exert sufficient magnetic forces on the mRBCs in order to separate and concentrate them in a specific region in the center of the channel. The trajectories of mRBCs inside the channel are determined using first-order stiff ordinary differential equations (ODE) that are solved numerically using the multistep ODE solver available from MATLAB. The mRBC trajectories reveal that it is possible to separate and concentrate the mRBCs in less than 5 minutes, including cases of low parasitemia (1-10 parasites/μL of blood). These results suggest that it is possible to develop an inexpensive and easy to use lab-on-a-chip device for separating and concentating the mRBCs for diagnostic purposes.

3.1. Malaria as a global problem

Malaria which is transmitted by the bites of infected mosquitoes is a global concern. According to the World Health Organization (WHO) an estimated 1.2 billion people are at high risk of contracting malaria infection. Around 198 million cases of malaria occurred globally in 2013 and the disease led to 584000 deaths (uncertainty range 367000 – 755000). The burden is heaviest on the African countries, where an estimated

90% of all malaria deaths occur, and in children aged under 5 years, who account for 78% of all deaths [114].

3.2. Review of Current Methods of Malaria Diagnosis

Microscopic examination of Romanowsky stained thick blood films and thin blood films continues to be the gold standard for the diagnosis of malaria. In this procedure blood sample is obtained by pricking a finger or earlobe and two drops of blood are placed on a glass slide to prepare the thick film and the thin film smears [115-117]. Blood samples collected in EDTA anticoagulant-coated tubes are also acceptable if used shortly after being drawn in order to prevent alteration in the morphology of the blood cells and the parasites [115, 117]. The probability of detecting malarial infection depends on the density of parasites and the volume of blood examined. Thin smears allow one to identify the parasite species whereas the thick smears are used to quantify parasitemia (number of parasites/μL of blood) in cases of low parasitemia [115, 117, 118].

In order to quantify parasitemia, the microscopist has to manually count the number of parasites/blood-cells in a given number of microscope fields. This entire process requires an ability to differentiate between non-parasitic stained components/bodies (e.g. red blood cells, white blood cells, platelets, and artefacts) and the malarial parasites using visual information [115, 117, 118]. For efficient examination of the films, it is important to continuously focus and refocus the microscope when moving from one field of view to another [118]. The standard basis of examination of a thick film is usually 100-200 microscope fields [115, 117], it is recommended that 100-400 fields be examined before declaring a slide negative [119, 120]. The infected-cells are randomly distributed in the

smear, this makes the microscopic examination of blood films laborious and time-consuming, especially in cases of low parasitemia where a large number of fields have to examined [116, 121].

Although, some studies [122, 123] have demonstrated the ability of polymerase chain reaction (PCR) based diagnostic techniques to detect 1-10 parasites/μL of blood, their use remains limited in resource deficient settings of poor countries due to requirements of sophisticated technology and expertise [124-126]. In addition, the volume of blood examined during microscopic examination, if 100 high-powered fields are screened, is 0.1-0.25 μL, which is much lower than 5-100 μL of blood that is required by most protocols for PCR based detection [115, 121, 127]. Thin film smears usually require less than 1 μL of blood and the thick film smears usually require 3-5 μL of blood [115]. This is important because drawing larger amounts of blood can be problematic when dealing with children [128]. Also, the choice between microscopy and rapid diagnostic tests is not a very simple one because the performance of both diagnostic techniques in operational conditions varies depending on transmission intensity, prevalence of infections, and parasite density [129-131]. Nevertheless, microscopic diagnosis of malaria continues to be the most widely used diagnostic technique for malaria all over the world because of its simplicity, low cost, its ability to identify the presence of parasites, and assess parasite density [116, 132].

3.3. Quality of Blood Smear Based Malaria Diagnosis

The quality of malaria diagnosis through microscopy is a function of multiple factors, including training and skills maintenance, slide preparation techniques, conditions of the microscope etc. Even among local laboratories with similar equipment

and training, diagnostic abilities vary significantly [133, 134]. The expected sensitivity that can be achieved by an average microscopist for the examination of the thick blood film is about 50-100 parasites/μL of blood [135, 136]. Microscopy diagnostic errors are not uncommon for low parasitemias (10-100 parasites/μL of blood) [131, 137, 138]. It is extremely difficult to achieve high detection accuracy at very low parasitemias (1-10 parasites/μL of blood) and in cases of asymptomatic malaria [127, 137]. Asymptomatic malaria-infection with low parasitemia (1-10 parasites/μL of blood) is a major obstacle in controlling and eliminating malaria in endemic regions [127, 139]. Accurate microscopic diagnosis is a skill that is still learned with extended training and experience, whether in countries where malaria is prevalent or in countries where malaria is imported [132, 140].

3.4. Life Cycle of Malaria Parasite and Changes in its Magnetic Properties

The life-cycle of Plasmodium parasites follow one of the two pathways: i) Asexual reproduction for propagation within the human host or, ii) Development of sexual reproductive blood stages (gametocytes) which can infect the mosquito vector when taken up with a blood meal. While asexual reproduction causes the clinical symptoms associated with malaria, sexual reproduction is responsible for inter-host spread of the parasite [127, 141]. It has been reported that gametocyte densities of 1-10 parasites/μL of blood can result in inter-host spread of the parasite [142]. With respect to the first pathway it is well known that after infection, within the human host, the malaria-parasite catabolizes up to 80% of cellular hemoglobin and liberates haem which is later converted to hemozoin [141, 143]. The iron (Fe^{3+}) in hemozoin has a stronger paramagnetic effect than the iron (Fe^{2+}) in hemoglobin; mature malaria-infected red blood cells (mRBCs)

therefore usually behave as paramagnetic particles in a magnetic field [144, 145]. Specifically, it is the late-stage schizonts ($\Delta\chi \approx 1.8\times10^{-6}$ SI units) and gametocytes that are known to behave as paramagnetic particles [10, 144, 145]. The first symptoms and signs of malaria are associated with the rupture of erythrocytic-stage schizonts [141].

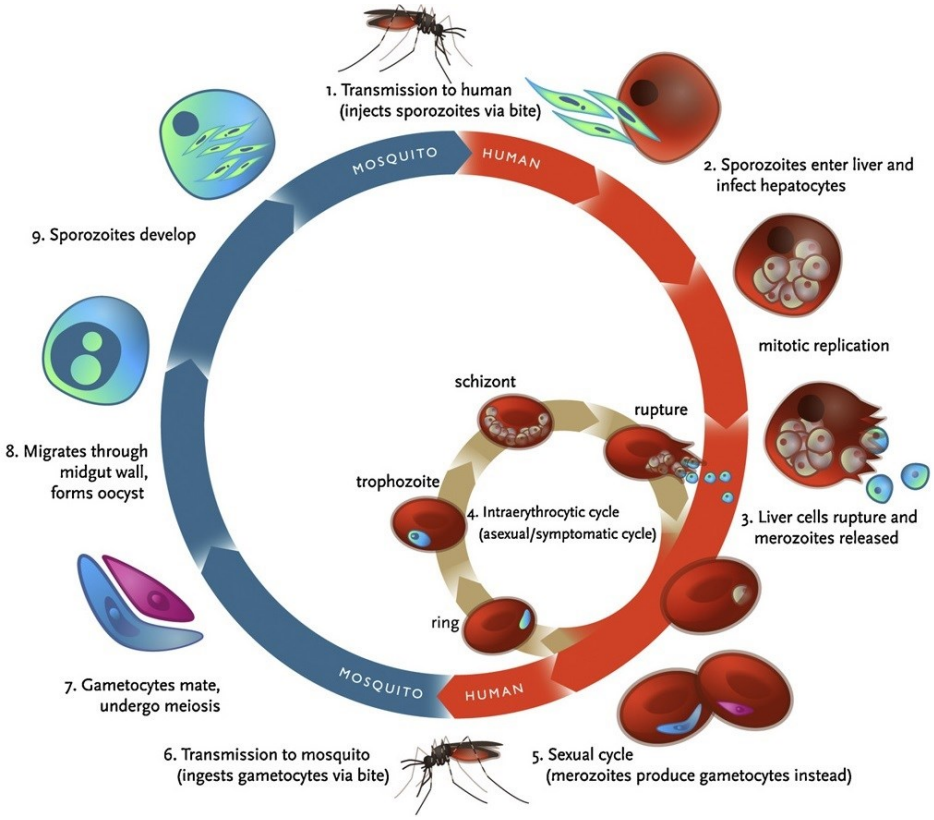

Figure 37. Life cycle of malaria parasite in the mosquito and the human host [146].

3.5. Review of Magnetic Diagnosis of Malaria

In an attempt to improve the microscopic diagnosis of malaria, some researchers have utilized magnetic properties of mRBCs in order to separate/concentrate them for easier examination under the microscope [10, 11]. Concentrating the mRBCs in smaller number of microscope fields can improve counting of mRBCs and estimation of parasitemia, in cases of low parasitemia this can improve diagnosis while making the

process less laborious and time consuming. Karl et al. in their magnetic deposition microscopy method showed good improvement in concentration of gametocytes, however, they had limited success in concentrating ring stage parasites [10]. Nam et al. through their high gradient magnetic separation (HGMS) based design were able to separate ring stage parasites better than other researchers that used conventional magnetic separation systems [11]. HGMS based designs produce higher magnetic field gradients than conventional magnetic separation systems, and this could be part of the reason that Nam et al. were able to separate ring stage parasites better than other researchers. Even though the design by Nam et al. separates the parasites, it does not concentrate them on a slide for easier examination under the microscope. Further steps would be needed to transfer the separated parasites on to a microscope glass slide and to assess the improvement in microscopic examination. In addition, their design requires external sheath flows, which makes it more complicated and expensive. For implementation in poorer parts of the world, it is important that the design should be inexpensive, and simple and easier to operate as there could be a shortage of laboratory personnel and equipment, a lack of effective quality assurance programs, and a lack of interest in training [140, 147, 148].

Even though these studies [10, 11] show an improvement in separation/concentration of malaria-infected cells, so far, improvement in microscopic diagnosis of low-parasitemia malaria and asymptomatic malaria has not been studied. It is in these cases of low-parasitemia and asymptomatic malaria where improvement in diagnosis is most needed. In this paper, we introduce a new design for a microfluidic system to separate and concentrate mRBCs using the magnetic properties of accumulated hemozoin in the

mRBCs. The concentrated mRBCs can then be fixed and stained and observed under the microscope to estimate parasitemia. We believe that this novel design will significantly improve the diagnosis of low-parasitemia and asymptomatic malaria.

3.6. Magnetic Repulsion Based Malaria Diagnosis

3.6.1. Specific Geometric Configuration for Fluid Flow and Magnetic Field Gradient Sources

The specific configuration consists of a 5 μm deep rectangular microfluidic channel where two magnetic wires are strategically placed in a V-shape on top of and underneath it along the length of the channel. Figure. 38 shows the 3D diagram of the design. An external homogenous magnetic field of magnitude 1T is applied perpendicular to the axis of the wires and along the thickness (along z-axis) of the channel in order to magnetize the wires and the mRBCs to saturation. The sample containing the mRBCs is allowed to flow through the channel through the sample inlet of the design. The magnetic wires are strategically placed to separate and concentrate the mRBCs which are present in flow in the region of concentration. It is important to note that the magnetic wires are placed on top of both the upper plate and the lower plate of the channel and are not obstructing the flow.

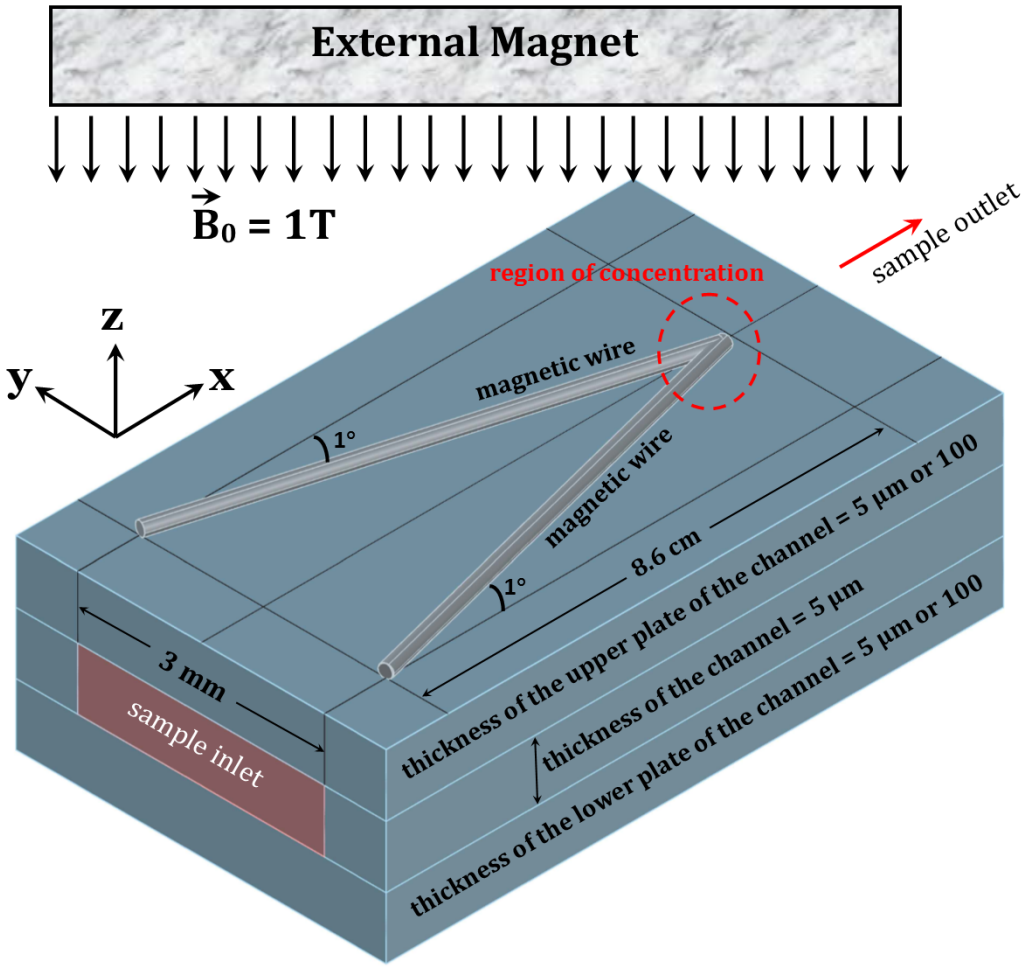

Figure 38. Three dimensional diagram of the repulsion based magnetic design for improving the diagnosis of malaria. The volume of the channel (8.6 cm × 3 mm × 5 µm) is 1.29 µL, and the wires are placed at an angle of 1° with respect to the x-axis.

Red blood cells have a hydrodynamic radius of 3.85 µm [149]. Based on the study by Shelby et al. [150], we expect the uninfected and the infected red blood cells to readily traverse through the 5 µm deep and 3 mm wide channel. The height of the channel (along z-axis) is fixed at 5 µm to limit the movement of the mRBCs to x-y plane. This essentially reduces the design to a 2D geometry [46].

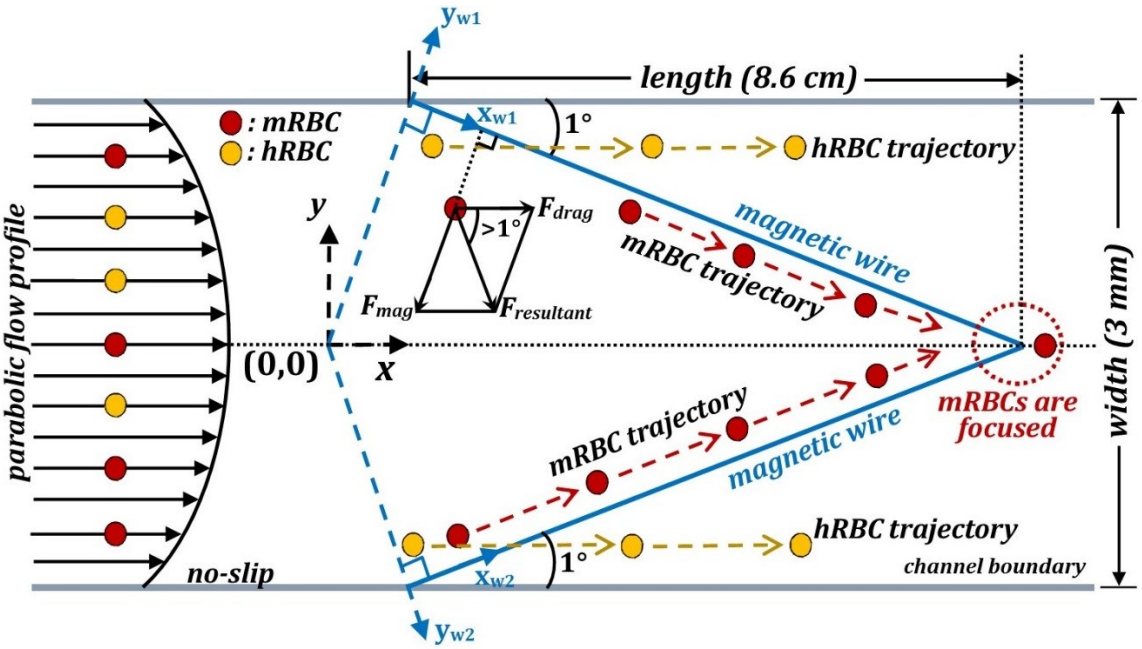

Figure 39. Top view of the repulsion based magnetic focusing design to improve the diagnosis of malaria. The mRBCs are focused towards the center of the channel, while the healthy rbcs continue to flow past the magnetic wires.

3.6.2. Illustration of the Magnetic Repulsion Principle used to Separate and Focus Malaria-Infected Red Blood Cells

The principle here is that the mRBCs will be constrained to move along the length of the wires in the x-y plane because the component of the magnetic force that is along the y-direction and perpendicular to the flow will repel the mRBCs away from the wires and cause their lateral movement in the x-y plane thereby focusing them towards the center of the channel where the wires meet (see Figure. 39). Designs based on a similar principle where high magnetic field gradients provide forces at an angle to the flow of paramagnetic micro/nano meter sized particles in an essentially 2D geometry in order to sort them have been used before by other researchers [46, 81, 151]. The aim of our design is to use the high magnetic field gradients (~ 10,000 T/m) produced by the strategically placed

magnetic wires in order to exert sufficiently strong magnetic forces on the mRBCs in order to separate and concentrate them in a small region inside the channel for easy viewing under the microscope.

3.6.3. Mathematical Model of mRBC Motion in Low Reynold's Number Fluid Flow

The model is developed to determine the trajectory of a single mRBC in order to investigate the possibility of focusing it to the center of the channel (where the wires meet) with the help of the strategically placed magnetic wires. Figure. 39 shows the coordinate system for the model. Several studies on the motion of red blood cells in fluid flow in HGMS systems have established that it is the viscous and the magnetic forces that are most dominant, and it is fairly reasonable to ignore other forces [151, 152]. By considering only the dominant fluidic and magnetic forces, the mRBC motion can be predicted using Newton's third law as [104, 151, 153]:

$$\vec{F}_m = -\vec{F}_d \tag{3.1}$$

where $\vec{F}_m$ and $\vec{F}_d$ are the magnetic and the drag forces, respectively. Flow in microfluidic devices is usually laminar; the Reynolds number, the ratio of inertial to viscous forces, is low, meaning inertial effects are usually considered negligible. Cells entrained in such flows are usually expected to follow fluidic streamlines unless deflected by an external force or restricted by an obstacle [154, 155]. Therefore, in this study, we model flow as a two-dimensional laminar (parabolic) flow of Newtonian fluid between parallel plates. The drag force on an mRBC can then be approximated by Stoke's law in the form [104, 151, 153]:

$$\vec{F}_d = 6\pi\eta r_m \vec{v}_f \tag{3.2}$$

where η is the blood viscosity, r_m is the radius of mRBC, and $\vec{v}_f$ is the fluid velocity. Red blood cells have a hydrodynamic radius of 3.85 μm and a volume of 88.4 μm^3 [145, 149]. For a parabolic laminar flow profile, the flow velocity can be approximated as [92]:

$$\vec{v}_f = 1.5\ \vec{v}_{avg}\left(1 - \left(\frac{2y}{w}\right)^2\right) \tag{3.3}$$

where $\vec{v}_{avg}$ is the average flow velocity in the channel, (x,y) is the position of the mRBC in the channel, and w is the width of the channel. The magnetic force on an mRBC, acted upon by a magnetic field gradient can be expressed as [46, 153]:

$$\vec{F}_m = \frac{\Delta\chi V}{\mu_0}(B.\nabla)B \tag{3.4}$$

where $\Delta\chi$ is the magnetic susceptibility of the mRBC, V is the volume of one mRBC, and μ_0 is the magnetic permeability of free space. In this study, we will be using the magnetic susceptibility of late-stage schizonts ($\Delta\chi \approx 1.8\times10^{-6}$ SI units) for plotting the trajectories of mRBC. We assume that in the presence of the powerful external magnetic field the magnetic moments of all the mRBCs and all the magnetic wires are aligned with the external magnetic field. Because of the relative difference between the size of the mRBC and the length of the magnetic wires, the wires are modeled as infinite cylinders [156]. The external magnetic field of a homogeneously magnetized cylinder of infinite length, magnetized by a constant magnetic field B_0, which is perpendicular to its axis in the z-direction, is given by [100, 102]:

$$\vec{B} = \frac{\mu_0 M}{2}(r_w)^2\left\{\frac{2y_w z}{\left(y_w^2+z^2\right)^2}.\widehat{y_w} + \frac{z^2-y_w^2}{\left(y_w^2+z^2\right)^2}.\hat{z}\right\} + B_0.\hat{z} \tag{3.5}$$

where M is the magnetization saturation of the wire, r_w is the radius of the wire, and y_w is the perpendicular distance from the axis of the wire. The mRBCs are assumed to be identical and non-interacting. It is also important to mention that the magnetic field in the x-y plane does not change because of the characteristics of blood. Taking the ratio of the y and the x velocity components of the mRBC and using Eqs. (1), (2), and (4), the trajectory of the mRBC in the x-y plane can be obtained as [95, 157]:

$$\frac{dy}{dx} = \frac{\sum F_{mag}\hat{y}}{F_{drag}\hat{x}+\sum F_{mag}\hat{x}} \tag{3.6}$$

3.6.4. Optimization of Geometric Configuration: Estimation of Wire Diameter

The diameter of the magnetic wires to be used in the design is determined based on the thickness of the upper plate and the lower plate of the channel. It is well known that the magnetic interactions exerted by a larger wire, although much weaker, are longer ranged, i.e., the magnetic particles can feel the magnetic effect of the wire at farther distances away from it [99]. In our design, we will consider two separate thicknesses (upper and lower plate thickness: 5 μm, and upper and lower plate thickness: 100 μm) for the upper and the lower plates of the channel and determine the corresponding wire diameters needed for the design. We will use Eq. (4) to determine the wire diameter as it gives the maximum magnetic force that can be experienced by one mRBC because of one magnetic wire placed on top of the upper plate or the lower plate of the channel.

In order to optimize the design, we will be using commonly available iron (Fe) and stainless steel grade 430 (SS 430) wires in this study, these wires have a higher average magnetization saturation than the commonly used nickel wires [99]. Iron (Fe) wires

(average magnetization saturation: 1735 kA/m [99]) are used to determine the magnetic force experienced by one mRBC. The mRBC's z-position is fixed at half the height of the channel at 2.5 μm. We expect that a larger diameter wire would be needed for the case where the thickness of the upper plate and the lower plate is 100 μm in comparison to the case where the thickness of the upper plate and the lower plate is 5 μm because the mRBC is farther away from the wire for the case where the thickness of the upper plate and the lower plate is 100 μm. It is clear from Figure 40 that a 50 μm diameter magnetic wire will be most suitable for the design when the thickness of the upper plate and the lower plate is equal to 5 μm, and a 0.5 mm diameter magnetic wire will be most suitable for the design when the thickness of the upper plate and the lower plate is equal to 100 μm (Figure 41). This is in agreement with the theory presented in [99] that the magnetic interactions exerted by a larger wire, although much weaker, are longer ranged. Our calculations also show that for the case where the thickness of the upper plate and the lower plate is 5 μm, the gradients produced by the 50 μm diameter wire within the 5 μm deep channel are of the order of 10,000 T/m, whereas for the case where the thickness of the upper plate and the lower plate is 100 μm, the gradients produced by the 0.5 mm diameter wire within the 5 μm deep channel are of the order of 1000 T/m.

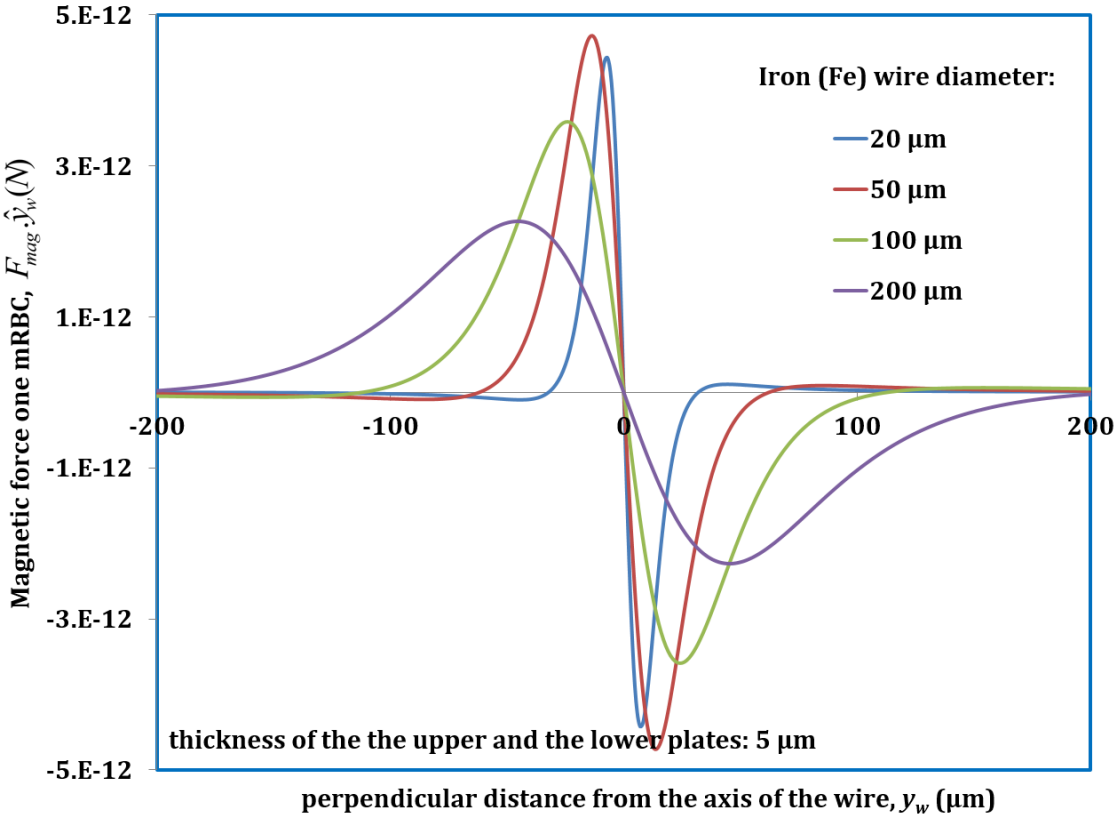

Figure 40. Magnetic force experienced by one mRBC for magnetic wires of different diameter. Thickness of the upper plate and the lower plate is 5 µm.

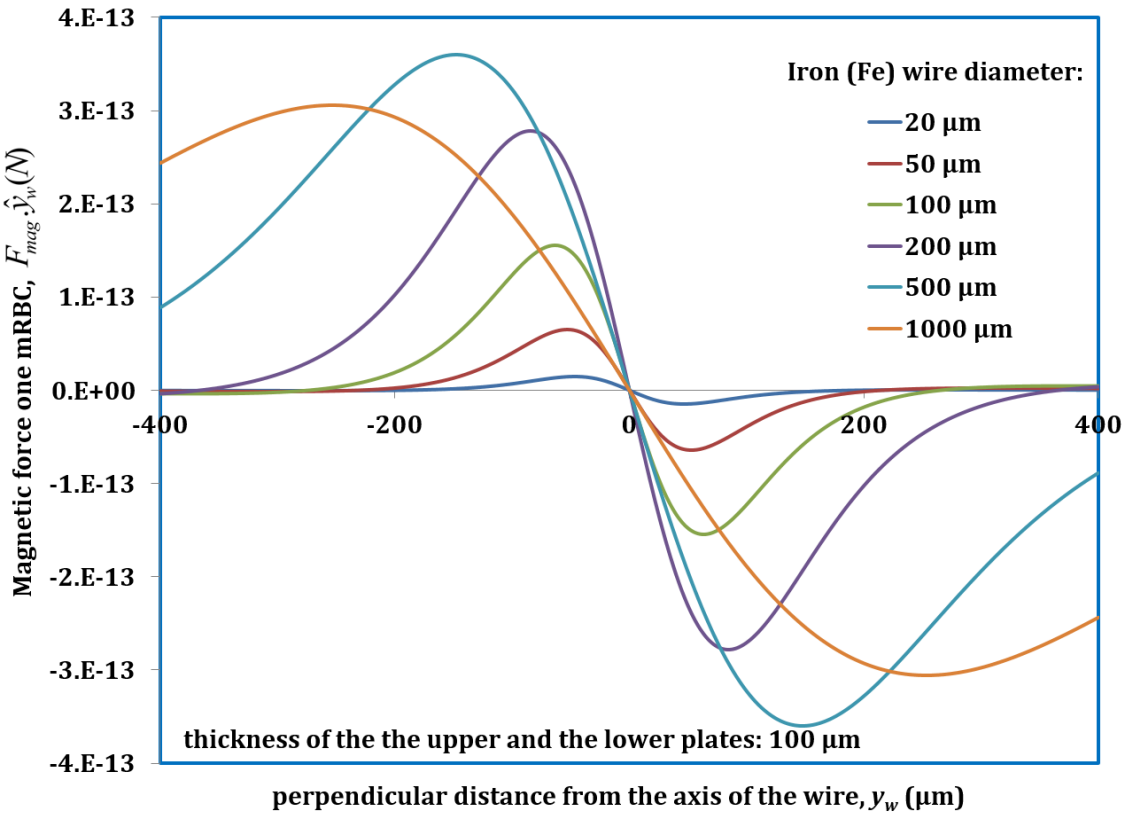

Figure 41. Magnetic force experienced by one mRBC for magnetic wires of different diameter. Thickness of the upper plate and the lower plate is 100 µm.

3.6.5. MATLAB Simulated Trajectory Properties of mRBC

The values of the magnetic and the drag forces experienced by the mRBC can be used to plot the mRBC's trajectory of slopes in the x-y plane. MATLAB's quiver function is used to plot Figure 42. The shape and positioning of the wire affects the field of trajectory slopes. Our goal is to determine the design parameters that result in a trajectory slope field which brings all particle trajectories regardless of their starting point to the

same final target area within a short amount of time and using less than a few microliters of blood.

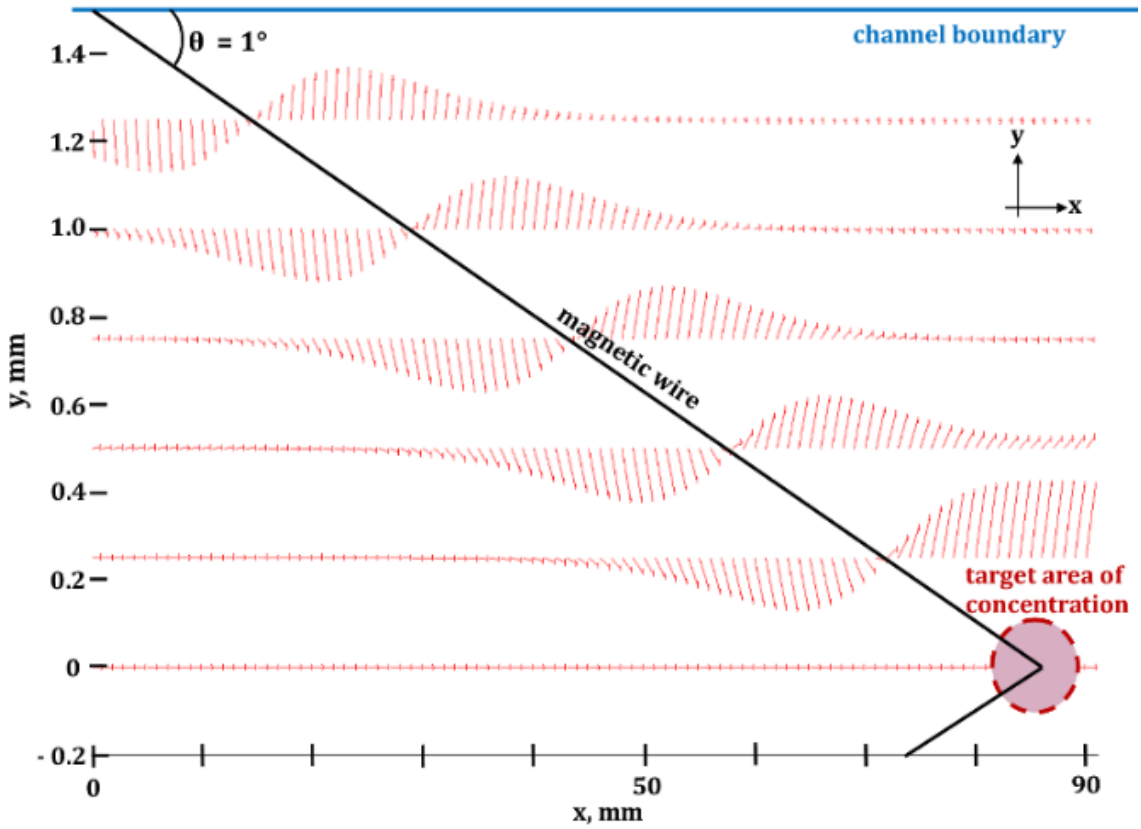

Figure 42. 2D field of trajectory slopes around the magnetic wire in the repulsion based magnetic focusing design.

3.6.6. MATLAB Simulated Trajectories of mRBCs

The trajectories of an mRBC inside the channel is determined by numerically solving Eq. (3.6) using the multistep ODE solver available from MATLAB (ODE15s). The number of wires in the design (two on upper plate and two on lower plate) and the angle they make with the x-axis are accounted for in the MATLAB code. In ODE15s, the initial

value is represented by the starting position of the mRBC along the width (along y-axis) of the channel. The z-coordinate of the mRBC is fixed at half the height of the channel at 2.5 μm. The step size in this numerical computation is 0.01 μm. With the help of this numerical analysis, we are able to determine the value of inlet average flow velocity in the channel for which an mRBC irrespective of its starting y-position in the channel will get focused towards the center of the channel where the wires meet.

Figures 43 and 44 show the simulated trajectory of one mRBC for different starting positions inside the 3 mm wide channel. These trajectories reveal that it is possible to separate and focus mRBCs at the center of the channel in less than 5 minutes. The values of inlet average flow velocity obtained numerically using Eq. (7) were in close agreement with the average flow velocity values obtained analytically using Eq. (8).

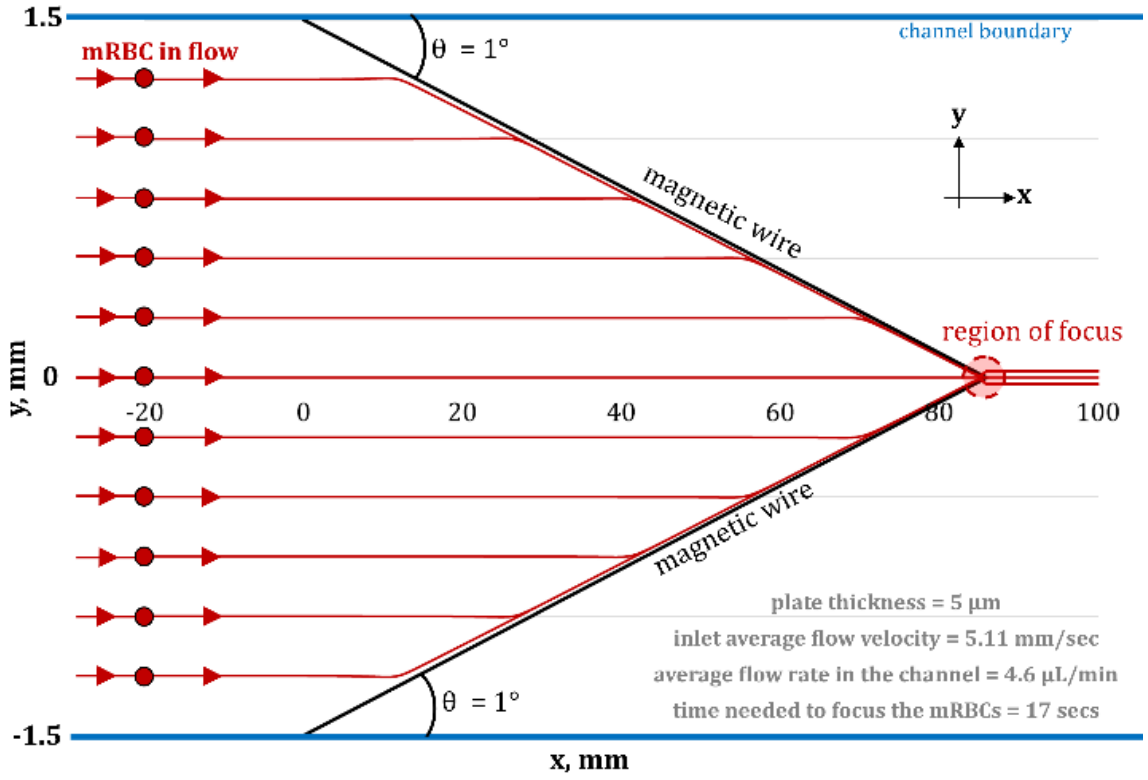

Figure 43. Trajectory of the mRBCs for various starting positions inside the channel. Average flow rate in the channel is 4.6 µL/min.

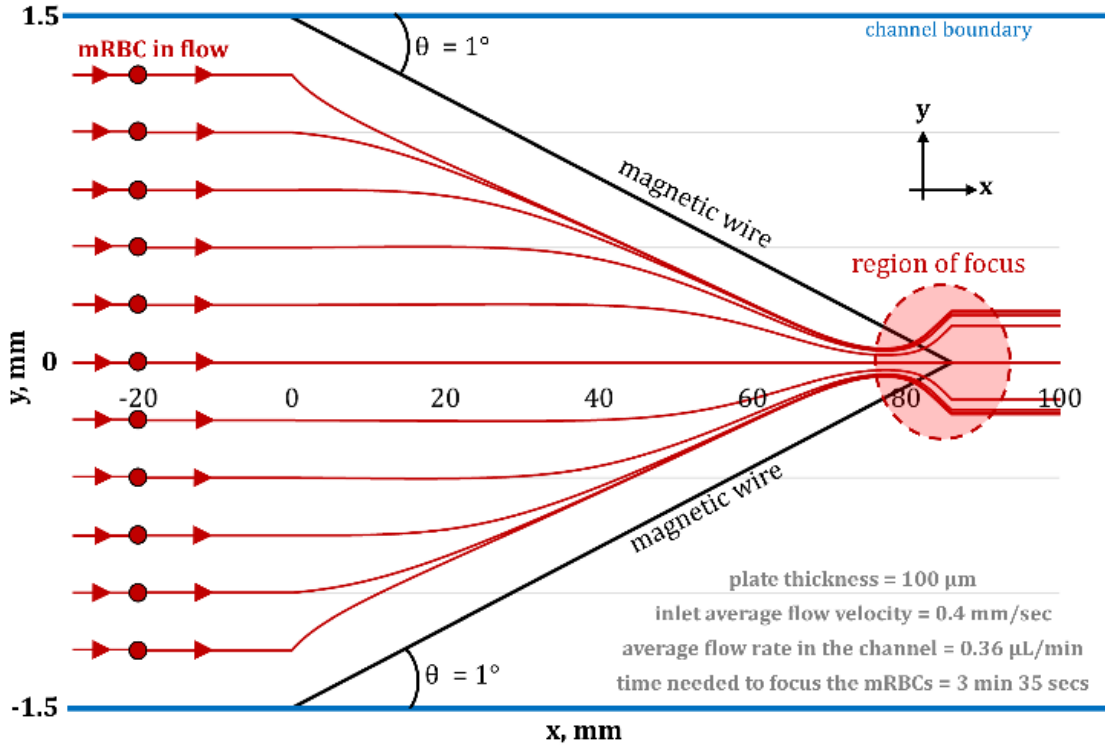

Figure 44. Trajectory of the mRBCs for various starting positions inside the channel. Average flow rate in the channel is 0.36 µL/min.

Unlike the mRBCs, the trajectories of healthy red blood cells owing to their very low magnetic susceptibility were found to be vastly unaffected by the magnetic wires. Figures 43 and 44 also reveal that even though the mRBC gets focused towards the center of the channel, it does not stay at the position where the wires meet and continues to flow past the point of intersection of wires. In order to concentrate the mRBCs in the region of focus, mechanical modifications can be made inside the channel in the region of focus where the wires meet. It has been found that the changes in mRBC rigidity as the parasite matures within can cause the mRBCs to block 2 µm wide channels, while the healthy cells can readily squeeze through the blockages formed by immobile schizonts in a 6 µm capillary [150]. Our design employs the reduced deformability of mRBCs to block a 2 µm

wide sub-channel in the region of focus after they have been brought there by magnetic means (Figure 45). Table 1. lists the complete set of design parameters needed to implement this design in practice.

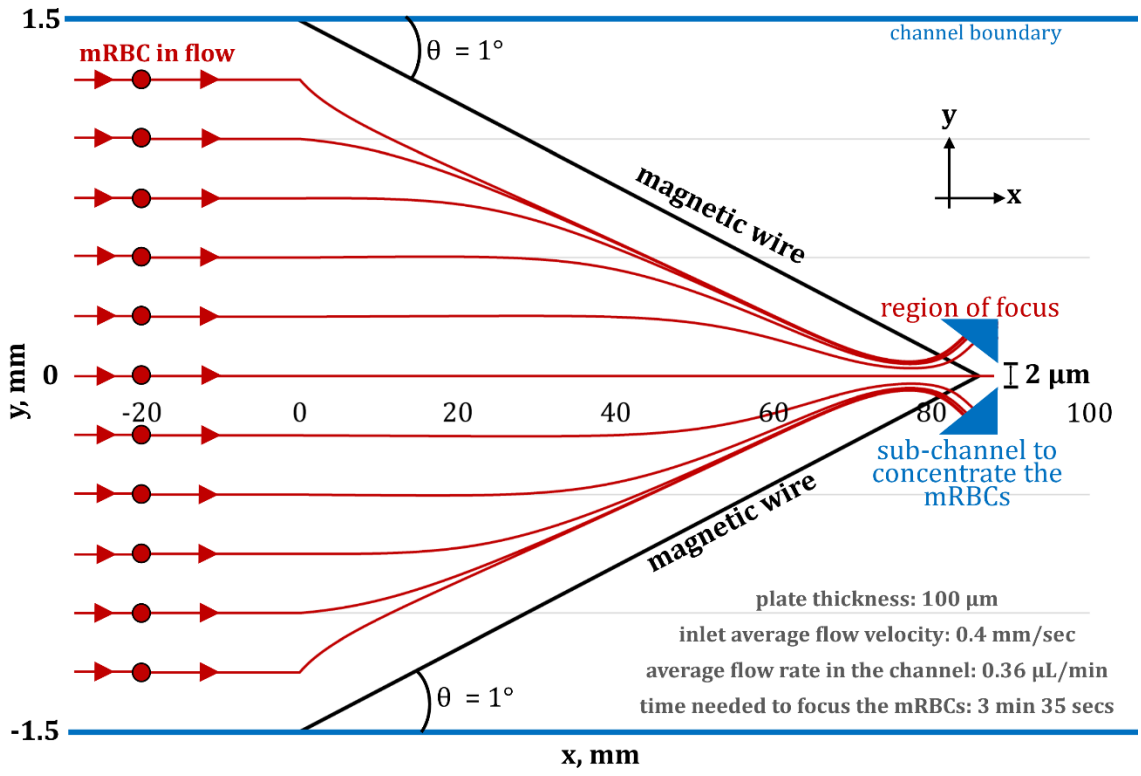

Figure 45. Mechanical modification [150] of the channel in the region of focus to concentrate the mRBCs.

3.6.7. Complete Set of Design Parameters Needed to Implement the Model in Practice

Table 3. Complete set of design parameters needed to implement the magnetic repulsion based focusing design in order to improve the diagnosis of malaria.

Design parameter	Fe Wire	SS 430 Wire	Fe Wire	SS 430 Wire
plate thickness (μm)	5	5	100	100
wire diameter (μm)	50	50	500	500
volume of Blood (μL)	1.29	1.29	1.29	1.29
average flow velocity (mm/sec)	5.11	3.49	0.4	0.31
average flow rate (μL/min)	4.6	3.14	0.36	0.28
Pressure ΔP (atm)	20.8	14.22	1.63	1.26
time needed to focus mRBCs	17 sec	25 sec	3 min 35 sec	4 min 37 sec

We have presented a simple, efficient, and cost-effective method for separating and concentrating malaria-infected red blood cells in flow using a HGMS design. This design uses inherent magnetic properties of mRBCs and is a label free method. Based on the results obtained, we believe that our design can significantly improve the diagnosis of low

parasitemia and asymptomatic malaria. As the design utilizes a simple microfluidic channel and inexpensive magnetic wires and magnet, we believe that the cost of diagnosis will be similar to the cost of diagnosis through conventional blood smear microscopy [158].

It is important to note that our design is able to concentrate the mRBCs in a very small area of less than 0.5 mm^2 (see Figures. 43 and 44), this area of concentration is significantly smaller than the area of concentration (~ 8 mm^2) that was achieved by Zimmerman et al. in their magnetic deposition microscopy method [158]. The typical area of examination of a conventional thick film is ~1 cm^2 [115]. According to the WHO the sensitivity of conventional microscopic diagnosis is directly related to the time available to examine the slides. The ability to detect infection by microscopy depends on the number of fields inspected and the experience of the technician reading the slide. It is widely accepted that no more than 30–40 slides can be effectively read per day. It is also recommended that the workload of each technician be monitored, considering fatigue or the pressure to return results can lead to a significant loss of efficiency and accuracy [132, 140, 159]. In addition, many microscopes in the field, through age, deterioration, and hard use, are nearing or are at the end of their useful working lives [159, 160]. In light of all of the above, we believe that the reduced area of inspection can significantly aid in better examination of the slides thereby improving the efficiency of microscopists.

4. Example Application II: Magnetic-Stent Assisted Drug Targeting

4.1. Introduction

Researchers have been studying the capture of drug-carrying magnetic particles by magnetic stent wires for over a decade now. The computational studies so far have revealed that the capture of drug carrying magnetic particles by magnetic stent wires is very small (≈ 10%) for practical blood flow velocities in arteries where the stent could potentially be placed. At the same time physical experiments performed in-vivo continue to show uneven capture of magnetic particles. The aim of this chapter is to help understand the kinematics of capture of drug-carrying magnetic particles which are present in flow by magnetic wires. The stent is modeled as an array of magnetic wires which are aligned perpendicular to Poiseuille flow in a 2D channel. The magnetic wires are magnetized both perpendicular to the flow and along the flow. It is revealed that the magnetic particles that are not captured by the first wire are repelled towards the center of the channel when compared to their starting position. This is an unexpected phenomenon indicating that the repulsive effect of the magnetic stent is stronger than the attractive effect, the simplicity of our model allowed us to expose this previously undiscovered effect.

4.1.1. Coronary Heart Disease

Coronary heart disease is characterized by a narrowing (stenosis) of the arteries that supply blood to the tissue of the heart. Continued restriction of blood flow manifests itself as angina and ultimately myocardial infarction (heart attack) for the patient. Coronary heart disease alone caused nearly 1 of every 7 deaths in the United States in 2013. In 2013, 370213 Americans died of coronary heart disease. Each year, an estimated ≈

660000 Americans have a new coronary attack (defined as first hospitalized myocardial infarction or coronary heart disease death) and ≈ 305000 have a recurrent attack. It is estimated that an additional 160000 silent myocardial infarctions occur each year. Approximately every 34 seconds, 1 American has a coronary event, and approximately every 1 minute 24 seconds, an American will die of one [161].

4.1.2. Vascular Stents and In-stent Restenosis

The use of vascular stents, a medical device designed to serve as a temporary or permanent internal scaffold, was initiated in 1986 by Sigwart *et al*. in order to maintain or increase the lumen of a blood vessel [162]. Stents are very small tubular structures that can be inserted via balloon catheter into the narrowed segment of the artery. When the balloon is inflated, the stent expands and is embedded into the artery vessel wall, which thus opens the previously narrowed segment of the artery. The balloon is then deflated and removed along with the catheter, and the stent is left behind to serve as a metal framework for the artery. In 1993, the FDA approved the balloon-expandable stent to treat acute or threatened closure [163, 164]. Today, stents are used in over 70% of the cases of coronary angioplasty. Stents are usually made of metal or polymer filamentous tube. The metals used to prepare these stents are selected for strength, elasticity, and malleability or shape memory. Stainless steel, tantalum, and nitinol alloys are among the most commonly used materials. Their diameter may vary from 2.5 to 3.5 mm, and their length is typically in the range of 15–18 mm [165-167].

In-stent restenosis (ISR) is defined as a decrease in the luminal diameter by greater than 50% in the stented area of the vessel. Similar to post-angioplasty restenosis, in-stent restenosis also occurs within 6 months of stenting [168, 169]. The incidence of ISR may

vary from 8% to as high as 80% at 6 months, according to both anatomic and clinical risk factors [170]. The problem of in-stent restenosis has been difficult to overcome and made PCI a less definitive treatment. The process of ISR peaks at about the third month and reaches a plateau between the third and sixth months after procedure. Although stented arteries have less chance of renarrowing than arteries opened with a balloon alone, in-stent restenosis can still occur in more than 1 in 5 patients after stent placement [171].

4.1.3. Treatment of Restenosis and Demand for Local Drug Delivery

Without exception, all interventions designed to treat coronary heart disease are complicated by restenosis. The development of recurrent restenotic disease affects not only vessels treated with angioplasty or stent, but also surgical bypasses or endarterectomy for coronary as well as peripheral arterial disease. Restenosis severely limits the overall efficacy of these interventions and can occur in up to 80% of patients. Despite many advances in the fields of vascular biology, pharmacology and bioengineering, restenosis remains a significant problem. The mechanism of restenosis after balloon angioplasty is a combination of recoil, arterial vessel remodelling, and neointimal hyperplasia. Stents inhibit both recoil and the vascular remodelling process, however, they are not immune to intimal hyperplasia which results in late lumen loss.

As stents alone cannot eliminate restenosis, systemic drugs are required to be administrated in conjunction. The majority of the drugs used and studied have been antiplatelets and antithrombogenic. However, systemic administration of a variety of agents has not had a significant impact on post-PCI restenosis rates in various clinical trials. The lack of effect of systemically administrated agents has been attributed to their potential toxicity leading to various side-effects and inadequate drug concentrations at

the site of stent insertion. On the other hand temporary local delivery of antiproliferative agents with the use of microperforated balloons has been found to cause vascular damage and has been associated with fast washout and a delayed effect of the drug.

These outcomes have led to the requirement and concept of local drug delivery where high doses of a therapeutic agent are administered directly to a treated artery or vein without engendering adverse systemic effects or vascular damage. Local drug delivery can result in drug concentrations in vascular tissues that are 400-1000 higher than that achieved following systemic administration of the same compound [172]. The concept of applying pharmacologic agents directly to vessel wall is an attractive strategy that is likely to be effective if several conditions can be met:

1) there is steady delivery of the drug over time

2) effective drug concentrations can be maintained,

3) there is absence of local or systemic toxicity and importantly

4) the mechanism of delivery does not insight vascular damage and restenosis.

Fortunately, restenosis lends itself to treatment by local drug delivery because it is often a focal process.

4.2. Magnetic Drug Targeting

4.2.1. Introduction

Magnetic drug targeting (MDT) is emerging as a promising technique for treatment of localized diseases. One of the biggest problems with non-targeted treatment of many diseases is that the drug spreads through the circulatory system, leading to low concentrations in the diseased tissue and side effects in healthy tissues. The aim of MDT is to concentrate drugs, attached to magnetic particles, in a specific part of the human

body by application of magnetic fields. By applying a magnetic field at the target region, the particles can be slowed down or even captured from the bloodstream. This MDT technique can significantly increase the specificity of certain medical treatments, lowering the required dose and reducing side-effects. MDT treatments start with the bonding of the drug to magnetic particles either chemically or by embedding magnetic particles in a drug carrier particle. The magnetic drug particles are then injected into the bloodstream at a convenient location, steered towards the disease site via externally-applied magnetic fields, and pushed into the capillary bed of the diseased tissue.

4.2.2. Magnetic stent assisted drug targeting

Magnetic stent assisted drug targeting (SADT) continues to draw considerable attention as a potential therapeutic aid for in-stent restenosis [173-175]. SADT has shown a lot of promise in delivering anti-proliferative drugs and native endothelial cells to the stent region by use of magnetic particles, as described in [173, 175]. In comparison to other drug targeting methodologies, magnetic targeting of therapeutic agents to specific sites in the body offers the advantage that it requires only a simple injection at the site of interest; this makes magnetic targeting a far less invasive procedure than other surgical methods for targeted drug delivery. The magnetic particles, once injected into the bloodstream can be guided to the targeted area with help of an external magnetic field. The common idea is to achieve the ability to deliver high effective dosages of the drug to specific sites in the human body while decreasing the amount of drug delivered to normal and healthy tissue.

Many researchers have examined the feasibility and performance of SADT systems [92, 93, 110, 112, 176, 177]. However, the kinematics of capture of magnetic particles (MPs) by stent wires is still poorly understood. This information is important for the

improvement of SADT systems. In this study, we incorporate a simplified 2D configuration of a SADT system in order to examine the kinematics of capture of MPs by a periodic array of wires in a large design parameter space that includes: variable number of wires, variable spacing between wires, and different orientations of external magnetizing field with respect to the flow and the stent wire. The advantage of using a 2D configuration is that it helps in the quick implementation of a simple magneto-hydrodynamic model in the formulation, and in our study, this also allowed us to expose a previously undiscovered and non-intuitive effect that the cumulative repulsive effect of the wires is stronger than the attractive effect.

4.3. Mathematical Model of Magnetic Particle Motion in Low Reynold's Number Flows

The model is used to study the capture of 1 μm diameter spherical MPs by a periodic array of magnetic wires which are aligned perpendicular to the flow in a rectangular 2D channel. The number of wires and the separation between the wires is varied in the study. Figure 46 shows the 2D configuration of the system. Figure 46 is not drawn to scale. Similar 2D configurations of SADT systems have been studied before by other researchers [92, 95, 108, 109]. However, in our configuration, the wires are embedded in the vessel walls and are not obstructing the flow. This is a more realistic scenario for blood vessel models [171, 178]. An external homogenous magnetic field is applied perpendicular to the axis of the wires and either perpendicular to or along the direction of flow in order to magnetize the MPs and wires to saturation. Prior studies related to SADT systems had limitedly considered the external magnetic field orientation to be perpendicular to the flow and wires. Therefore, one of our goals in this study is to examine the effects of

external field orientation [179]. Using external field along the flow, but still perpendicular to the wires can be viewed as the most extreme deviation from prior work. Results of other field orientations will likely fall between these two extremes and can be studied in later work.

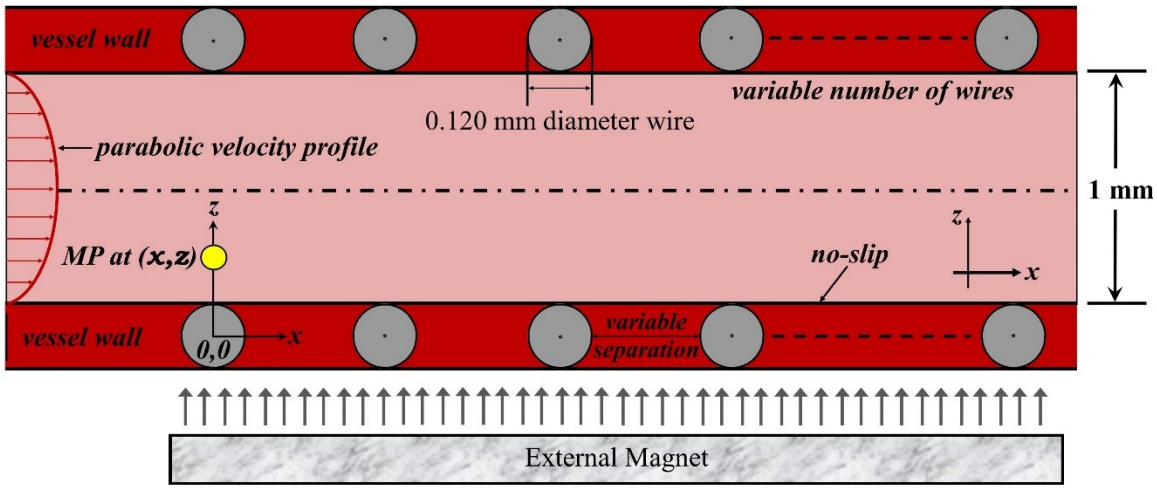

Figure 46. 2D schematic of the magnetic stent-assisted drug-targeting system.

Magnetic particle transport in blood vessel is dependent on several factors including magnetic force, viscous drag, and MP's interaction with cells in the blood [95, 180]. Several studies on motion of MPs in blood stream for magnetic drug targeting systems have established that effective fluid viscosity (η) can, to some extent, account for the particle blood-cell interactions, while the other forces are an order of magnitude smaller than the magnetic forces and can be neglected [177, 181, 182]. By considering only the dominant viscous and magnetic forces, the MP's motion can be predicted using Newton's law as [110, 180]:

$$m_p \frac{d\vec{v}_p}{dt} = \vec{F}_m + \vec{F}_d \tag{4.1}$$

where m_p is the mass of the MP, $\vec{v}_p$ is the velocity of the MP, and $\vec{F}_m$ and $\vec{F}_d$ are the magnetic and drag forces experienced by the particle, respectively. The inertia term $m_p \frac{d\vec{v}_p}{dt}$is very small and can be neglected [180]. So, the final force balance can be written as [95, 110, 157]:

$$\vec{F}_m = -\vec{F}_d \tag{4.2}$$

The flow in the channel is modeled as a two-dimensional laminar flow of Newtonian fluid between parallel plates. For conditions of low Reynolds number as applicable in SADT systems, the drag force on a suspended spherical particle is given by Stoke's law in the form [92, 95, 108]:

$$\vec{F}_d = 6\pi\eta r_p(\vec{v}_f - \vec{v}_p) \tag{4.3}$$

Where r_p is the radius of the MP, and $\vec{v}_f$ and $\vec{v}_p$ are the fluid and MP velocities respectively. Although, in reality the MPs may have a preferred position in the flow, the main goal of this study is to understand the kinematics of MP's magnetic capture, and to determine the effect of MP's initial positioning on its capture. Therefore, in this first order approximation, the effects of interactions that may influence MP's true positioning with respect to the vessel walls are neglected and the MPs are assumed to be uniformly distributed in the fluid [92]. For the same reason, we assume a low concentration limit of MPs in the fluid so that the MPs are non-interacting [183]. For a parabolic laminar flow profile, the fluid velocity can be approximated as:

$$\vec{v}_f = 1.5\,\vec{v}_{avg}\left(1 - \left(\frac{r_c + r_s - z}{r_c}\right)^2\right) \tag{4.4}$$

Where $\vec{v}_{avg}$ is the average fluid velocity in the channel, (x, z) is the position of the MP in the channel, r_c is half the width of the channel, and r_s is the radius of the wire. The magnetic force on a micrometer sized particle of magnetic moment m, acted upon by a magnetic field gradient ∇B, can be expressed as:

$$\vec{F}_m = (\vec{m}.\nabla)\vec{B} \tag{4.5}$$

In this study, we assume that the magnetic moments are all aligned with the external magnetic field, so above can be simplified as:

$$\vec{F}_m = |\vec{m}|\nabla\left|\vec{B}\right| = m\nabla B \tag{4.6}$$

The stent wires are modeled as infinite cylinders. The external magnetic field of a homogeneously magnetized cylinder of infinite length, magnetized by a constant magnetic field B_0, which is perpendicular to its axis in the z direction, is given by:

$$\vec{B} = \frac{\mu_0 M}{2}(r_s)^2\left\{\frac{2xz}{(x^2+z^2)^2}.\hat{x} + \frac{z^2-x^2}{(x^2+z^2)^2}.\hat{z}\right\} + \vec{B}_0.\hat{z} \tag{4.7}$$

Where μ_0 is the permeability of free space, M is the magnetization saturation of the wire, and B_0 is the strength of the external magnetizing field. The magnetization saturation of 127 μm diameter SS 430 wires used in this study is 1261 kA/m. Typical magnetic field values required to reach saturation magnetization in SADT systems are of the order of 0.4 T. The value of B_0 in this study is 1 T. The MP properties are listed in Table 5.

Table 4. Magnetic particle properties for the magnetic-stent assisted drug targeting system [92].

Particle diameter μm	Magnetite weight content %	Magnetite volume content %	Magnetite saturation magnetization kAm^{-1}	Magnetic moment of the particle Am^2
1	60	24.1	304.2	3.4×10^{-14}

It is also important to mention that the magnetic field in the x-z plane does not change because of the characteristics of fluid. The trajectory of the MP can be obtained as [95, 182]:

$$\frac{dz}{dx} = \frac{\vec{F}_m.\hat{z}}{\vec{F}_d.\hat{x}+\vec{F}_m.\hat{x}} \tag{4.8}$$

It is important to note that $\vec{F}_m$ represents the sum of magnetic forces due to all the wires present in the system. The number of wires is varied from 1 to 10 in this study. The separation between the wires is varied from 0.5×diameter to 4×diameter. A separation of 1× diameter means that one wire can be placed between the surfaces of two consecutive wires. The number of wires and the separation between the wires are accounted for in the MATLAB code. The trajectories of MPs are determined by numerically solving (4.8) using the multistep ODE solver available from MATLAB (ODE15s). The step size in the numerical computation is 0.01 μm. The starting position of the particle in x-direction is 10 mm away from the first wire. The theoretical capture efficiency is calculated using the starting position (distance from channel boundary, z_0 in Fig. 47) of the MP in the z-

direction, below which the MP will always be captured. The percentage capture efficiency can be expressed as [92]:

$$CE\% = 100\left(\frac{z_0 - r_s}{r_c}\right) \tag{4.9}$$

4.4. MATLAB Simulated Trajectories of Magnetic Particles in the Fluid Channel

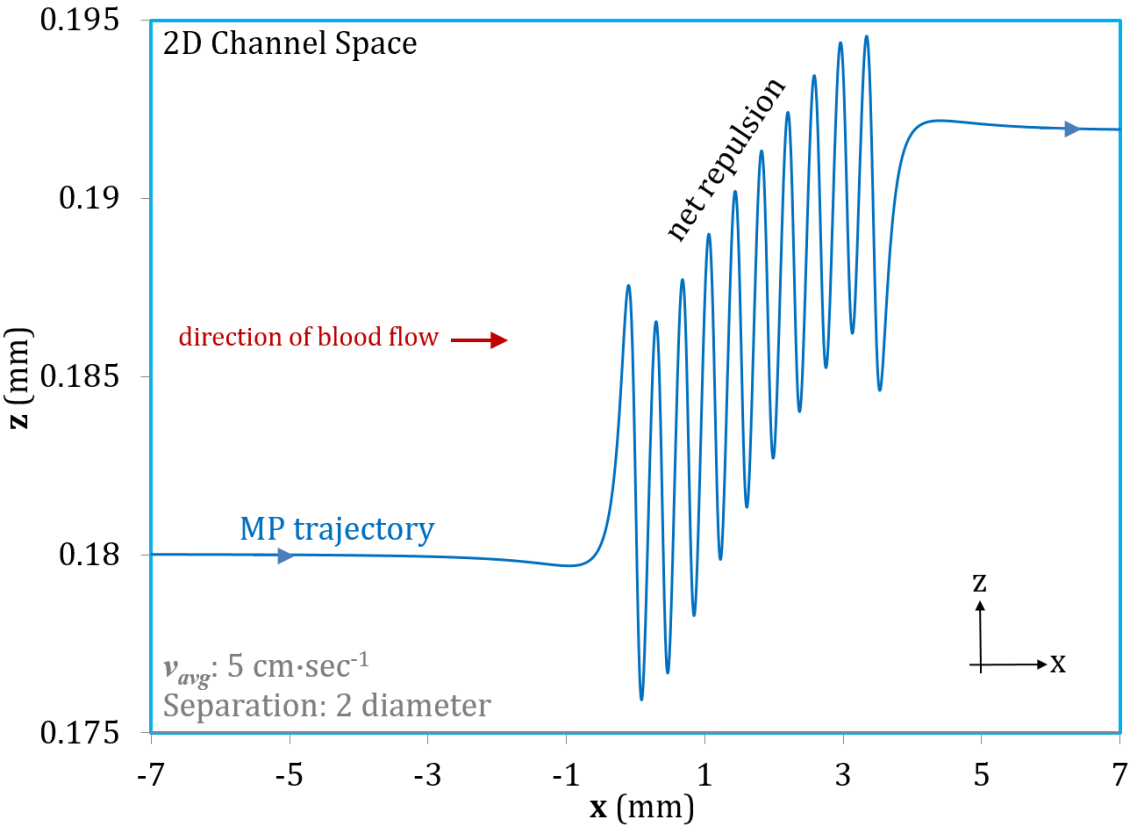

Figure 47. Trajectory of an uncaptured MP. The wires are magnetized perpendicular to the direction of flow.

Figures 47 and 48 show the trajectory of an uncaptured MP in the 2D-channel space of Figure 46. The first wire (not shown in Figures 47 and 48) is located at (0, 0).

Figures 47 and 48 show an oscillatory movement of the MP in the region above the wires. It is revealed that regardless of the orientation of external magnetic field, the MPs that are not captured are always repelled to the center of the channel when compared to their starting position. This new and unexpected result suggests that the cumulative repulsive effect of the wires is stronger than the attractive effect. The simplicity of our model allowed us to expose this previously undiscovered effect.

The external magnetizing field magnetizes the wires and the MPs to saturation with their dipoles aligned in the direction of the external field. The force between an MP and a wire then depends on the relative position of the MP with respect to the wire as shown in Figure 49. If the MP is situated outside the region of attraction of the wire, then it is repelled away from the wire; if the MP is situated within the region of attraction of the wire, then it is attracted towards the wire. This phenomenon is repeated consecutively as the MP travels with the flow above each of the wires, giving rise to an oscillatory movement of the MP in the channel.

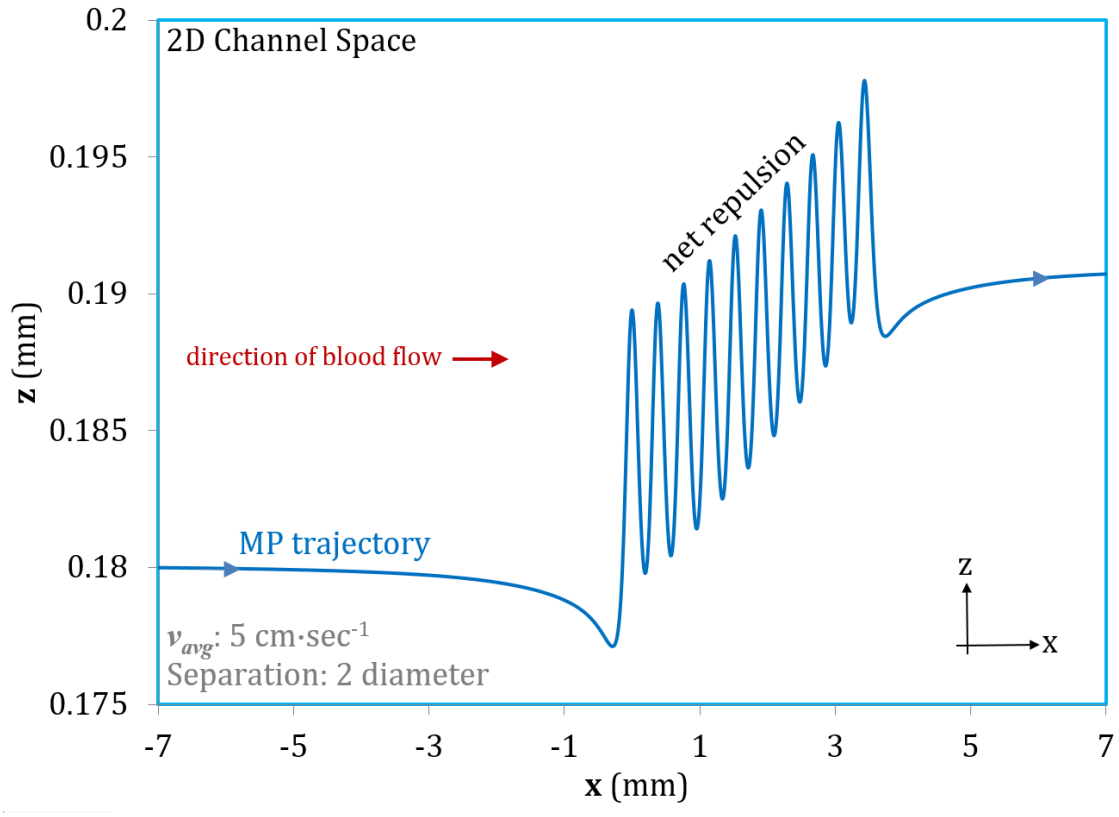

Figure 48. Trajectory of an uncaptured MP. Wires are magnetized along the direction of flow.

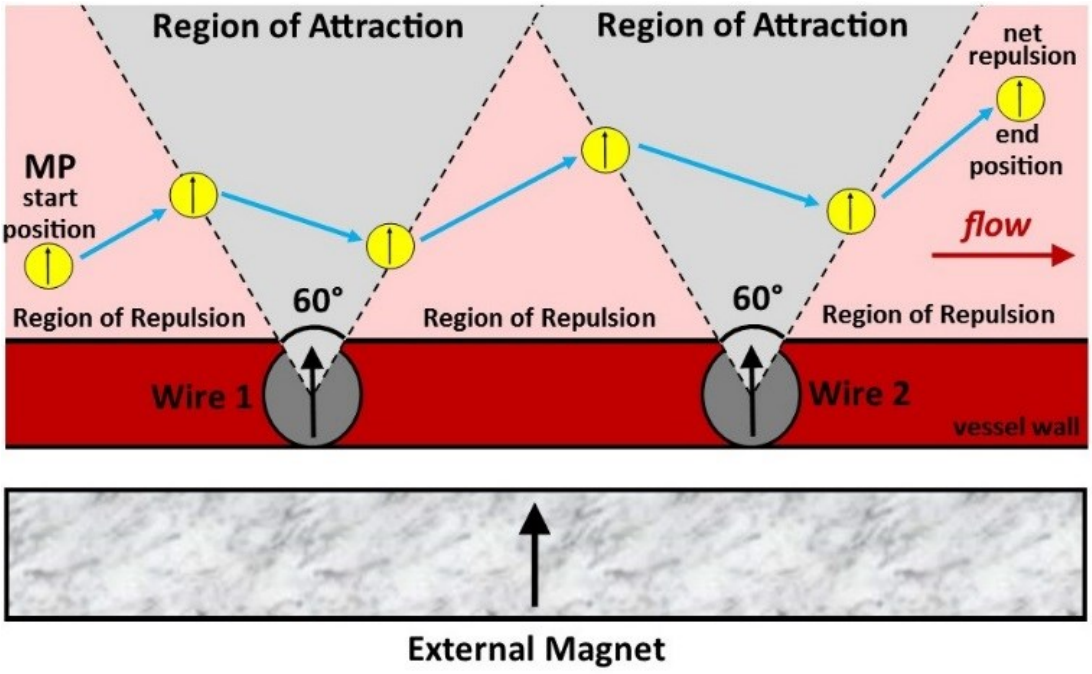

Figure 49. Trajectory of an uncaptured magnetic particle showing the oscillatory movement of the particle in presence of the magnetic wires.

It is important to note that the trajectory of the MP is sensitive to the component of magnetic force that is along the direction of flow. The repulsive effect is very weak when the component of magnetic force along the direction of flow is not included in the model (not shown in the figures). Apparently, the component of magnetic force along the direction of flow slows down the MP in the region of repulsion and speeds it up in the region of attraction.

It is also important to note that regardless of the orientation of external magnetic field, it is always the first wire that captures the MP. This behavior is in agreement with the previously reported results in [92]. The MPs that are not captured by the first wire are repelled towards the center of the channel. This suggests that the captured MPs will be

concentrated at the beginning of the stent which will result in a non-uniform distribution of MPs across the stent.

Figure 50 shows that regardless of the orientation of external magnetic field, as the average fluid flow velocity increases the capture efficiency of the wires decreases. These results are intuitive because as the value of average fluid flow velocity increases there is an increase in the value of drag force while the magnetic forces remain fixed. The CE values (when wires are magnetized perpendicular to the direction of flow) obtained by our model are in close agreement with the values achieved in [92], this validates our model. From a drug-targeting perspective these results are not very promising as the CE values are below 5% for inlet average velocities over 2 cm/sec. However, it is important to note that the CE values are almost twice when the wires are magnetized along the direction of flow in comparison to perpendicular to the direction of flow for same conditions.

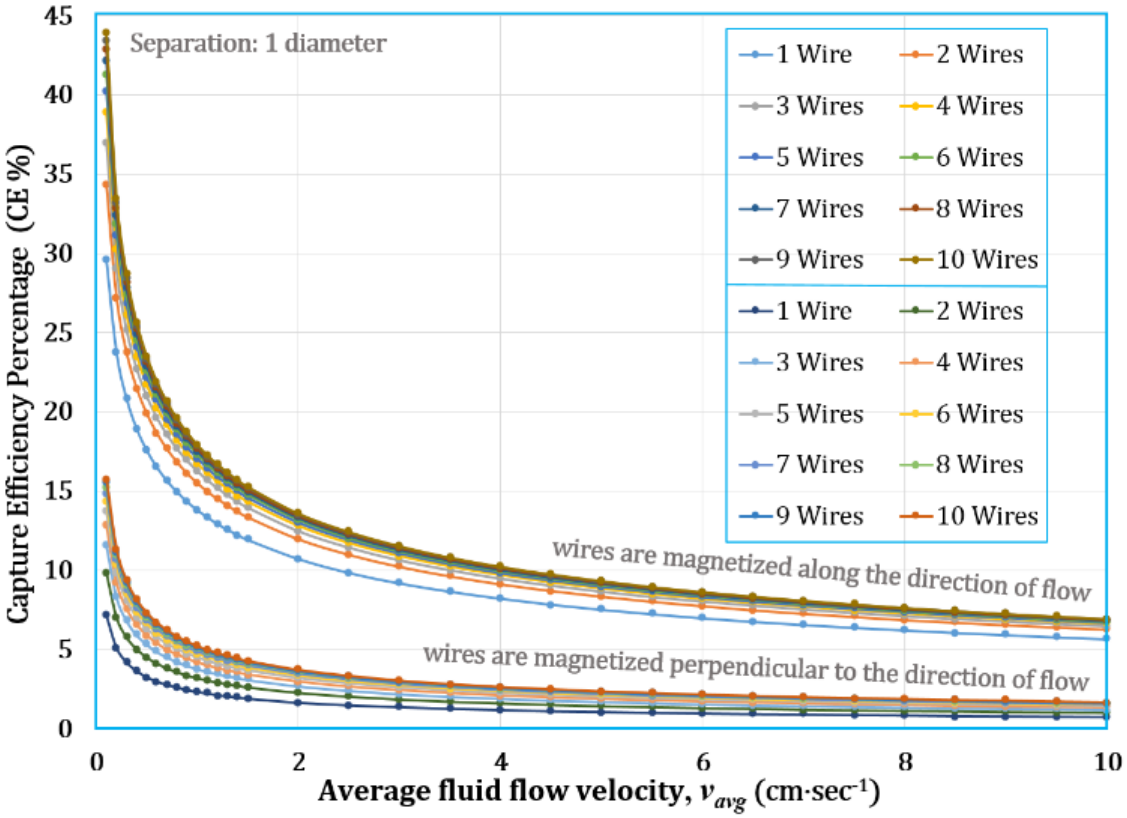

Figure 50. Capture efficiency of the magnetic wires vs average fluid flow velocity in the channel.

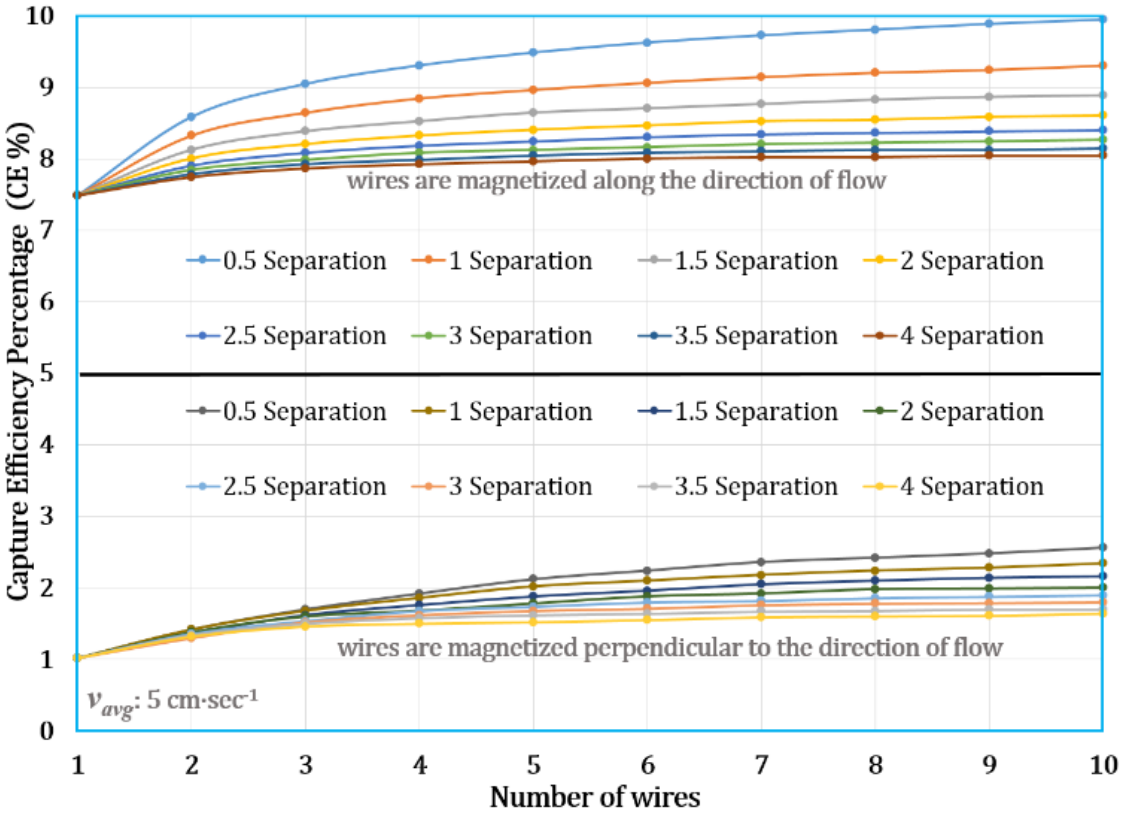

Figure 51. Capture efficiency of the magnetic wires vs number of wires in the channel.

Figure 51 shows that regardless of the orientation of external magnetic field, there is minimal increase in CE values with the increase in number of wires. It can also be seen that smaller separation between consecutive wires results in slightly larger CE values.

4.5. Discussion

Experimental results obtained by Aviles et. al. show that there is a much larger increase in CE values with the increase in number of wires [92]. However, theoretical/computational studies so far, have failed to corroborate those experimental results. We believe that, in experimental scenarios, the direction in which the magnetic wires get magnetized involves a more complex situation. Depending on the orientation of

magnetic wires inside the channel, they can get magnetized in different ways by an external magnetizing field as shown in Figure 52.

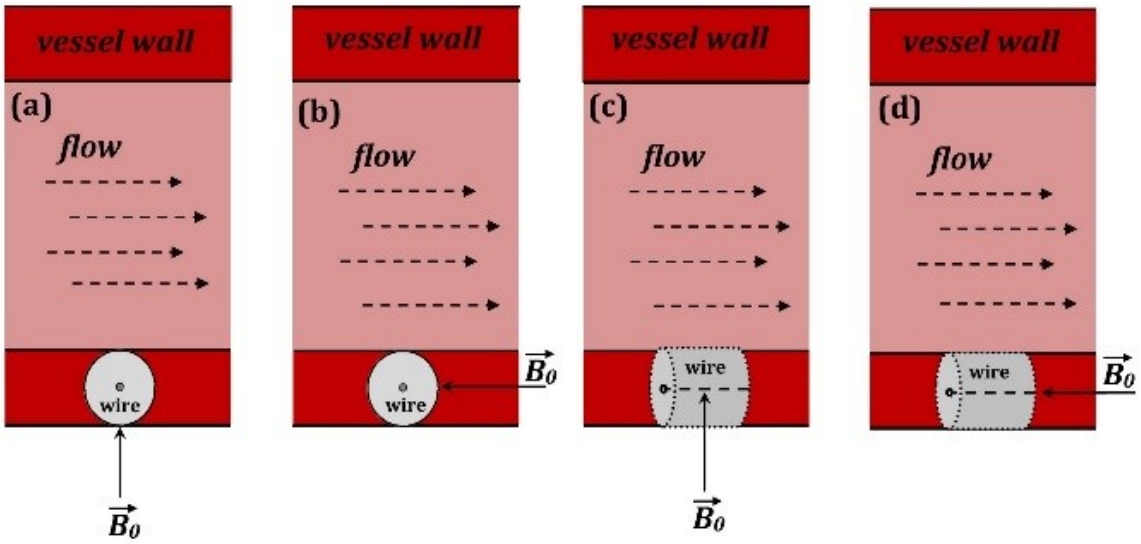

Figure 52. Orientation of magnetic wire and direction of external magnetizing field with respect to the flow in the channel.

So far, most of the theoretical and computational studies have focused on the situation depicted in Figure 52 (a). In this dissertation, the situations depicted in Figures 52(a) and 52(b) were. A more comprehensive theoretical analysis shall include all possible scenarios shown in Figure 52. It is possible that the sections of magnetic wires that are oriented along the direction of flow might be contributing more towards total capture when compared to the contribution of sections that are oriented perpendicular to the direction of flow, and this might be causing a much larger increase in CE values with the increase in number of wires in experimental studies. More analysis is needed.

The main aim of this computational study was to gain an understanding of the kinematics of capture of MPs for a SADT system without the use of computationally exhaustive and time consuming simulations which make it extremely difficult to explore the performance of a SADT system in a larger design parameter space. Two new results were obtained. Firstly, it is always the first wire that captures the MP and the MPs that are not captured are repelled to the center of the channel when compared to their starting position. Secondly, it is better to magnetize the wires along the direction of flow in comparison to perpendicular to the direction of flow for increased capture of MPs.

5. Contributions and Future Work

5.1. Contributions

5.1.1. Principal Finding

In mechanical equilibrium it is not possible to repel magnetic particles from magnets (consequence of Earnshaw's theorem [184]). This dissertation found the possibility that relative motion between magnetic particles and magnetic field gradient producing features can cause repulsion of magnetic particles. This phenomenon of magnetic repulsion can allow magnetic particles to experience much larger magnetic forces throughout the trajectory of the particles. In contrast, magnetic attraction can only be used at relatively large distances from gradient producing features reducing the average magnetic force throughout the particle trajectory. Attractive forces near gradient producing features are difficult to use because they cause aggregation and flow obstruction.

In regards to cell/biomolecule separation and focusing methods in flow, this phenomenon of magnetic repulsion can be exploited to significantly improve the throughput of separation and focusing by employing much larger flow-rates in the focusing and separation channels in comparison to the flow-rates employed in other methods of separation and focusing in microfluidic systems.

5.1.2. Example Application I: Magnetic Diagnosis of Malaria

This phenomenon of magnetic repulsion can be used to separate and focus very weakly magnetic particles such as malaria-infected red blood cells using very simple design. These designs allow concentration of malaria-infected red blood cells in less than

5 minutes which is significantly smaller than the time needed to prepare conventional blood smears (≈ 1 hour) [185] that continue to be the gold standard for malaria diagnosis. This magnetic repulsion based focusing of malaria-infected red blood cells can also potentially aid in the in the next step towards eradication of malaria by screening people for presence of gametocytes in cases of asymptomatic malaria.

5.1.3. Example Application II: Magnetic Stent Assisted Drug Targeting

Researchers have been suggesting the use of magnetic-stents to capture drug-carrying magnetic particles in order to reduce the problem of in-stent restenosis. However, in a range of studies, the capture of drug-carrying magnetic particles by those magnetic stent wires continues to be very small for practical blood flow velocities. Aviles et. al. [92] through their model and experiment suggested that it is only the first wire that captures the magnetic particles. However, as far as we know, so far, the kinematics of capture of magnetic particles has not been studied. This dissertation shows that the relative motion of drug-carrying magnetic particles and the magnetic field gradient producing wires causes repulsion of drug-carrying magnetic particles that were not captured by the first wire. The very low capture of drug-carrying magnetic particles by magnetic-stent wires in magnetic-stent assisted drug targeting systems can be partly attributed to the repulsion of magnetic particles that were not captured by the first wire.

5.2. Future Work

5.2.1. Physical Experiments for Magnetic Repulsion based Focusing of mRBCs

This dissertation presented computational study of one of the applications of the phenomenon of magnetic repulsion in separating and focusing malaria-infected red blood

cells. The future work shall include experimental work demonstrating the feasibility of the phenomenon of magnetic repulsion in separating and focusing malaria-infected red blood cells. The computational model presented in this dissertation provides ways to optimize the separation and focusing design in regards to the dimensions of the channel, the angle θ that the magnetic wires make with the direction of the flow along the length of the channel, and the corresponding diameter of the magnetic wires needed to focus the malaria-infected red blood cells.

This section on future work will focus on physical properties of the channel, means to maintain required flow rates through the channel, and the magnetic particles that can be utilized for experimentally demonstrating the feasibility of the magnetic repulsion based separation and focusing design for separating, focusing, and concentrating the malaria-infected red blood cells.

5.2.2. Fabrication and Surface Treatment of Separation and Focusing Channel

Owing to recent advancements in rapid prototyping, microfluidic systems are easy to fabricate and provide an ideal environment for testing either bulk samples or single entities, such as individual cells. Capillary like channel systems fabricated on silicon and glass substrates are now commonly employed by researchers. The ability to fabricate micrometer-sized features in glass and silicon makes these materials attractive options for making microfluidic channels. These microfluidic channels can also be integrated into comprehensive test platforms with controlled flow rate, temperature, and pressure [150].

For example Shelby et. al. [150] used polydimethylsiloxane (PDMS) rapid prototyping to fabricate narrow test channels in order to study the mechanical property

of deformability of malaria-infected erythrocytes. The channels were fabricated by MicroChem, Newton, MA, USA. It is important to note that the PDMS channel surface was oxidized in oxygen plasma to make the surface of the channel more hydrophilic. This was done to prevent the erythrocytes from sticking to the channel surface. In all of their tests, Shelby et. al. found that the uninfected erythrocytes did not stick to the plasma treated channel walls.

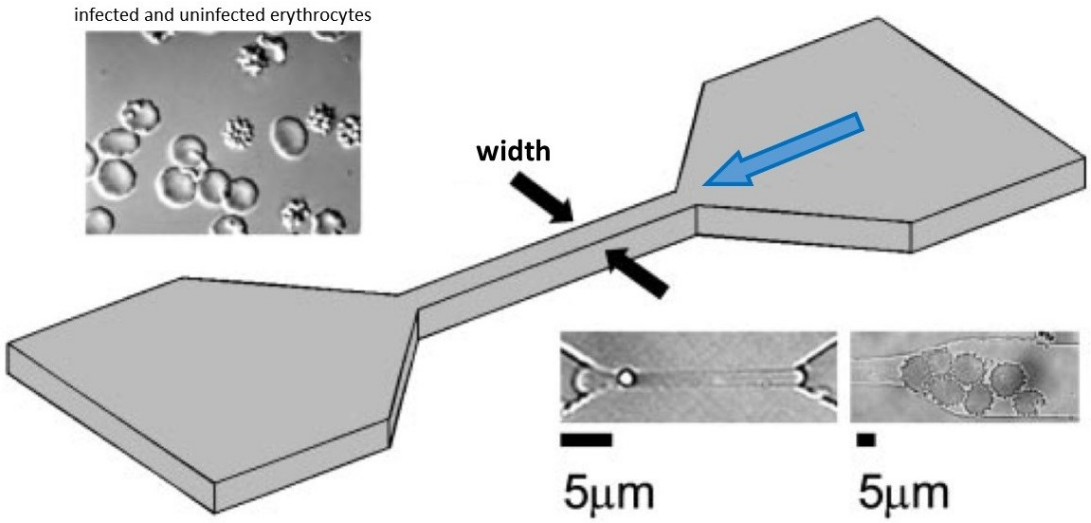

Figure 53. Schematic illustrating the geometry of the microchannel in the study by Shelby et. al. [150]. The width of the channel is 8, 6, 4, and 2 µm. The height of the channel is 2 µm. The blue arrow represents the direction of fluid flow. The flow rate in the channel varies from 0.1 – 0.5 mm sec^{-1}. This suggests that it is possible to construct very narrow channels that allow erythrocytes that are present in flow to pass through them.

Similarly, Nam et. al. [11] utilized a polydimethylsiloxane (PDMS) microfluidic channel, that was 50 µm in height and 100 µm in width to separate malaria-infected red blood cells. This channel was also fabricated by MicroChem, Newton, MA, USA. The channel was also treated with oxygen plasma to prevent the erythrocytes from sticking to

the channel walls. Before sample injection, it is suggested that the channel wall surface should be treated with 1% bovine serum albumin (BSA) to further prevent cell adhesion to the channel walls.

5.2.3. Maintaining Flow Rate in the Separation and Focusing Channel

These days several injection pumps are available that can be used to maintain a required flow rate through the microfluidic channels. Nam et. al. [11] were able to incorporate flow rates from 0.1 μL/min to 2 μL/min in their microfluidic channel. Karl et. al. [10] utilized syringe pump model R99-EJM, that is available from Razel Scientific Instruments, St Albans, VT. This syringe pump maintained a flow rate of 8.3 μl/min in their microfluidic channel.

5.2.4. Magnetic Particles for Physical Experiments

Red-blood cells have a hydrodynamic radius of ≈ 4 μm [149]. As preparation of samples with malaria-parasites involve a lot of rules and regulations, physical experiments can be started with commercially available magnetic particles that have a diameter of 3-5 μm. Once it is established that it is possible to focus to these magnetic particles using the phenomenon of magnetic repulsion, then deoxygenated red blood cells (magnetic susceptibility of $\Delta\chi = 3.9\times10^{-6}$) [11] can be used for further studies, eventually malaria-infected red blood cells and gametocytes can be utilized to study the efficiency of the design in separating and concentrating them.

5.2.4.1. Commercially Available Magnetic Particles

Cell separation methods typically use magnetic particles from 0.5-5 μm in diameter. For example, such particles are available commercially from Dynal® (microbeads 1–3 μm; Invitrogen, Carlsbad, USA) [76]. At the same time, magnetic particles (1-120 μm diameter) with different surface properties are available from Spherotech, Lake Forest, IL, USA.

5.2.4.2. Preparation of Samples with Deoxygenated Red Blood Cells

The next step in physical experiments of separation and focusing can utilize deoxygenated red blood cells. While, malaria-infected red blood cells have a relative magnetic susceptibility of $\Delta\chi = 1.8\times10^{-6}$, deoxygenated red blood cells have a relative magnetic susceptibility of $\Delta\chi = 3.9\times10^{-6}$ [11]. For the preparation of deoxygenated red blood cells, the red blood cells can be treated with $NaNO_2$. Blood samples can be obtained from healthy volunteers who are not on any medication and who provide informed consent while following all the required rules and regulations. A venous blood sample can be drawn from the antecubital vein and collected in (K2) ethylenediaminetetraacetic acid (EDTA) (as an anticoagulant) vacuum tubes. The blood sample should then be mixed with 5 mM $NaNO_2$ solution in a ratio of 1:40 (v/v) to oxidize the hemoglobin in the RBCs into paramagnetic form and then kept at 4 °C for 40 min before use [105, 186]. With the NaNO2 treatment of the RBCs, the ferrous ions (Fe2+) gets converted to the ferric (Fe3+) state. This conversion can be regarded in the same way as the paramagnetic changes of malaria-infected red blood cells.

5.2.4.3. Preparation of Samples with Malaria-Infected Red Blood Cells

Preparation of samples containing malaria-infected red blood cells requires significant expertise and training and shall follow the required rules and regulations associated with the preparation of such samples. Dr. Akhil Vaidya's malaria lab at the Department of Microbiology and Immunology at the Queen Lane campus of Drexel University specializes in preparation of cultures involving malaria-parasites.

Nam et. al. [11] in their magnetic separation of malaria-infected red blood cells method prepared sample cultures following an elaborate procedure. In their procedure, laboratory line 3D7 P. falciparum malaria parasites were grown with human erythrocytes (group O, Rh-positive, 3% hematocrit) in RPMI-HEPES medium (developed at Roswell Park Memorial Institute, RPMI) supplemented with 40 mg/L gentamicin (Invitrogen Co., Carlsbad, CA), 1.36 g/L hypoxanthine (Sigma-Aldrich, St. Louis, MO), 25 mM HEPES [2-(4-(2-hydroxyethyl)-1-piperazinyl) ethanesulfonic acid] (Sigma-Aldrich, St. Louis, MO), 7.5% sodium bicarbonate (Invitrogen Co., Carlsbad, CA), 20% glucose (Sigma-Aldrich, St. Louis, MO), 1 M NaOH (Sigma-Aldrich, St. Louis, MO), and 20% AlbuMAX (Invitrogen Co., Carlsbad, CA). All cultures were maintained at 37 °C in an atmosphere of 5% CO_2, 1% O_2, and 94% N_2, with daily medium changes in accordance with [187]. Synchronization of the culture was achieved through sorbitol lysis at the mature stage using 5% sorbitol (Sigma-Aldrich, St. Louis, MO) and fine-tuned by another lysis after 8 h [188]. Cells were harvested after being cultured for 48 hours.

In the study by Karl et. al. [10] blood samples from actual infected individuals were collected over a period of two months during the wet season, at health centers in Madang Province in Papua New Guinea in accordance with the required protocols. In

their study, a total of 55 whole blood samples (1 ml) were collected from *Plasmodium*-infected individuals in heparin Vacutainer® tubes (Greiner bio one GmbH, Kremsmuenster, Austria).

It is important to note that magnetic particles of different sizes and different magnetic content can be separated and focused by positioning high magnetic field gradient producing wires at different angles with respect to the flow and also by incorporating different flow rates through the separation and focusing chamber.

The ability to separate and focus magnetic particles using the phenomenon of magnetic repulsion was a major focus of this thesis. The computational models, example designs, and optimizations presented in this thesis can also be employed in a number of applications beyond just focusing of malaria-infected red blood cells [65].

Bibliography

[1] A. Orfao and A. Ruiz-Arguelles, "General concepts about cell sorting techniques," *Clin Biochem,* vol. 29, pp. 5-9, Feb 1996.

[2] A. Boyum, "Isolation of mononuclear cells and granulocytes from human blood. Isolation of monuclear cells by one centrifugation, and of granulocytes by combining centrifugation and sedimentation at 1 g," *Scand J Clin Lab Invest Suppl,* vol. 97, pp. 77-89, 1968.

[3] H. R. Hulett, W. A. Bonner, J. Barrett, and L. A. Herzenberg, "Cell sorting: automated separation of mammalian cells as a function of intracellular fluorescence," *Science,* vol. 166, pp. 747-9, Nov 07 1969.

[4] A. J. Armstrong, M. S. Marengo, S. Oltean, G. Kemeny, R. L. Bitting, J. D. Turnbull, *et al.*, "Circulating tumor cells from patients with advanced prostate and breast cancer display both epithelial and mesenchymal markers," *Mol Cancer Res,* vol. 9, pp. 997-1007, Aug 2011.

[5] A. W. Wognum, A. C. Eaves, and T. E. Thomas, "Identification and isolation of hematopoietic stem cells," *Arch Med Res,* vol. 34, pp. 461-75, Nov-Dec 2003.

[6] F. Z. Bischoff, D. A. Marquez-Do, D. I. Martinez, D. Dang, C. Horne, D. Lewis, *et al.*, "Intact fetal cell isolation from maternal blood: improved isolation using a simple whole blood progenitor cell enrichment approach (RosetteSep)," *Clin Genet,* vol. 63, pp. 483-9, Jun 2003.

[7] Y. Chen, P. Li, P. H. Huang, Y. Xie, J. D. Mai, L. Wang, *et al.*, "Rare cell isolation and analysis in microfluidics," *Lab Chip,* vol. 14, pp. 626-45, Feb 21 2014.

[8] W. A. O'Brien, P. M. Hartigan, E. S. Daar, M. S. Simberkoff, and J. D. Hamilton, "Changes in plasma HIV RNA levels and CD4+ lymphocyte counts predict both response to antiretroviral therapy and therapeutic failure. VA Cooperative Study Group on AIDS," *Ann Intern Med,* vol. 126, pp. 939-45, Jun 15 1997.

[9] X. Cheng, D. Irimia, M. Dixon, K. Sekine, U. Demirci, L. Zamir, *et al.*, "A microfluidic device for practical label-free CD4(+) T cell counting of HIV-infected subjects," *Lab Chip,* vol. 7, pp. 170-8, Feb 2007.

[10] S. Karl, M. David, L. Moore, B. T. Grimberg, P. Michon, I. Mueller, *et al.*, "Enhanced detection of gametocytes by magnetic deposition microscopy predicts higher potential for Plasmodium falciparum transmission," *Malar J,* vol. 7, p. 66, 2008.

[11] J. Nam, H. Huang, H. Lim, C. Lim, and S. Shin, "Magnetic separation of malaria-infected red blood cells in various developmental stages," *Anal Chem,* vol. 85, pp. 7316-23, Aug 6 2013.

[12] J. A. Korecka, J. Verhaagen, and E. M. Hol, "Cell-replacement and gene-therapy strategies for Parkinson's and Alzheimer's disease," *Regen Med,* vol. 2, pp. 425-46, Jul 2007.

[13] Z. Wu, K. Hjort, G. Wicher, and A. Fex Svenningsen, "Microfluidic high viability neural cell separation using viscoelastically tuned hydrodynamic spreading," *Biomed Microdevices,* vol. 10, pp. 631-8, Oct 2008.

[14] E. Hedlund, J. Pruszak, A. Ferree, A. Vinuela, S. Hong, O. Isacson*, et al.*, "Selection of embryonic stem cell-derived enhanced green fluorescent protein-positive dopamine neurons using the tyrosine hydroxylase promoter is confounded by reporter gene expression in immature cell populations," *Stem Cells,* vol. 25, pp. 1126-35, May 2007.

[15] A. Mavrou, E. Kouvidi, A. Antsaklis, A. Souka, S. Kitsiou Tzeli, and A. Kolialexi, "Identification of nucleated red blood cells in maternal circulation: a second step in screening for fetal aneuploidies and pregnancy complications," *Prenat Diagn,* vol. 27, pp. 150-3, Feb 2007.

[16] L. Chin, J. N. Andersen, and P. A. Futreal, "Cancer genomics: from discovery science to personalized medicine," *Nat Med,* vol. 17, pp. 297-303, Mar 2011.

[17] M. J. Tomlinson, S. Tomlinson, X. B. Yang, and J. Kirkham, "Cell separation: Terminology and practical considerations," *Journal of Tissue Engineering,* vol. 4, January 1, 2013 2013.

[18] M. Kamihira and A. Kumar, "Development of separation technique for stem cells," *Adv Biochem Eng Biotechnol,* vol. 106, pp. 173-93, 2007.

[19] R. E. Nordon, D. N. Haylock, L. Gaudry, and K. Schindhelm, "Hollow-fibre affinity cell separation system for CD34+ cell enrichment," *Cytometry,* vol. 24, pp. 340-7, Aug 01 1996.

[20] G. Bell, "Models for the specific adhesion of cells to cells," *Science,* vol. 200, pp. 618-627, 1978.

[21] A. Kumar and A. Bhardwaj, "Methods in cell separation for biomedical application: cryogels as a new tool," *Biomed Mater,* vol. 3, p. 034008, Sep 2008.

[22] A. A. Bhagat, H. Bow, H. W. Hou, S. J. Tan, J. Han, and C. T. Lim, "Microfluidics for cell separation," *Med Biol Eng Comput,* vol. 48, pp. 999-1014, Oct 2010.

[23] C. W. t. Shields, C. D. Reyes, and G. P. Lopez, "Microfluidic cell sorting: a review of the advances in the separation of cells from debulking to rare cell isolation," *Lab Chip,* vol. 15, pp. 1230-49, Mar 07 2015.

[24] D. R. Gossett, W. M. Weaver, A. J. Mach, S. C. Hur, H. T. Tse, W. Lee*, et al.*, "Label-free cell separation and sorting in microfluidic systems," *Anal Bioanal Chem,* vol. 397, pp. 3249-67, Aug 2010.

[25] S. Gronthos, M. Mankani, J. Brahim, P. G. Robey, and S. Shi, "Postnatal human dental pulp stem cells (DPSCs) in vitro and in vivo," *Proc Natl Acad Sci U S A,* vol. 97, pp. 13625-30, Dec 05 2000.

[26] K. Nagase, A. Kimura, T. Shimizu, K. Matsuura, M. Yamato, N. Takeda*, et al.*, "Dynamically cell separating thermo-functional biointerfaces with densely packed polymer brushes," *Journal of Materials Chemistry,* vol. 22, pp. 19514-19522, 2012.

[27] R. G. Miller and R. A. Phillips, "Separation of cells by velocity sedimentation," *J Cell Physiol,* vol. 73, pp. 191-201, Jun 1969.

[28] W. A. Bonner, H. R. Hulett, R. G. Sweet, and L. A. Herzenberg, "Fluorescence activated cell sorting," *Rev Sci Instrum,* vol. 43, pp. 404-9, Mar 1972.

[29] S. Miltenyi, W. Muller, W. Weichel, and A. Radbruch, "High gradient magnetic cell separation with MACS," *Cytometry,* vol. 11, pp. 231-8, 1990.

[30] A. Rembaum, R. C. Yen, D. H. Kempner, and J. Ugelstad, "Cell labeling and magnetic separation by means of immunoreagents based on polyacrolein microspheres," *J Immunol Methods,* vol. 52, pp. 341-51, Aug 13 1982.

[31] J. El-Ali, P. K. Sorger, and K. F. Jensen, "Cells on chips," *Nature,* vol. 442, pp. 403-11, Jul 27 2006.

[32] M. E. Piyasena and S. W. Graves, "The intersection of flow cytometry with microfluidics and microfabrication," *Lab Chip,* vol. 14, pp. 1044-59, Mar 21 2014.

[33] M. Zhao, P. G. Schiro, J. S. Kuo, K. M. Koehler, D. E. Sabath, V. Popov*, et al.*, "An automated high-throughput counting method for screening circulating tumor cells in peripheral blood," *Anal Chem,* vol. 85, pp. 2465-71, Feb 19 2013.

[34] W. Sheng, O. O. Ogunwobi, T. Chen, J. Zhang, T. J. George, C. Liu*, et al.*, "Capture, release and culture of circulating tumor cells from pancreatic cancer patients using an enhanced mixing chip," *Lab Chip,* vol. 14, pp. 89-98, Jan 07 2014.

[35] G. Mernier, N. Piacentini, T. Braschler, N. Demierre, and P. Renaud, "Continuous-flow electrical lysis device with integrated control by dielectrophoretic cell sorting," *Lab Chip,* vol. 10, pp. 2077-82, Aug 21 2010.

[36] S. Yang, A. Undar, and J. D. Zahn, "A microfluidic device for continuous, real time blood plasma separation," *Lab Chip,* vol. 6, pp. 871-80, Jul 2006.

[37] S. Yan, J. Zhang, D. Yuan, and W. Li, "Hybrid microfluidics combined with active and passive approaches for continuous cell separation," *Electrophoresis,* Oct 08 2016.

[38] J. Voldman, "ELECTRICAL FORCES FOR MICROSCALE CELL MANIPULATION," *Annual Review of Biomedical Engineering,* vol. 8, pp. 425-454, 2006.

[39] A. Lenshof and T. Laurell, "Continuous separation of cells and particles in microfluidic systems," *Chem Soc Rev,* vol. 39, pp. 1203-17, Mar 2010.

[40] O. D. Velev and K. H. Bhatt, "On-chip micromanipulation and assembly of colloidal particles by electric fields," *Soft Matter,* vol. 2, pp. 738-750, 2006.

[41] A. Y. Fu, C. Spence, A. Scherer, F. H. Arnold, and S. R. Quake, "A microfabricated fluorescence-activated cell sorter," *Nat Biotechnol,* vol. 17, pp. 1109-11, Nov 1999.

[42] P. S. Dittrich and P. Schwille, "An integrated microfluidic system for reaction, high-sensitivity detection, and sorting of fluorescent cells and particles," *Anal Chem,* vol. 75, pp. 5767-74, Nov 01 2003.

[43] P. G. Erlandsson and N. D. Robinson, "Electrolysis-reducing electrodes for electrokinetic devices," *Electrophoresis,* vol. 32, pp. 784-90, Mar 2011.

[44] S. Valagerahally Puttaswamy, S. Sivashankar, C.-H. Yeh, R.-J. Chen, and C. H. Liu, "Electrodynamically actuated on-chip flow cytometry with low shear stress for electro-osmosis based sorting using low conductive medium," *Microelectronic Engineering,* vol. 87, pp. 2582-2591, 12// 2010.

[45] A. Thiel, A. Scheffold, and A. Radbruch, "Immunomagnetic cell sorting--pushing the limits," *Immunotechnology,* vol. 4, pp. 89-96, Oct 1998.

[46] M. Berger, J. Castelino, R. Huang, M. Shah, and R. H. Austin, "Design of a microfabricated magnetic cell separator," *Electrophoresis,* vol. 22, pp. 3883-92, Oct 2001.

[47] H. Tsutsui and C. M. Ho, "Cell Separation by Non-Inertial Force Fields in Microfluidic Systems," *Mech Res Commun,* vol. 36, pp. 92-103, Jan 01 2009.

[48] N. Pamme, "Continuous flow separations in microfluidic devices," *Lab on a Chip,* vol. 7, pp. 1644-1659, 2007.

[49] M. Zborowski and J. J. Chalmers, "Rare Cell Separation and Analysis by Magnetic Sorting," *Analytical Chemistry,* vol. 83, pp. 8050-8056, 2011/11/01 2011.

[50] Y. Chen, P. Li, P.-H. Huang, Y. Xie, J. D. Mai, L. Wang, *et al.*, "Rare cell isolation and analysis in microfluidics," *Lab on a Chip,* vol. 14, pp. 626-645, 2014.

[51] L. Gwo-Bin, C. Chih-Chang, H. Sung-Bin, and Y. Ruey-Jen, "The hydrodynamic focusing effect inside rectangular microchannels," *Journal of Micromechanics and Microengineering,* vol. 16, p. 1024, 2006.

[52] A. Kummrow, J. Theisen, M. Frankowski, A. Tuchscheerer, H. Yildirim, K. Brattke, *et al.*, "Microfluidic structures for flow cytometric analysis of hydrodynamically focussed blood cells fabricated by ultraprecision micromachining," *Lab on a Chip,* vol. 9, pp. 972-981, 2009.

[53] C.-H. Tsai, H.-H. Hou, and L.-M. Fu, "An optimal three-dimensional focusing technique for micro-flow cytometers," *Microfluidics and Nanofluidics,* vol. 5, pp. 827-836, 2008.

[54] L.-M. Fu, R.-J. Yang, C.-H. Lin, Y.-J. Pan, and G.-B. Lee, "Electrokinetically driven micro flow cytometers with integrated fiber optics for on-line cell/particle detection," *Analytica Chimica Acta,* vol. 507, pp. 163-169, 4/1/ 2004.

[55] X. Xuan and D. Li, "Focused electrophoretic motion and selected electrokinetic dispensing of particles and cells in cross-microchannels," *Electrophoresis,* vol. 26, pp. 3552-60, Sep 2005.

[56] Y. Ruey-Jen, C. Chih-Chang, H. Sung-Bin, and L. Gwo-Bin, "A new focusing model and switching approach for electrokinetic flow inside microchannels," *Journal of Micromechanics and Microengineering,* vol. 15, p. 2141, 2005.

[57] P. B. Howell Jr, J. P. Golden, L. R. Hilliard, J. S. Erickson, D. R. Mott, and F. S. Ligler, "Two simple and rugged designs for creating microfluidic sheath flow," *Lab on a Chip,* vol. 8, pp. 1097-1103, 2008.

[58] M. G. Lee, S. Choi, and J.-K. Park, "Three-dimensional hydrodynamic focusing with a single sheath flow in a single-layer microfluidic device," *Lab on a Chip,* vol. 9, pp. 3155-3160, 2009.

[59] X. Mao and T. J. Huang, "Focusing fluids and light," *IEEE Nanotechnology Magazine,* vol. 2, pp. 22-27, 2008.

[60] P. R. C. Gascoyne and J. Vykoukal, "Particle separation by dielectrophoresis," *Electrophoresis,* vol. 23, pp. 1973-1983, 2002.

[61] C. Liu, T. Stakenborg, S. Peeters, and L. Lagae, "Cell manipulation with magnetic particles toward microfluidic cytometry," *Journal of Applied Physics,* vol. 105, p. 102014, 2009.

[62] Y. Zhao, B. S. Fujimoto, G. D. M. Jeffries, P. G. Schiro, and D. T. Chiu, "Optical gradient flow focusing," *Optics Express,* vol. 15, pp. 6167-6176, 2007/05/14 2007.

[63] S. Choi, S. Song, C. Choi, and J. K. Park, "Sheathless focusing of microbeads and blood cells based on hydrophoresis," *Small,* vol. 4, pp. 634-41, May 2008.

[64] D. Di Carlo, "Inertial microfluidics," *Lab on a Chip,* vol. 9, pp. 3038-3046, 2009.

[65] X. Xuan, J. Zhu, and C. Church, "Particle focusing in microfluidic devices," *Microfluidics and Nanofluidics,* vol. 9, pp. 1-16, 2010.

[66] K. Kim, H.-K. Seo, and Y.-J. Kim, "Sheathless microfluidic particle focusing technique using slanted microstructure array," *Microfluidics and Nanofluidics,* vol. 16, pp. 159-166, 2014.

[67] T. Zhu, R. Cheng, and L. Mao, "Focusing microparticles in a microfluidic channel with ferrofluids," in *2011 16th International Solid-State Sensors, Actuators and Microsystems Conference*, 2011, pp. 1280-1283.

[68] R. Afshar, Y. Moser, T. Lehnert, and M. A. M. Gijs, "Three-Dimensional Magnetic Focusing of Superparamagnetic Beads for On-Chip Agglutination Assays," *Analytical Chemistry,* vol. 83, pp. 1022-1029, 2011/02/01 2011.

[69] J. Shi, X. Mao, D. Ahmed, A. Colletti, and T. J. Huang, "Focusing microparticles in a microfluidic channel with standing surface acoustic waves (SSAW)," *Lab Chip,* vol. 8, pp. 221-3, Feb 2008.

[70] L. Che-Hsin, L. Gwo-Bin, F. Lung-Ming, and H. Bao-Herng, "Vertical focusing device utilizing dielectrophoretic force and its application on microflow cytometer," *Journal of Microelectromechanical Systems,* vol. 13, pp. 923-932, 2004.

[71] I. Šafařík and M. Šafaříková, "Use of magnetic techniques for the isolation of cells," *Journal of Chromatography B: Biomedical Sciences and Applications,* vol. 722, pp. 33-53, 2/5/ 1999.

[72] A. Bee, R. Massart, and S. Neveu, "Synthesis of very fine maghemite particles," *Journal of Magnetism and Magnetic Materials,* vol. 149, pp. 6-9, 1995/08/01 1995.

[73] Y.-k. Sun, M. Ma, Y. Zhang, and N. Gu, "Synthesis of nanometer-size maghemite particles from magnetite," *Colloids and Surfaces A: Physicochemical and Engineering Aspects,* vol. 245, pp. 15-19, 9/24/ 2004.

[74] D. Horák, M. Babič, H. Macková, and M. J. Beneš, "Preparation and properties of magnetic nano- and microsized particles for biological and environmental separations," *Journal of Separation Science,* vol. 30, pp. 1751-1772, 2007.

[75] R. S. Molday, S. P. S. Yen, and A. Rembaum, "Application of magnetic microspheres in labelling and separation of cells," *Nature,* vol. 268, pp. 437-438, 08/04/print 1977.

[76] A. Grutzkau and A. Radbruch, "Small but mighty: how the MACS-technology based on nanosized superparamagnetic particles has helped to analyze the immune system within the last 20 years," *Cytometry A,* vol. 77, pp. 643-7, Jul 2010.

[77] I. Safarik and M. Safarikova, "Magnetic techniques for the isolation and purification of proteins and peptides," *Biomagnetic Research and Technology,* vol. 2, pp. 7-7, 11/26 2004.

[78] G. Blankenstein, "Microfabricated Flow System for Magnetic Cell and Particle Separation," in *Scientific and Clinical Applications of Magnetic Carriers*, U. Häfeli, W. Schütt, J. Teller, and M. Zborowski, Eds., ed Boston, MA: Springer US, 1997, pp. 233-245.

[79] K. S. Kim and J. K. Park, "Magnetic force-based multiplexed immunoassay using superparamagnetic nanoparticles in microfluidic channel," *Lab Chip,* vol. 5, pp. 657-64, Jun 2005.

[80] N. Pamme and A. Manz, "On-Chip Free-Flow Magnetophoresis: Continuous Flow Separation of Magnetic Particles and Agglomerates," *Analytical Chemistry,* vol. 76, pp. 7250-7256, 2004/12/01 2004.

[81] D. W. Inglis, R. Riehn, R. H. Austin, and J. C. Sturm, "Continuous microfluidic immunomagnetic cell separation," *Applied Physics Letters,* vol. 85, pp. 5093-5095, 2004.

[82] K.-H. Han and A. B. Frazier, "Paramagnetic capture mode magnetophoretic microseparator for high efficiency blood cell separations," *Lab on a Chip,* vol. 6, pp. 265-273, 2006.

[83] R. Afshar Ghasemlouy, Y. Moser, T. Lehnert, and M. Gijs, "Three-dimensional hydro-magnetic focusing and in-flow separation of superparamagnetic beads," presented at the 14th International Conference on Miniaturized Systems for Chemistry and Life Sciences (MicroTAS 2010), Groningen, Netherlands, 2010.

[84] R. Afshar, Y. Moser, T. Lehnert, and M. Gijs, "Magneto-Microfluidic Three-Dimensional Focusing of Magnetic Particles," *AIP Conference Proceedings,* vol. 1311, pp. 161-166, 2010.

[85] S. Rampini, D. Kilinc, P. Li, C. Monteil, D. Gandhi, and G. U. Lee, "Micromagnet arrays for on-chip focusing, switching, and separation of superparamagnetic beads and single cells," *Lab Chip,* vol. 15, pp. 3370-9, Jul 28 2015.

[86] G. M. Whitesides, "The origins and the future of microfluidics," *Nature,* vol. 442, pp. 368-373, 07/27/print 2006.

[87] Q. A. Pankhurst, J. Connolly, S. K. Jones, and J. Dobson, "Applications of magnetic nanoparticles in biomedicine," *Journal of Physics D: Applied Physics,* vol. 36, p. R167, 2003.

[88] M. A. M. Gijs, "Magnetic bead handling on-chip: new opportunities for analytical applications," *Microfluidics and Nanofluidics,* vol. 1, pp. 22-40, 2004.

[89] D. L. Leslie-Pelecky and R. D. Rieke, "Magnetic Properties of Nanostructured Materials," *Chemistry of Materials,* vol. 8, pp. 1770-1783, 1996/01/01 1996.

[90] Y. Hou, J. Yu, and S. Gao, "Solvothermal reduction synthesis and characterization of superparamagnetic magnetite nanoparticles," *Journal of Materials Chemistry,* vol. 13, pp. 1983-1987, 2003.

[91] S. J. Kemp, R. M. Ferguson, A. P. Khandhar, and K. M. Krishnan, "Monodisperse magnetite nanoparticles with nearly ideal saturation magnetization," *RSC Advances,* vol. 6, pp. 77452-77464, 2016.

[92] M. O. Avilés, A. D. Ebner, and J. A. Ritter, "Implant assisted-magnetic drug targeting: Comparison of in vitro experiments with theory," *Journal of Magnetism and Magnetic Materials,* vol. 320, pp. 2704-2713, 11// 2008.

[93] A. D. Grief and G. Richardson, "Mathematical modelling of magnetically targeted drug delivery," *Journal of Magnetism and Magnetic Materials,* vol. 293, pp. 455-463, 5// 2005.

[94] L. Blaney, "Magnetite (Fe3O4): Properties, synthesis, and applications," 2007.

[95] A. E. David, A. J. Cole, B. Chertok, Y. S. Park, and V. C. Yang, "A combined theoretical and in vitro modeling approach for predicting the magnetic capture and retention of magnetic nanoparticles in vivo," *J Control Release,* vol. 152, pp. 67-75, May 30 2011.

[96] M. Zborowski, "Physics of Magnetic Cell Sorting," in *Scientific and Clinical Applications of Magnetic Carriers*, U. Häfeli, W. Schütt, J. Teller, and M. Zborowski, Eds., ed Boston, MA: Springer US, 1997, pp. 205-231.

[97] G. P. Hatch and R. E. Stelter, "Magnetic design considerations for devices and particles used for biological high-gradient magnetic separation (HGMS) systems," *Journal of Magnetism and Magnetic Materials,* vol. 225, pp. 262-276, // 2001.

[98] J. M. C. a. V. Sosa, "Alternative method to calculate the magnetic field of permanent magnets with azimuthal symmetry," *Revista Mexicana de F´ısica E,* vol. 59, pp. 8-17, 2013.

[99] H. Chen, A. D. Ebner, A. J. Rosengart, M. D. Kaminski, and J. A. Ritter, "Analysis of magnetic drug carrier particle capture by a magnetizable intravascular stent: 1. Parametric study with single wire correlation," *Journal of Magnetism and Magnetic Materials,* vol. 284, pp. 181-194, 12// 2004.

[100] J. M. Peeters, E. E. H. van Faassen, and C. J. G. Bakker, "Magnetic resonance imaging of microstructure transition in stainless steel," *Magnetic Resonance Imaging,* vol. 24, pp. 663-672, 6// 2006.

[101] R. Bhagwandien, R. van Ee, R. Beersma, C. J. G. Bakker, M. A. Moerland, and J. J. W. Lagendijk, "Numerical analysis of the magnetic field for arbitrary magnetic susceptibility distributions in 2D," *Magnetic Resonance Imaging,* vol. 10, pp. 299-313, // 1992.

[102] J. F. Schenck, "The role of magnetic susceptibility in magnetic resonance imaging: MRI magnetic compatibility of the first and second kinds," *Med Phys,* vol. 23, pp. 815-50, Jun 1996.

[103] K. M. Lüdeke, P. Röschmann, and R. Tischler, "Susceptibility artefacts in NMR imaging," *Magnetic Resonance Imaging,* vol. 3, pp. 329-343, 1985/01/01 1985.

[104] K.-H. Han and A. Bruno Frazier, "Continuous magnetophoretic separation of blood cells in microdevice format," *Journal of Applied Physics,* vol. 96, pp. 5797-5802, 2004.

[105] B. Y. Qu, Z. Y. Wu, F. Fang, Z. M. Bai, D. Z. Yang, and S. K. Xu, "A glass microfluidic chip for continuous blood cell sorting by a magnetic gradient without labeling," *Anal Bioanal Chem,* vol. 392, pp. 1317-24, Dec 2008.

[106] K. H. Han and A. B. Frazier, "Paramagnetic capture mode magnetophoretic microseparator for high efficiency blood cell separations," *Lab Chip,* vol. 6, pp. 265-73, Feb 2006.

[107] P. J. Cregg, K. Murphy, A. Mardinoglu, and A. Prina-Mello, "Many particle magnetic dipole–dipole and hydrodynamic interactions in magnetizable stent assisted magnetic drug targeting," *Journal of Magnetism and Magnetic Materials,* vol. 322, pp. 2087-2094, 8// 2010.

[108] S. Kayal, D. Bandyopadhyay, T. K. Mandal, and R. V. Ramanujan, "The flow of magnetic nanoparticles in magnetic drug targeting," *RSC Advances,* vol. 1, pp. 238-246, 2011.

[109] P. Yue, S. Lee, S. Afkhami, and Y. Renardy, "On the motion of superparamagnetic particles in magnetic drug targeting," *Acta Mechanica,* vol. 223, pp. 505-527, 2012/03/01 2012.

[110] J. W. Haverkort, S. Kenjereš, and C. R. Kleijn, "Computational Simulations of Magnetic Particle Capture in Arterial Flows," *Annals of Biomedical Engineering,* vol. 37, pp. 2436-2448, 09/16 04/15/received 08/26/accepted 2009.

[111] K. W. Yung, P. B. Landecker, and D. D. Villani, "An Analytic Solution for the Force Between Two Magnetic Dipoles," *Magnetic and Electrical Separation,* vol. 9, pp. 39-52, 1998.

[112] E. M. Cherry, P. G. Maxim, and J. K. Eaton, "Particle size, magnetic field, and blood velocity effects on particle retention in magnetic drug targeting," *Med Phys,* vol. 37, pp. 175-82, Jan 2010.

[113] E. Cherry and J. Eaton, "Simulation of magnetic particles in the bloodstream for magnetic drug targeting applications," in *International Conference on Multiphase Flow*, 2013.

[114] W. H. Organization, "World Malaria report 2014," 2014.

[115] D. C. Warhurst and J. E. Williams, "ACP Broadsheet no 148. July 1996. Laboratory diagnosis of malaria," *J Clin Pathol,* vol. 49, pp. 533-8, Jul 1996.

[116] N. Tangpukdee, C. Duangdee, P. Wilairatana, and S. Krudsood, "Malaria diagnosis: a brief review," *Korean J Parasitol,* vol. 47, pp. 93-102, Jun 2009.

[117] J. W. Bailey, J. Williams, B. J. Bain, J. Parker-Williams, P. L. Chiodini, and H. The General Haematology Task Force of the British Committee for Standards in, "Guideline: the laboratory diagnosis of malaria," *British Journal of Haematology,* vol. 163, pp. 573-580, 2013.

[118] W. H. Organization, "Basic Malaria Microscopy-Part I. Learner's Guide. ; 2010," *Geneva: WHO,* pp. 65-68, 1991.

[119] A. Trampuz, M. Jereb, I. Muzlovic, and R. M. Prabhu, "Clinical review: Severe malaria," *Critical Care,* vol. 7, pp. 315-323, 04/14 2003.

[120] J. F. Trape, "Rapid evaluation of malaria parasite density and standardization of thick smear examination for epidemiological investigations," *Trans R Soc Trop Med Hyg,* vol. 79, pp. 181-4, 1985.

[121] D. Payne, "Use and limitations of light microscopy for diagnosing malaria at the primary health care level," *Bull World Health Organ,* vol. 66, pp. 621-6, 1988.

[122] R. E. Coleman, J. Sattabongkot, S. Promstaporm, N. Maneechai, B. Tippayachai, A. Kengluecha*, et al.*, "Comparison of PCR and microscopy for the detection of asymptomatic malaria in a Plasmodium falciparum/vivax endemic area in Thailand," *Malar J,* vol. 5, p. 121, 2006.

[123] C. Fançony, Y. V. Sebastião, J. E. Pires, D. Gamboa, and S. V. Nery, "Performance of microscopy and RDTs in the context of a malaria prevalence survey in Angola: a comparison using PCR as the gold standard," *Malaria Journal,* vol. 12, pp. 1-7, 2013.

[124] S. Shillcutt, C. Morel, C. Goodman, P. Coleman, D. Bell, C. J. Whitty, *et al.*, "Cost-effectiveness of malaria diagnostic methods in sub-Saharan Africa in an era of combination therapy," *Bull World Health Organ,* vol. 86, pp. 101-10, Feb 2008.

[125] J. C. Mouatcho and J. P. Goldring, "Malaria rapid diagnostic tests: challenges and prospects," *J Med Microbiol,* vol. 62, pp. 1491-505, Oct 2013.

[126] T. Hänscheid and M. P. Grobusch, "How useful is PCR in the diagnosis of malaria?," *Trends in Parasitology,* vol. 18, pp. 395-398, 9/1/ 2002.

[127] L. C. Okell, T. Bousema, J. T. Griffin, A. L. Ouedraogo, A. C. Ghani, and C. J. Drakeley, "Factors determining the occurrence of submicroscopic malaria infections and their relevance for control," *Nat Commun,* vol. 3, p. 1237, 2012.

[128] J. Luchavez, M. E. Lintag, M. Coll-Black, F. Baik, and D. Bell, "An assessment of various blood collection and transfer methods used for malaria rapid diagnostic tests," *Malaria Journal,* vol. 6, pp. 1-5, 2007.

[129] H. Hopkins, L. Bebell, W. Kambale, C. Dokomajilar, P. J. Rosenthal, and G. Dorsey, "Rapid diagnostic tests for malaria at sites of varying transmission intensity in Uganda," *J Infect Dis,* vol. 197, pp. 510-8, Feb 15 2008.

[130] D. Francis, A. Gasasira, R. Kigozi, S. Kigozi, S. Nasr, M. R. Kamya, *et al.*, "Health facility-based malaria surveillance: The effects of age, area of residence and diagnostics on test positivity rates," *Malar J,* vol. 11, p. 229, 2012.

[131] L. C. Okell, A. C. Ghani, E. Lyons, and C. J. Drakeley, "Submicroscopic Infection in Plasmodium falciparum-Endemic Populations: A Systematic Review and Meta-Analysis," *Journal of Infectious Diseases,* vol. 200, pp. 1509-1517, November 15, 2009 2009.

[132] W. H. Organization, "Malaria microscopy quality assurance manual-version 2," 2016.

[133] D. N. Durrhelm, P. J. Becker, K. Billinghurst, and A. Brink, "Diagnostic disagreement--the lessons learnt from malaria diagnosis in Mpumalanga," *S Afr Med J,* vol. 87, pp. 609-11, May 1997.

[134] J. D. Maguire, E. R. Lederman, M. J. Barcus, W. A. P. O'Meara, R. G. Jordon, S. Duong, *et al.*, "Production and validation of durable, high quality standardized malaria microscopy slides for teaching, testing and quality assurance during an era of declining diagnostic proficiency," *Malaria Journal,* vol. 5, pp. 1-8, 2006.

[135] C. Wongsrichanalai, M. J. Barcus, S. Muth, A. Sutamihardja, and W. H. Wernsdorfer, "A review of malaria diagnostic tools: microscopy and rapid diagnostic test (RDT)," *Am J Trop Med Hyg,* vol. 77, pp. 119-27, Dec 2007.

[136] L. M. Milne, M. S. Kyi, P. L. Chiodini, and D. C. Warhurst, "Accuracy of routine laboratory diagnosis of malaria in the United Kingdom," *Journal of Clinical Pathology,* vol. 47, pp. 740-742, 1994.

[137] C. K. Murray, R. A. Gasser, Jr., A. J. Magill, and R. S. Miller, "Update on rapid diagnostic testing for malaria," *Clin Microbiol Rev,* vol. 21, pp. 97-110, Jan 2008.

[138] W. H. Organization, "Malaria diagnosis: memorandum from a WHO meeting," *Bulletin of the World Health Organization (WHO),* vol. 66, pp. 575-94, 1988.

[139] E. Lo, G. Zhou, W. Oo, Y. Afrane, A. Githeko, and G. Yan, "Low parasitemia in submicroscopic infections significantly impacts malaria diagnostic sensitivity in the highlands of Western Kenya," *PLoS One,* vol. 10, p. e0121763, 2015.

[140] S. Moura, C. Fançony, C. Mirante, M. Neves, L. Bernardino, F. Fortes, *et al.*, "Impact of a training course on the quality of malaria diagnosis by microscopy in Angola," *Malaria Journal,* vol. 13, pp. 1-7, 2014/11/18 2014.

[141] S. E. Francis, D. J. Sullivan, Jr., and D. E. Goldberg, "Hemoglobin metabolism in the malaria parasite Plasmodium falciparum," *Annu Rev Microbiol,* vol. 51, pp. 97-123, 1997.

[142] R. Carter and R. W. Gwadz, "Infectiousness and gamete immunization in malaria," *Research in Malaria. Volume,* vol. 3, pp. 263-298, 1980.

[143] D. E. Goldberg, A. F. Slater, A. Cerami, and G. B. Henderson, "Hemoglobin degradation in the malaria parasite Plasmodium falciparum: an ordered process in a unique organelle," *Proc Natl Acad Sci U S A,* vol. 87, pp. 2931-5, Apr 1990.

[144] S. Hackett, J. Hamzah, T. M. E. Davis, and T. G. St Pierre, "Magnetic susceptibility of iron in malaria-infected red blood cells," *Biochimica et Biophysica Acta (BBA) - Molecular Basis of Disease,* vol. 1792, pp. 93-99, 2// 2009.

[145] L. R. Moore, H. Fujioka, P. S. Williams, J. J. Chalmers, B. Grimberg, P. A. Zimmerman, *et al.*, "Hemoglobin degradation in malaria-infected erythrocytes determined from live cell magnetophoresis," *Faseb j,* vol. 20, pp. 747-9, Apr 2006.

[146] E. Y. Klein, "Antimalarial drug resistance: a review of the biology and strategies to delay emergence and spread," *Int J Antimicrob Agents,* vol. 41, pp. 311-7, Apr 2013.

[147] M. Kiggundu, S. L. Nsobya, M. R. Kamya, S. Filler, S. Nasr, G. Dorsey, *et al.*, "Evaluation of a Comprehensive Refresher Training Program in Malaria Microscopy Covering Four Districts of Uganda," *Am J Trop Med Hyg,* vol. 84, pp. 820-4, May 5 2011.

[148] J. Nankabirwa, D. Zurovac, J. N. Njogu, J. B. Rwakimari, H. Counihan, R. W. Snow, *et al.*, "Malaria misdiagnosis in Uganda--implications for policy change," *Malar J,* vol. 8, p. 66, 2009.

[149] M. Zborowski, G. R. Ostera, L. R. Moore, S. Milliron, J. J. Chalmers, and A. N. Schechter, "Red blood cell magnetophoresis," *Biophys J,* vol. 84, pp. 2638-45, Apr 2003.

[150] J. P. Shelby, J. White, K. Ganesan, P. K. Rathod, and D. T. Chiu, "A microfluidic model for single-cell capillary obstruction by Plasmodium falciparum-infected erythrocytes," *Proc Natl Acad Sci U S A,* vol. 100, pp. 14618-22, Dec 9 2003.

[151] J. D. Adams, U. Kim, and H. T. Soh, "Multitarget magnetic activated cell sorter," *Proceedings of the National Academy of Sciences,* November 17, 2008 2008.

[152] F. Paul, D. Melville, and S. Roath, "Inviscid approximation trajectories in high gradient magnetic separation," *Magnetics, IEEE Transactions on,* vol. 18, pp. 792-795, 1982.

[153] J. Svoboda, "Separation of red blood cells by magnetic means," *Journal of Magnetism and Magnetic Materials,* vol. 220, pp. 103-105, 10// 2000.

[154] N. Pamme, "Continuous flow separations in microfluidic devices," *Lab Chip,* vol. 7, pp. 1644-59, Dec 2007.

[155] M. Suwa and H. Watarai, "Magnetoanalysis of micro/nanoparticles: a review," *Anal Chim Acta,* vol. 690, pp. 137-47, Apr 1 2011.

[156] A. Eisenträger, D. Vella, and I. M. Griffiths, "Particle capture efficiency in a multi-wire model for high gradient magnetic separation," *Applied Physics Letters,* vol. 105, p. 033508, 2014.

[157] S. Shaw, P. V. S. N. Murthy, and P. Sibanda, "Magnetic drug targeting in a permeable microvessel," *Microvascular Research,* vol. 85, pp. 77-85, 1// 2013.

[158] P. A. Zimmerman, J. M. Thomson, H. Fujioka, W. E. Collins, and M. Zborowski, "Diagnosis of malaria by magnetic deposition microscopy," *Am J Trop Med Hyg,* vol. 74, pp. 568-72, Apr 2006.

[159] S. C. Oaks Jr, V. S. Mitchell, G. W. Pearson, and C. C. Carpenter, *Malaria: obstacles and opportunities*: National Academies Press, 1991.

[160] L. L. Ekawati, H. Herdiana, M. E. Sumiwi, C. Barussanah, C. Ainun, S. Sabri*, et al.*, "A comprehensive assessment of the malaria microscopy system of Aceh, Indonesia, in preparation for malaria elimination," *Malaria Journal,* vol. 14, pp. 1-17, 2015.

[161] D. Mozaffarian, E. J. Benjamin, A. S. Go, D. K. Arnett, M. J. Blaha, M. Cushman*, et al.*, "Heart Disease and Stroke Statistics—2016 Update," *A Report From the American Heart Association,* 2015.

[162] U. Sigwart, J. Puel, V. Mirkovitch, F. Joffre, and L. Kappenberger, "Intravascular stents to prevent occlusion and restenosis after transluminal angioplasty," *N Engl J Med,* vol. 316, pp. 701-6, Mar 19 1987.

[163] A. J. Lansky, G. S. Roubin, C. D. O'Shaughnessy, P. B. Moore, L. S. Dean, A. E. Raizner*, et al.*, "Randomized Comparison of GR-II Stent and Palmaz-Schatz Stent for Elective Treatment of Coronary Stenoses," *Circulation,* vol. 102, pp. 1364-1368, 2000.

[164] J. Iqbal, J. Gunn, and P. W. Serruys, "Coronary stents: historical development, current status and future directions," *Br Med Bull,* vol. 106, pp. 193-211, 2013.

[165] A. Fortier, V. Gullapalli, and R. A. Mirshams, "Review of biomechanical studies of arteries and their effect on stent performance," *IJC Heart & Vessels,* vol. 4, pp. 12-18, 2014 2014.

[166] E. Wajnberg, G. Rodrigues, and D. G. Abud, "O uso de stents farmacológicos no tratamento da estenose das artérias vertebrais," *Radiologia Brasileira,* vol. 44, pp. 343-348, 2011.

[167] M. E. Wiisanen, A. Abdel-Latif, D. Mukherjee, and K. M. Ziada, "Drug-eluting stents versus bare-metal stents in saphenous vein graft interventions: a systematic review and meta-analysis," *JACC Cardiovasc Interv,* vol. 3, pp. 1262-73, Dec 2010.

[168] H. Hamid and J. Coltart, "'Miracle stents' - a future without restenosis," *McGill Journal of Medicine : MJM,* vol. 10, pp. 105-111, 2007.

[169] A. K. Mitra and D. K. Agrawal, "In stent restenosis: bane of the stent era," *J Clin Pathol,* vol. 59, pp. 232-9, Mar 2006.

[170] A. Kraitzer, Y. Kloog, and M. Zilberman, "Approaches for prevention of restenosis," *Journal of Biomedical Materials Research Part B: Applied Biomaterials,* vol. 85B, pp. 583-603, 2008.

[171] W. H. Maisel and W. K. Laskey, "Cardiology patient page. Drug-eluting stents," *Circulation,* vol. 115, pp. e426-7, May 01 2007.

[172] S. M. Seedial, S. Ghosh, R. S. Saunders, P. A. Suwanabol, X. Shi, B. Liu*, et al.*, "Local Drug Delivery to Prevent Restenosis," *Journal of vascular surgery,* vol. 57, pp. 1403-1414, 2013.

[173] M. Chorny, I. Fishbein, R. F. Adamo, S. P. Forbes, Z. Folchman-Wagner, and I. S. Alferiev, "Magnetically Targeted Delivery of Therapeutic Agents to Injured Blood Vessels for Prevention of In-Stent Stenosis," *Methodist DeBakey Cardiovascular Journal,* vol. 8, pp. 23-27, Jan-Mar 2012.

[174] B. Polyak, I. Fishbein, M. Chorny, I. Alferiev, D. Williams, B. Yellen*, et al.*, "High field gradient targeting of magnetic nanoparticle-loaded endothelial cells to the

surfaces of steel stents," *Proceedings of the National Academy of Sciences of the United States of America,* vol. 105, pp. 698-703, 01/08 09/05/received 2008.

[175] K. Hournkumnuard and M. Natenapit, "Magnetic drug targeting by ferromagnetic microwires implanted within blood vessels," *Med Phys,* vol. 40, p. 062302, Jun 2013.

[176] H. Chen, M. D. Kaminski, P. Pytel, L. Macdonald, and A. J. Rosengart, "Capture of magnetic carriers within large arteries using external magnetic fields," *J Drug Target,* vol. 16, pp. 262-8, May 2008.

[177] J. B. Freund and B. Shapiro, "Transport of particles by magnetic forces and cellular blood flow in a model microvessel," *Physics of Fluids,* vol. 24, p. 051904, 2012.

[178] M. El Feghaly, P. Soula, H. Rousseau, F. Chaiban, P. Otal, F. Joffre*, et al.*, "Endovascular retrieval of two migrated venous stents by means of balloon catheters," *Journal of Vascular Surgery,* vol. 28, pp. 541-546, 9// 1998.

[179] L. Chen, "Effect of magnetic field orientation on high gradient magnetic separation performance," *Minerals Engineering,* vol. 24, pp. 88-90, 1// 2011.

[180] S. Shaw and P. V. S. N. Murthy, "Magnetic Drug Targeting in the Permeable Blood Vessel—The Effect of Blood Rheology," *Journal of Nanotechnology in Engineering and Medicine,* vol. 1, pp. 021001-021001, 2010.

[181] B. Gleich, N. Hellwig, H. Bridell, R. Jurgons, C. Seliger, C. Alexiou*, et al.*, "Design and Evaluation of Magnetic Fields for Nanoparticle Drug Targeting in Cancer," *Nanotechnology, IEEE Transactions on,* vol. 6, pp. 164-170, 2007.

[182] J. B. Freund, "Numerical Simulation of Flowing Blood Cells," *Annual Review of Fluid Mechanics,* vol. 46, pp. 67-95, 2014.

[183] H.-W. Yang, M.-Y. Hua, H.-L. Liu, C.-Y. Huang, and K.-C. Wei, "Potential of magnetic nanoparticles for targeted drug delivery," *Nanotechnology, Science and Applications,* vol. 5, pp. 73-86, 08/27 2012.

[184] S. Earnshaw, "On the nature of the molecular forces which regulate the constitution of the luminiferous ether.," *Trans. Camb. Phil. Soc,* vol. 7, pp. 97-112, // 1842.

[185] A. Moody, "Rapid diagnostic tests for malaria parasites," *Clin Microbiol Rev,* vol. 15, pp. 66-78, Jan 2002.

[186] C. S. Owen, "High gradient magnetic separation of erythrocytes," *Biophysical Journal,* vol. 22, pp. 171-178, 1978.

[187] W. Trager and J. B. Jensen, "Human malaria parasites in continuous culture," *Science,* vol. 193, pp. 673-5, Aug 20 1976.

[188] C. Lambros and J. P. Vanderberg, "Synchronization of Plasmodium falciparum erythrocytic stages in culture," *J Parasitol,* vol. 65, pp. 418-20, Jun 1979.

Appendix A.

Appendix A provides the derivation of the expression for magnetic force experienced by a magnetic particle in presence of a magnetic wire that is magnetized perpendicular to its axis and also perpendicular to the flow in a HGMS system.

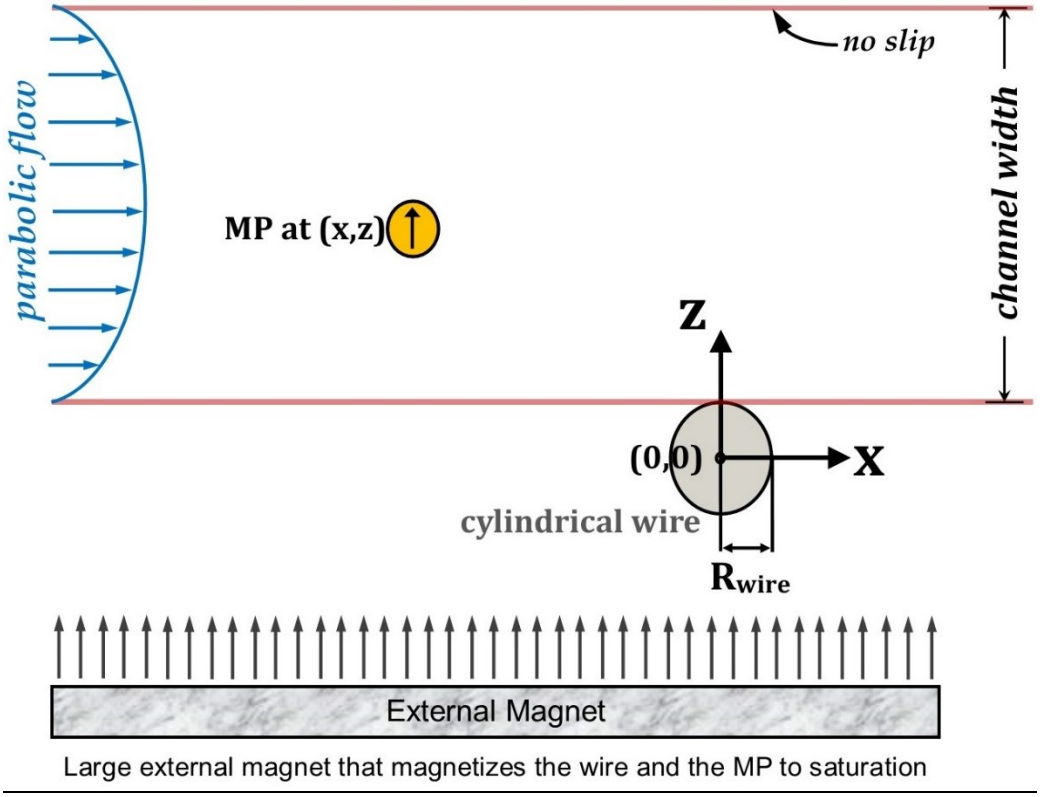

Magnetic Field in the x-z plane: This field is equal to the sum of the magnetic field of the wire and the external magnetizing field of the large external magnet.

$$\vec{B}\,(x,z) = \frac{\mu_0 M}{2} R_{wire}^2 [B_x(x,z).\hat{x} + B_z(x,z).\hat{z}] + B_0.\hat{z}$$

$$M = Magnetization\ of\ the\ wire\ in\ A/m$$

$$B_x(x,z) = \frac{2xz}{(x^2+z^2)^2} \qquad B_z(x,z) = \frac{z^2-x^2}{(x^2+z^2)^2}$$

Magnetic Field Gradients of the Infinite Cylindrical Wire's Field Components

$$B_x(x,z) = \frac{2xz}{(x^2+z^2)^2}$$

$$\frac{\partial}{\partial x}B_x(x,z) = \frac{(x^2+z^2)^2\frac{\partial}{\partial x}(2xz) - 2xz\frac{\partial}{\partial x}\{(x^2+z^2)^2\}}{\{(x^2+z^2)^2\}^2}$$

$$\frac{\partial}{\partial x}B_x(x,z) = \frac{(x^2+z^2)^2(2z) - 2xz\{2(x^2+z^2)(2x)\}}{\{(x^2+z^2)^2\}^2}$$

$$\frac{\partial}{\partial x}B_x(x,z) = \frac{(2z)(x^2+z^2)^2 - 8x^2z(x^2+z^2)}{\{(x^2+z^2)^2\}^2} = \frac{2z}{(x^2+z^2)^2} - \frac{8x^2z}{(x^2+z^2)^3}$$

$$\frac{\partial}{\partial x}B_x(x,z) = \frac{2z(x^2+z^2) - 8x^2z}{(x^2+z^2)^3} = \frac{2x^2z + 2z^3 - 8x^2z}{(x^2+z^2)^3} = \frac{2z^3 - 6x^2z}{(x^2+z^2)^3}$$

$$\frac{\partial}{\partial x}B_x(x,z) = \frac{-2z(3x^2 - z^2)}{(x^2+z^2)^3}$$

$$\frac{\partial}{\partial z}B_x(x,z) = \frac{(x^2+z^2)^2\frac{\partial}{\partial z}(2xz) - 2xz\frac{\partial}{\partial z}\{(x^2+z^2)^2\}}{\{(x^2+z^2)^2\}^2}$$

$$\frac{\partial}{\partial z}B_x(x,z) = \frac{(x^2+z^2)^2(2x) - 2xz\{2(x^2+z^2)(2z)\}}{\{(x^2+z^2)^2\}^2}$$

$$\frac{\partial}{\partial z}B_x(x,z) = \frac{(2x)(x^2+z^2)^2 - 8xz^2(x^2+z^2)}{\{(x^2+z^2)^2\}^2} = \frac{2x}{(x^2+z^2)^2} - \frac{8xz^2}{(x^2+z^2)^3}$$

$$\frac{\partial}{\partial z}B_x(x,z) = \frac{2x(x^2+z^2) - 8xz^2}{(x^2+z^2)^3} = \frac{2x^3 + 2xz^2 - 8xz^2}{(x^2+z^2)^3} = \frac{2x^3 - 6xz^2}{(x^2+z^2)^3}$$

$$\frac{\partial}{\partial z}B_x(x,z) = \frac{2x(x^2 - 3z^2)}{(x^2+z^2)^3}$$

$$B_z(x,z) = \frac{z^2 - x^2}{(x^2 + z^2)^2}$$

$$\frac{\partial}{\partial x} B_z(x,z) = \frac{(x^2 + z^2)^2 \frac{\partial}{\partial x}(z^2 - x^2) - (z^2 - x^2)\frac{\partial}{\partial x}\{(x^2 + z^2)^2\}}{\{(x^2 + z^2)^2\}^2}$$

$$\frac{\partial}{\partial x} B_z(x,z) = \frac{(x^2 + z^2)^2(-2x) - (z^2 - x^2)\{2(x^2 + z^2)(2x)\}}{\{(x^2 + z^2)^2\}^2}$$

$$\frac{\partial}{\partial x} B_z(x,z) = \frac{(-2x)(x^2 + z^2)^2 - 4x(z^2 - x^2)(x^2 + z^2)}{\{(x^2 + z^2)^2\}^2}$$

$$\frac{\partial}{\partial x} B_z(x,z) = -\frac{2x}{(x^2 + z^2)^2} - \frac{4x(z^2 - x^2)}{(x^2 + z^2)^3} = \frac{-2x(x^2 + z^2) - 4x(z^2 - x^2)}{(x^2 + z^2)^3}$$

$$\frac{\partial}{\partial x} B_z(x,z) = \frac{-2x^3 - 2xz^2 - 4xz^2 + 4x^3}{(x^2 + z^2)^3} = \frac{2x^3 - 6xz^2}{(x^2 + z^2)^3} = \frac{2x(x^2 - 3z^2)}{(x^2 + z^2)^3}$$

$$\frac{\partial}{\partial z} B_z(x,z) = \frac{(x^2 + z^2)^2 \frac{\partial}{\partial z}(z^2 - x^2) - (z^2 - x^2)\frac{\partial}{\partial z}\{(x^2 + z^2)^2\}}{\{(x^2 + z^2)^2\}^2}$$

$$\frac{\partial}{\partial z} B_z(x,z) = \frac{(x^2 + z^2)^2(2z) - (z^2 - x^2)\{2(x^2 + z^2)(2z)\}}{\{(x^2 + z^2)^2\}^2}$$

$$\frac{\partial}{\partial z} B_z(x,z) = \frac{(2z)(x^2 + z^2)^2 - 4z(z^2 - x^2)(x^2 + z^2)}{\{(x^2 + z^2)^2\}^2}$$

$$\frac{\partial}{\partial z} B_z(x,z) = \frac{2z}{(x^2 + z^2)^2} - \frac{4z(z^2 - x^2)}{(x^2 + z^2)^3} = \frac{2z(x^2 + z^2) - 4z(z^2 - x^2)}{(x^2 + z^2)^3}$$

$$\frac{\partial}{\partial z} B_z(x,z) = \frac{2x^2z + 2z^3 - 4z^3 + 4x^2z}{(x^2 + z^2)^3} = \frac{6x^2z - 2z^3}{(x^2 + z^2)^3} = \frac{2z(3x^2 - z^2)}{(x^2 + z^2)^3}$$

Magnetic Field Gradients of the Infinite Cylindrical Wire's Field Components Written in Simplified Form

$$B_x(x,z) = \frac{2xz}{(x^2+z^2)^2}$$

$$\frac{\partial}{\partial x}B_x(x,z) = \frac{-2z(3x^2-z^2)}{(x^2+z^2)^3}$$

$$\frac{\partial}{\partial z}B_x(x,z) = \frac{2x(x^2-3z^2)}{(x^2+z^2)^3}$$

$$B_z(x,z) = \frac{z^2-x^2}{(x^2+z^2)^2}$$

$$\frac{\partial}{\partial x}B_z(x,z) = \frac{2x(x^2-3z^2)}{(x^2+z^2)^3}$$

$$\frac{\partial}{\partial z}B_z(x,z) = \frac{2z(3x^2-z^2)}{(x^2+z^2)^3}$$

Determining Magnetic Force

$$\vec{B}\,(x,z) = \frac{\mu_0 M}{2} R_{wire}^2 [B_x(x,z).\hat{x} + B_z(x,z).\hat{z}] + B_0.\hat{z}$$

or

$$\vec{B}\,(x,z) = \frac{\mu_0 M}{2} R_{wire}^2 [B_x(x,z).\hat{x} + B_{z0}(x,z).\hat{z}]$$

where

$$B_{z0} = B_z + {B_0}\Big/{\frac{\mu_0 M\, R_{wire}^2}{2}}$$

$$\vec{F}_m(x,z) = F_{mx}(x,z).\hat{x} + F_{mz}(x,z).\hat{z}$$

$$\vec{F}_m(x,z) = |\vec{m}|\big(\hat{B}.\nabla\big)\vec{B} = \frac{|\vec{m}|}{|\vec{B}|}\big(\vec{B}.\nabla\big)\vec{B}$$

$$m = magnetic\ moment; units = Am^2$$

$$\vec{F}_m(x,z) = Am^2\frac{T}{m} = Am^2\frac{N}{Am}\frac{1}{m} = N$$

$$\big(\vec{B}.\nabla\big) = \frac{\mu_0 M}{2} R_{wire}^2 \left(B_x\frac{\partial}{\partial x} + B_{z0}\frac{\partial}{\partial z}\right)$$

$$\big(\vec{B}.\nabla\big)\vec{B} = \frac{\mu_0 M}{2} R_{wire}^2 \left(B_x\frac{\partial}{\partial x} + B_{z0}\frac{\partial}{\partial z}\right)\frac{\mu_0 M}{2} R_{wire}^2 (B_x.\hat{x} + B_{z0}.\hat{z})$$

$$\big(\vec{B}.\nabla\big)\vec{B} = \left(\frac{\mu_0 M}{2} R_{wire}^2\right)^2 \left[\left(B_x\frac{\partial B_x}{\partial x} + B_{z0}\frac{\partial B_x}{\partial z}\right).\hat{x} + \left(B_x\frac{\partial B_{z0}}{\partial x} + B_{z0}\frac{\partial B_{z0}}{\partial z}\right).\hat{z}\right]$$

Evaluating Magnetic Force Components

$$F_{mx}(x,z).\hat{x} = \frac{|\vec{m}|}{|\vec{B}|}\left(\frac{\mu_0 M}{2}R_{wire}^2\right)^2\left(B_x\frac{\partial B_x}{\partial x} + B_{z0}\frac{\partial B_x}{\partial z}\right)$$

$$F_{mz}(x,z).\hat{z} = \frac{|\vec{m}|}{|\vec{B}|}\left(\frac{\mu_0 M}{2}R_{wire}^2\right)^2\left(B_x\frac{\partial B_{z0}}{\partial x} + B_{z0}\frac{\partial B_{z0}}{\partial z}\right)$$

$$|\vec{B}| = \frac{\mu_0 M}{2}R_{wire}^2\sqrt{(B_x)^2 + \left(B_z + \frac{B_0}{\frac{\mu_0 M\, R_{wire}^2}{2}}\right)^2}$$

$$B_x\frac{\partial B_x}{\partial x} = (B_x)\left(\frac{\partial}{\partial x}B_x(x,z)\right)$$

$$B_{z0}\frac{\partial B_x}{\partial z} = \left(B_z + \frac{B_0}{\frac{\mu_0 M\, R_{wire}^2}{2}}\right)\left(\frac{\partial}{\partial z}B_x(x,z)\right)$$

$$B_x\frac{\partial B_{z0}}{\partial x} = (B_x)\left(\frac{\partial}{\partial x}B_z(x,z) + \frac{\partial}{\partial x}\frac{B_0}{\frac{\mu_0 M\, R_{wire}^2}{2}}\right) = (B_x)\frac{\partial}{\partial x}B_z(x,z)$$

$$B_{z0}\frac{\partial B_{z0}}{\partial z} = (B_{z0})\left(\frac{\partial}{\partial z}B_z(x,z) + \frac{\partial}{\partial z}\frac{B_0}{\frac{\mu_0 M\, R_{wire}^2}{2}}\right) = (B_{z0})\frac{\partial}{\partial z}B_z(x,z)$$

Magnitude of the Magnetic Field

$$|\vec{B}| = \frac{\mu_0 M}{2} R_{wire}^2 \sqrt{(B_x)^2 + \left(B_z + \frac{B_0}{\frac{\mu_0 M\, R_{wire}^2}{2}} \right)^2}$$

$$Let's\ say, \qquad \frac{\mu_0 M}{2} R_{wire}^2 = k$$

$$|\vec{B}| = k \sqrt{(B_x)^2 + \left(B_z + \frac{B_0}{k} \right)^2}$$

$$|\vec{B}| = k \sqrt{\left\{ \frac{2xz}{(x^2 + z^2)^2} \right\}^2 + \left\{ \frac{z^2 - x^2}{(x^2 + z^2)^2} + \frac{B_0}{k} \right\}^2}$$

Determining Axial Component of the Magnetic Force

$$F_{mx}(x,z).\hat{x} = \frac{|\vec{m}|}{|\vec{B}|}\left(\frac{\mu_0 M}{2}R_{wire}^2\right)^2\left(B_x\frac{\partial B_x}{\partial x} + B_{z0}\frac{\partial B_x}{\partial z}\right)$$

$$F_{mx}(x,z).\hat{x} = \frac{|\vec{m}|k^2}{|\vec{B}|}\left[(B_x)\left(\frac{\partial}{\partial x}B_x(x,z)\right) + (B_{z0})\left(\frac{\partial}{\partial z}B_x(x,z)\right)\right]$$

$$F_{mx}(x,z).\hat{x} = \frac{|\vec{m}|k^2}{|\vec{B}|}\left[\left\{\frac{2xz}{(x^2+z^2)^2}\right\}\left\{\frac{-2z(3x^2-z^2)}{(x^2+z^2)^3}\right\} + \left\{\frac{z^2-x^2}{(x^2+z^2)^2} + \frac{B_0}{k}\right\}\left\{\frac{2x(x^2-3z^2)}{(x^2+z^2)^3}\right\}\right]$$

$$F_{mx}(x,z).\hat{x} = \frac{|\vec{m}|k^2}{|\vec{B}|}\left[\left\{\frac{2xz}{(x^2+z^2)^2}\right\}\left\{\frac{-2z(3x^2-z^2)}{(x^2+z^2)^3}\right\} + \left\{\frac{z^2-x^2}{(x^2+z^2)^2}\right\}\left\{\frac{2x(x^2-3z^2)}{(x^2+z^2)^3}\right\} + \left(\frac{B_0}{k}\right)\left\{\frac{2x(x^2-3z^2)}{(x^2+z^2)^3}\right\}\right]$$

$$F_{mx}(x,z).\hat{x} = \frac{|\vec{m}|k^2}{|\vec{B}|}\left[\left\{\frac{2xz\{-2z(3x^2-z^2)\} + (z^2-x^2)\{2x(x^2-3z^2)\}}{(x^2+z^2)^5}\right\} + \left(\frac{B_0}{k}\right)\left\{\frac{2x(x^2-3z^2)}{(x^2+z^2)^3}\right\}\right]$$

$$F_{mx}(x,z).\hat{x} = \frac{|\vec{m}|k^2}{|\vec{B}|}\left[\left\{\frac{-4xz^2(3x^2-z^2) + (z^2-x^2)(2x^3-6xz^2)}{(x^2+z^2)^5}\right\} + \left(\frac{B_0}{k}\right)\left\{\frac{2x(x^2-3z^2)}{(x^2+z^2)^3}\right\}\right]$$

$$F_{mx}(x,z).\hat{x} = \frac{|\vec{m}|k^2}{|\vec{B}|}\left[\left\{\frac{-12x^3z^2 + 4xz^4 + z^2(2x^3 - 6xz^2) - x^2(2x^3 - 6xz^2)}{(x^2+z^2)^5}\right\} + \left(\frac{B_0}{k}\right)\left\{\frac{2x(x^2-3z^2)}{(x^2+z^2)^3}\right\}\right]$$

$$F_{mx}(x,z).\hat{x} = \frac{|\vec{m}|k^2}{|\vec{B}|}\left[\left\{\frac{-12x^3z^2 + 4xz^4 + 2x^3z^2 - 6xz^4 - 2x^5 + 6x^3z^2}{(x^2+z^2)^5}\right\} + \left(\frac{B_0}{k}\right)\left(\frac{2x(x^2-3z^2)}{(x^2+z^2)^3}\right)\right]$$

$$F_{mx}(x,z).\hat{x} = \frac{|\vec{m}|k^2}{|\vec{B}|}\left[\left\{\frac{-4x^3z^2 - 2xz^4 - 2x^5}{(x^2+z^2)^5}\right\} + \left(\frac{B_0}{k}\right)\left\{\frac{2x(x^2-3z^2)}{(x^2+z^2)^3}\right\}\right]$$

$$F_{mx}(x,z).\hat{x} = \frac{|\vec{m}|k^2}{|\vec{B}|}\left[\left\{\frac{-2x(2x^2z^2 + z^4 + x^4)}{(x^2+z^2)^5}\right\} + \left(\frac{B_0}{k}\right)\left\{\frac{2x(x^2-3z^2)}{(x^2+z^2)^3}\right\}\right]$$

$$F_{mx}(x,z).\hat{x} = \frac{|\vec{m}|k^2}{|\vec{B}|}\left[\left\{\frac{-2x(x^2+z^2)^2}{(x^2+z^2)^5}\right\} + \left(\frac{B_0}{k}\right)\left\{\frac{2x(x^2-3z^2)}{(x^2+z^2)^3}\right\}\right]$$

$$F_{mx}(x,z).\hat{x} = \frac{|\vec{m}|k^2}{|\vec{B}|}\left[\frac{-2x}{(x^2+z^2)^3} + \left(\frac{B_0}{k}\right)\left\{\frac{2x(x^2-3z^2)}{(x^2+z^2)^3}\right\}\right]$$

$$F_{mx}(x,z).\hat{x} = \frac{|\vec{m}|k^2}{|\vec{B}|}\left[\frac{-2kx + B_0\{2x(x^2-3z^2)\}}{k(x^2+z^2)^3}\right]$$

$$F_{mx}(x,z).\hat{x} = \frac{|\vec{m}|k}{|\vec{B}|}\left[\frac{-2kx + B_0\{2x(x^2-3z^2)\}}{(x^2+z^2)^3}\right]$$

$$F_{mx}(x,z).\hat{x} = \frac{|\vec{m}|k}{|\vec{B}|}\left[\frac{-2kx + B_0(2x^3 - 6xz^2)}{(x^2+z^2)^3}\right]$$

$$F_{mx}(x,z).\hat{x} = \frac{|\vec{m}|k}{|\vec{B}|}\left[\frac{-2kx + 2x^3B_0 - 6xz^2B_0}{(x^2+z^2)^3}\right]$$

$$F_{mx}(x,z).\hat{x} = \frac{|\vec{m}|k}{|\vec{B}|}\left[\frac{-2x(k - x^2B_0 + 3z^2B_0)}{(x^2+z^2)^3}\right]$$

$$F_{mx}(x,z).\hat{x} = \frac{|\vec{m}|k}{|\vec{B}|}\left[\frac{-2x(-x^2B_0 + 3z^2B_0 + k)}{(x^2+z^2)^3}\right]$$

$$F_{mx}(x,z).\hat{x} = |\vec{m}|\frac{\left[\frac{-2x(-x^2B_0 + 3z^2B_0 + k)}{(x^2+z^2)^3}\right]}{\sqrt{\left\{\frac{2xz}{(x^2+z^2)^2}\right\}^2 + \left\{\frac{z^2-x^2}{(x^2+z^2)^2} + \frac{B_0}{k}\right\}^2}}$$

Determining Perpendicular Component of the Magnetic Force

$$F_{mz}(x,z).\hat{z} = \frac{|\vec{m}|}{|\vec{B}|}\left(\frac{\mu_0 M}{2}R_{wire}^2\right)^2\left(B_x\frac{\partial B_{z0}}{\partial x} + B_{z0}\frac{\partial B_{z0}}{\partial z}\right)$$

$$F_{mz}(x,z).\hat{z} = \frac{|\vec{m}|k^2}{|\vec{B}|}\left[(B_x)\left(\frac{\partial}{\partial x}B_{z0}(x,z)\right) + (B_{z0})\left(\frac{\partial}{\partial z}B_{z0}(x,z)\right)\right]$$

$$F_{mz}(x,z).\hat{z} = \frac{|\vec{m}|k^2}{|\vec{B}|}\left[(B_x)\left(\frac{\partial}{\partial x}B_z(x,z)\right) + \left(B_z + \frac{B_0}{k}\right)\left(\frac{\partial}{\partial z}B_z(x,z)\right)\right]$$

$$F_{mz}(x,z).\hat{z} = \frac{|\vec{m}|k^2}{|\vec{B}|}\left[(B_x)\left(\frac{\partial}{\partial x}B_z(x,z)\right) + (B_z)\left(\frac{\partial}{\partial z}B_z(x,z)\right) + \left(\frac{B_0}{k}\right)\left(\frac{\partial}{\partial z}B_z(x,z)\right)\right]$$

$$F_{mz}(x,z).\hat{z} = \frac{|\vec{m}|k^2}{|\vec{B}|}\left[\left\{\frac{2xz}{(x^2+z^2)^2}\right\}\left\{\frac{2x(x^2-3z^2)}{(x^2+z^2)^3}\right\} + \left\{\frac{z^2-x^2}{(x^2+z^2)^2}\right\}\left\{\frac{2z(3x^2-z^2)}{(x^2+z^2)^3}\right\} + \left(\frac{B_0}{k}\right)\left\{\frac{2z(3x^2-z^2)}{(x^2+z^2)^3}\right\}\right]$$

$$F_{mz}(x,z).\hat{z} = \frac{|\vec{m}|k^2}{|\vec{B}|}\left[\left\{\frac{2xz}{(x^2+z^2)^2}\right\}\left\{\frac{2x^3-6xz^2}{(x^2+z^2)^3}\right\} + \left\{\frac{z^2-x^2}{(x^2+z^2)^2}\right\}\left\{\frac{6x^2z-2z^3}{(x^2+z^2)^3}\right\} + \left(\frac{B_0}{k}\right)\left\{\frac{6x^2z-2z^3}{(x^2+z^2)^3}\right\}\right]$$

$$F_{mz}(x,z).\hat{z} = \frac{|\vec{m}|k^2}{|\vec{B}|}\left[\left\{\frac{2xz(2x^3-6xz^2)}{(x^2+z^2)^5}\right\} + \left\{\frac{z^2(6x^2z-2z^3)-x^2(6x^2z-2z^3)}{(x^2+z^2)^5}\right\} + \left(\frac{B_0}{k}\right)\left\{\frac{6x^2z-2z^3}{(x^2+z^2)^3}\right\}\right]$$

$$F_{mz}(x,z).\hat{z} = \frac{|\vec{m}|k^2}{|\vec{B}|}\left[\left\{\frac{4x^4z - 12x^2z^3}{(x^2+z^2)^5}\right\} + \left\{\frac{6x^2z^3 - 2z^5 - 6x^4z + 2x^2z^3}{(x^2+z^2)^5}\right\} + \left(\frac{B_0}{k}\right)\left\{\frac{6x^2z - 2z^3}{(x^2+z^2)^3}\right\}\right]$$

$$F_{mz}(x,z).\hat{z} = \frac{|\vec{m}|k^2}{|\vec{B}|}\left[\left\{\frac{4x^4z - 12x^2z^3 + 6x^2z^3 - 2z^5 - 6x^4z + 2x^2z^3}{(x^2+z^2)^5}\right\} + \left(\frac{B_0}{k}\right)\left\{\frac{6x^2z - 2z^3}{(x^2+z^2)^3}\right\}\right]$$

$$F_{mz}(x,z).\hat{z} = \frac{|\vec{m}|k^2}{|\vec{B}|}\left[\left\{\frac{-4x^2z^3 - 2z^5 - 2x^4z}{(x^2+z^2)^5}\right\} + \left(\frac{B_0}{k}\right)\left\{\frac{6x^2z - 2z^3}{(x^2+z^2)^3}\right\}\right]$$

$$F_{mz}(x,z).\hat{z} = \frac{|\vec{m}|k^2}{|\vec{B}|}\left[\left\{\frac{-2z(2x^2z^2 + z^4 + x^4}{(x^2+z^2)^5}\right\} + \left(\frac{B_0}{k}\right)\left\{\frac{6x^2z - 2z^3}{(x^2+z^2)^3}\right\}\right]$$

$$F_{mz}(x,z).\hat{z} = \frac{|\vec{m}|k^2}{|\vec{B}|}\left[\left\{\frac{-2z(x^2+z^2)^2}{(x^2+z^2)^5}\right\} + \left(\frac{B_0}{k}\right)\left\{\frac{6x^2z - 2z^3}{(x^2+z^2)^3}\right\}\right]$$

$$F_{mz}(x,z).\hat{z} = \frac{|\vec{m}|k^2}{|\vec{B}|}\left[\frac{-2z}{(x^2+z^2)^3} + \left(\frac{B_0}{k}\right)\left\{\frac{6x^2z - 2z^3}{(x^2+z^2)^3}\right\}\right]$$

$$F_{mz}(x,z).\hat{z} = \frac{|\vec{m}|k^2}{|\vec{B}|}\left[\frac{-2kz + 6B_0x^2z - 2B_0z^3}{k(x^2+z^2)^3}\right]$$

$$F_{mz}(x,z).\hat{z} = \frac{|\vec{m}|k}{|\vec{B}|}\left[\frac{-2z(-3B_0x^2 + B_0z^2 + k)}{(x^2+z^2)^3}\right]$$

$$F_{mz}(x,z).\hat{z} = |\vec{m}| \frac{\left[\frac{-2z(-3B_0x^2 + B_0z^2 + k)}{(x^2+z^2)^3}\right]}{\sqrt{\left\{\frac{2xz}{(x^2+z^2)^2}\right\}^2 + \left\{\frac{z^2-x^2}{(x^2+z^2)^2} + \frac{B_0}{k}\right\}^2}}$$

Expression for the axial component of magnetic force:

$$F_{mx}(x,z).\hat{x} = |\vec{m}| \frac{\left[\frac{-2x(-x^2B_0 + 3z^2B_0 + k)}{(x^2+z^2)^3}\right]}{\sqrt{\left\{\frac{2xz}{(x^2+z^2)^2}\right\}^2 + \left\{\frac{z^2-x^2}{(x^2+z^2)^2} + \frac{B_0}{k}\right\}^2}}$$

Expression for the perpendicular component of magnetic force:

$$F_{mz}(x,z).\hat{z} = |\vec{m}| \frac{\left[\frac{-2z(-3B_0x^2 + B_0z^2 + k)}{(x^2+z^2)^3}\right]}{\sqrt{\left\{\frac{2xz}{(x^2+z^2)^2}\right\}^2 + \left\{\frac{z^2-x^2}{(x^2+z^2)^2} + \frac{B_0}{k}\right\}^2}}$$

Appendix B.

Appendix B provides the derivation of the expression for magnetic force experienced by a magnetic particle in presence of a magnetic wire that is magnetized perpendicular to its axis and along the flow in a HGMS system.

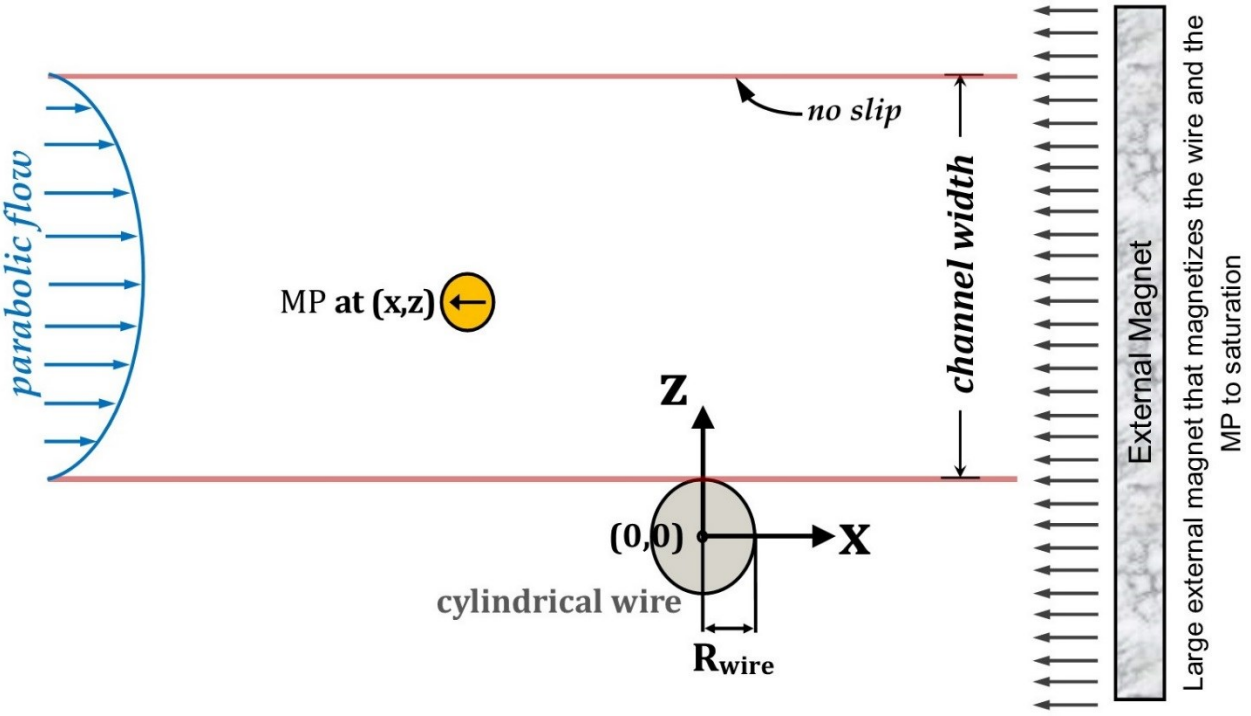

Magnetic Field in the x-z plane: This field is equal to the sum of the magnetic field of the wire and the external magnetizing field of the large external magnet.

$$\vec{B}\,(x,z) = \frac{\mu_0 M}{2} R_{wire}^2 [B_x(x,z).\hat{x} + B_z(x,z).\hat{z}] + B_0.\hat{x}$$

$$M = Magnetization\ of\ the\ wire\ in\ A/m$$

$$B_x(x,z) = \frac{x^2 - z^2}{(x^2 + z^2)^2} \qquad B_z(x,z) = \frac{2xz}{(x^2 + z^2)^2}$$

Magnetic Field Gradients of the Infinite Cylindrical Wire's Field Components:

$$B_x(x,z) = \frac{x^2 - z^2}{(x^2 + z^2)^2}$$

$$\frac{\partial}{\partial x} B_x(x,z) = \frac{(x^2+z^2)^2 \frac{\partial}{\partial x}(x^2 - z^2) - (x^2 - z^2)\frac{\partial}{\partial x}\{(x^2+z^2)^2\}}{\{(x^2+z^2)^2\}^2}$$

$$\frac{\partial}{\partial x} B_x(x,z) = \frac{(x^2+z^2)^2(2x) - (x^2 - z^2)\{2(x^2+z^2)(2x)\}}{\{(x^2+z^2)^2\}^2}$$

$$\frac{\partial}{\partial x} B_x(x,z) = \frac{(2x)(x^2+z^2)^2 - 4x(x^2+z^2)(x^2 - z^2)}{\{(x^2+z^2)^2\}^2}$$

$$\frac{\partial}{\partial x} B_x(x,z) = \frac{2x}{(x^2+z^2)^2} - \frac{4x(x^2 - z^2)}{(x^2+z^2)^3} = \frac{2x(x^2+z^2) - 4x(x^2 - z^2)}{(x^2+z^2)^3}$$

$$\frac{\partial}{\partial x} B_x(x,z) = \frac{2x^3 + 2xz^2 - 4x^3 + 4xz^2}{(x^2+z^2)^3} = \frac{-2x^3 + 6xz^2}{(x^2+z^2)^3}$$

$$= -\frac{2x(x^2 - 3z^2)}{(x^2+z^2)^3}$$

$$\frac{\partial}{\partial z} B_x(x,z) = \frac{(x^2+z^2)^2 \frac{\partial}{\partial z}(x^2 - z^2) - (x^2 - z^2)\frac{\partial}{\partial z}\{(x^2+z^2)^2\}}{\{(x^2+z^2)^2\}^2}$$

$$\frac{\partial}{\partial z} B_x(x,z) = \frac{(x^2+z^2)^2(-2z) - (x^2 - z^2)\{2(x^2+z^2)(2z)\}}{\{(x^2+z^2)^2\}^2}$$

$$\frac{\partial}{\partial z} B_x(x,z) = \frac{(-2z)(x^2+z^2)^2 - 4z(x^2+z^2)(x^2 - z^2)}{\{(x^2+z^2)^2\}^2}$$

$$\frac{\partial}{\partial z} B_x(x,z) = \frac{-2z}{(x^2+z^2)^2} - \frac{4z(x^2 - z^2)}{(x^2+z^2)^3} = \frac{-2z(x^2+z^2) - 4z(x^2 - z^2)}{(x^2+z^2)^3}$$

$$\frac{\partial}{\partial z} B_x(x,z) = \frac{-2x^2z - 2z^3 - 4x^2z + 4z^3}{(x^2+z^2)^3} = \frac{2z^3 - 6x^2z}{(x^2+z^2)^3}$$

$$= -\frac{2z(3x^2 - z^2)}{(x^2+z^2)^3}$$

$$B_z(x,z) = \frac{2xz}{(x^2+z^2)^2}$$

$$\frac{\partial}{\partial x}B_z(x,z) = \frac{(x^2+z^2)^2\frac{\partial}{\partial x}(2xz) - 2xz\frac{\partial}{\partial x}\{(x^2+z^2)^2\}}{\{(x^2+z^2)^2\}^2}$$

$$\frac{\partial}{\partial x}B_z(x,z) = \frac{(x^2+z^2)^2(2z) - 2xz\{2(x^2+z^2)(2x)\}}{\{(x^2+z^2)^2\}^2}$$

$$\frac{\partial}{\partial x}B_z(x,z) = \frac{(2z)(x^2+z^2)^2 - 8x^2z(x^2+z^2)}{\{(x^2+z^2)^2\}^2}$$

$$= \frac{2z}{(x'^2+z^2)^2} - \frac{8x^2z}{(x'^2+z^2)^3}$$

$$\frac{\partial}{\partial x}B_z(x,z) = \frac{2z(x^2+z^2) - 8x^2z}{(x'^2+z^2)^3} = \frac{2x^2z + 2z^3 - 8x^2z}{(x^2+z^2)^3}$$

$$\frac{\partial}{\partial x}B_z(x,z) = \frac{2z^3 - 6x^2z}{(x^2+z^2)^3} = \frac{-2z(3x^2-z^2)}{(x^2+z^2)^3}$$

$$\frac{\partial}{\partial z}B_z(x,z) = \frac{(x^2+z^2)^2\frac{\partial}{\partial z}(2xz) - 2xz\frac{\partial}{\partial z}\{(x^2+z^2)^2\}}{\{(x^2+z^2)^2\}^2}$$

$$\frac{\partial}{\partial z}B_z(x,z) = \frac{(x^2+z^2)^2(2x) - 2xz\{2(x^2+z^2)(2z)\}}{\{(x^2+z^2)^2\}^2}$$

$$\frac{\partial}{\partial z}B_z(x,z) = \frac{(2x)(x^2+z^2)^2 - 8xz^2(x^2+z^2)}{\{(x^2+z^2)^2\}^2}$$

$$\frac{\partial}{\partial z}B_z(x,z) = \frac{2x}{(x^2+z^2)^2} - \frac{8xz^2}{(x^2+z^2)^3}$$

$$\frac{\partial}{\partial z}B_z(x,z) = \frac{2x(x^2+z^2) - 8xz^2}{(x^2+z^2)^3} = \frac{2x^3 + 2xz^2 - 8xz^2}{(x^2+z^2)^3}$$

$$\frac{\partial}{\partial z}B_z(x,z) = \frac{2x^3 - 6xz^2}{(x^2+z^2)^3} = \frac{2x(x^2-3z^2)}{(x^2+z^2)^3}$$

Magnetic Field Gradients of the Infinite Cylindrical Wire's Field Components Written in Simplified Form:

$$B_x(x,z) = \frac{x^2 - z^2}{(x^2 + z^2)^2}$$

$$\frac{\partial}{\partial x} B_x(x,z) = -\frac{2x(x^2 - 3z^2)}{(x^2 + z^2)^3}$$

$$\frac{\partial}{\partial z} B_x(x,z) = -\frac{2z(3x^2 - z^2)}{(x^2 + z^2)^3}$$

$$B_z(x,z) = \frac{2xz}{(x^2 + z^2)^2}$$

$$\frac{\partial}{\partial x} B_z(x,z) = -\frac{2z(3x^2 - z^2)}{(x^2 + z^2)^3}$$

$$\frac{\partial}{\partial z} B_z(x,z) = \frac{2x(x^2 - 3z^2)}{(x^2 + z^2)^3}$$

Determining Magnetic Force

$$\vec{B}\ (x,z) = \frac{\mu_0 M}{2} R_{wire}^2 [B_x(x,z).\hat{x} + B_z(x,z).\hat{z}] + B_0.\hat{x}$$

or

$$\vec{B}\ (x,z) = \frac{\mu_0 M}{2} R_{wire}^2 [B_{x0}(x,z).\hat{x} + B_z(x,z).\hat{z}]$$

where

$$B_{x0} = B_x + {B_0}\Big/{\frac{\mu_0 M\ R_{wire}^2}{2}}$$

$$\vec{F}_m(x,z) = F_{mx}(x,z).\hat{x} + F_{mz}(x,z).\hat{z}$$

$$\vec{F}_m(x,z) = |\vec{m}|(\hat{B}.\nabla)\vec{B} = \frac{|\vec{m}|}{|\vec{B}|}(\vec{B}.\nabla)\vec{B}$$

$$m = magnetic\ moment; units = Am^2$$

$$\vec{F}_m(x,z) = Am^2 \frac{T}{m} = Am^2 \frac{N}{Am}\frac{1}{m} = N$$

$$(\vec{B}.\nabla) = \frac{\mu_0 M}{2} R_{wire}^2 \left(B_{x0}\frac{\partial}{\partial x} + B_z \frac{\partial}{\partial z}\right)$$

$$(\vec{B}.\nabla)\vec{B} = \frac{\mu_0 M}{2} R_{wire}^2 \left(B_{x0}\frac{\partial}{\partial x} + B_z \frac{\partial}{\partial z}\right)\frac{\mu_0 M}{2} R_{wire}^2 (B_{x0}.\hat{x} + B_z.\hat{z})$$

$$(\vec{B}.\nabla)\vec{B} = \left(\frac{\mu_0 M}{2} R_{wire}^2\right)^2 \left[\left(B_{x0}\frac{\partial B_{x0}}{\partial x} + B_z \frac{\partial B_{x0}}{\partial z}\right).\hat{x} + \left(B_{x0}\frac{\partial B_z}{\partial x} + B_z \frac{\partial B_z}{\partial z}\right).\hat{z}\right]$$

Evaluating Magnetic Force Components:

$$F_{mx}(x,z).\hat{x} = \frac{|\vec{m}|}{|\vec{B}|}\left(\frac{\mu_0 M}{2}R_{wire}^2\right)^2\left(B_{x0}\frac{\partial B_{x0}}{\partial x} + B_z\frac{\partial B_{x0}}{\partial z}\right)$$

$$F_{mz}(x,z).\hat{z} = \frac{|\vec{m}|}{|\vec{B}|}\left(\frac{\mu_0 M}{2}R_{wire}^2\right)^2\left(B_{x0}\frac{\partial B_z}{\partial x} + B_z\frac{\partial B_z}{\partial z}\right)$$

$$|\vec{B}| = \frac{\mu_0 M}{2}R_{wire}^2\sqrt{\left(B_x + \frac{B_0}{\frac{\mu_0 M\, R_{wire}^2}{2}}\right)^2 + (B_z)^2}$$

$$B_{x0}\frac{\partial B_{x0}}{\partial x} = \left(B_x + \frac{B_0}{\frac{\mu_0 M\, R_{wire}^2}{2}}\right)\left(\frac{\partial}{\partial x}B_x(x,z) + \frac{\partial}{\partial x}\frac{B_0}{\frac{\mu_0 M\, R_{wire}^2}{2}}\right)$$

$$B_z\frac{\partial B_{x0}}{\partial z} = (B_z)\left(\frac{\partial}{\partial z}B_x(x,z) + \frac{\partial}{\partial z}\frac{B_0}{\frac{\mu_0 M\, R_{wire}^2}{2}}\right)$$

$$B_{xo}\frac{\partial B_z}{\partial x} = \left(B_x + \frac{B_0}{\frac{\mu_0 M\, R_{wire}^2}{2}}\right)\left(\frac{\partial}{\partial x}B_z(x,z)\right)$$

$$B_z\frac{\partial B_z}{\partial z} = (B_z)\left(\frac{\partial}{\partial z}B_z(x,z)\right)$$

Magnitude of the Magnetic Field

$$\left|\vec{B}\right| = \frac{\mu_0 M}{2} R_{wire}^2 \sqrt{\left(B_x + \frac{B_0}{\frac{\mu_0 M\, R_{wire}^2}{2}} \right)^2 + (B_z)^2}$$

$$Let's\ say, \qquad \frac{\mu_0 M}{2} R_{wire}^2 = k$$

$$\left|\vec{B}\right| = k \sqrt{\left(B_x + \frac{B_0}{k} \right)^2 + (B_z)^2}$$

$$\left|\vec{B}\right| = k \sqrt{\left\{ \frac{x^2 - z^2}{(x^2 + z^2)^2} + \frac{B_0}{k} \right\}^2 + \left\{ \frac{2xz}{(x^2 + z^2)^2} \right\}^2}$$

Determining the Axial Component of the Magnetic Force:

$$F_{mx}(x,z).\hat{x} = \frac{|\vec{m}|}{|\vec{B}|}\left(\frac{\mu_0 M}{2}R_{wire}^2\right)^2\left(B_{x0}\frac{\partial B_{x0}}{\partial x} + B_z\frac{\partial B_{x0}}{\partial z}\right)$$

$$F_{mx}(x,z).\hat{x} = \frac{|\vec{m}|k^2}{|\vec{B}|}\left[\left(B_x + \frac{B_0}{k}\right)\left(\frac{\partial}{\partial x}B_x(x,z)\right) + (B_z)\left(\frac{\partial}{\partial z}B_x(x,z)\right)\right]$$

$$F_{mx}(x,z).\hat{x} = \frac{|\vec{m}|k^2}{|\vec{B}|}\left[\left\{\frac{x^2-z^2}{(x^2+z^2)^2} + \frac{B_0}{k}\right\}\left\{-\frac{2x(x^2-3z^2)}{(x^2+z^2)^3}\right\} + \left\{\frac{2xz}{(x^2+z^2)^2}\right\}\left\{-\frac{2z(3x^2-z^2)}{(x^2+z^2)^3}\right\}\right]$$

$$F_{mx}(x,z).\hat{x} = \frac{|\vec{m}|k^2}{|\vec{B}|}\left[\left\{\frac{x^2-z^2}{(x^2+z^2)^2}\right\}\left\{-\frac{2x(x^2-3z^2)}{(x^2+z^2)^3}\right\} + \left(\frac{B_0}{k}\right)\left\{-\frac{2x(x^2-3z^2)}{(x^2+z^2)^3}\right\} + \left\{\frac{2xz}{(x^2+z^2)^2}\right\}\left\{-\frac{2z(3x^2-z^2)}{(x^2+z^2)^3}\right\}\right]$$

$$F_{mx}(x,z).\hat{x} = \frac{|\vec{m}|k^2}{|\vec{B}|}\left[\left\{\frac{x^2-z^2}{(x^2+z^2)^2}\right\}\left\{\frac{-2x^3+6xz^2}{(x^2+z^2)^3}\right\} + \left(\frac{B_0}{k}\right)\left\{-\frac{2x(x^2-3z^2)}{(x^2+z^2)^3}\right\} + \left\{\frac{2xz}{(x^2+z^2)^2}\right\}\left\{\frac{-6x^2z+2z^3}{(x^2+z^2)^3}\right\}\right]$$

$$F_{mx}(x,z).\hat{x} = \frac{|\vec{m}|k^2}{|\vec{B}|}\left[\left\{\frac{x^2(-2x^3+6xz^2) - z^2(-2x^3+6xz^2)}{(x^2+z^2)^5}\right\} + \left(\frac{B_0}{k}\right)\left\{-\frac{2x(x^2-3z^2)}{(x^2+z^2)^3}\right\} + \left\{\frac{2xz(-6x^2z+2z^3)}{(x^2+z^2)^5}\right\}\right]$$

$$F_{mx}(x,z).\hat{x} = \frac{|\vec{m}|k^2}{|\vec{B}|}\left[\left\{\frac{-2x^5+6x^3z^2+2x^3z^2-6xz^4}{(x^2+z^2)^5}\right\} + \left(\frac{B_0}{k}\right)\left\{-\frac{2x(x^2-3z^2)}{(x^2+z^2)^3}\right\}+\left\{\frac{-12x^3z^2+4xz^4}{(x^2+z^2)^5}\right\}\right]$$

$$F_{mx}(x,z).\hat{x} = \frac{|\vec{m}|k^2}{|\vec{B}|}\left[\left\{\frac{-2x^5+6x^3z^2+2x^3z^2-6xz^4-12x^3z^2+4xz^4}{(x^2+z^2)^5}\right\} + \left(\frac{B_0}{k}\right)\left\{-\frac{2x(x^2-3z^2)}{(x^2+z^2)^3}\right\}\right]$$

$$F_{mx}(x,z).\hat{x} = \frac{|\vec{m}|k^2}{|\vec{B}|}\left[\left\{\frac{-2x^5-4x^3z^2-2xz^4}{(x^2+z^2)^5}\right\} + \left(\frac{B_0}{k}\right)\left\{-\frac{2x(x^2-3z^2)}{(x^2+z^2)^3}\right\}\right]$$

$$F_{mx}(x,z).\hat{x} = \frac{|\vec{m}|k^2}{|\vec{B}|}\left[\left\{\frac{-2x(x^4+2x^2z^2+z^4)}{(x^2+z^2)^5}\right\} + \left(\frac{B_0}{k}\right)\left\{-\frac{2x(x^2-3z^2)}{(x^2+z^2)^3}\right\}\right]$$

$$F_{mx}(x,z).\hat{x} = \frac{|\vec{m}|k^2}{|\vec{B}|}\left[\left\{-\frac{2x}{(x^2+z^2)^3}\right\} + \left(\frac{B_0}{k}\right)\left\{-\frac{2x(x^2-3z^2)}{(x^2+z^2)^3}\right\}\right]$$

$$F_{mx}(x,z).\hat{x} = \frac{|\vec{m}|k^2}{|\vec{B}|}\left[\left\{-\frac{2x}{(x^2+z^2)^3}\right\} + \left(\frac{B_0}{k}\right)\left\{\frac{-2x^3+6xz^2}{(x^2+z^2)^3}\right\}\right]$$

$$F_{mx}(x,z).\hat{x} = \frac{|\vec{m}|k^2}{|\vec{B}|}\left[\frac{-2kx - 2B_0x^3 + 6B_0xz^2}{k(x^2+z^2)^3}\right]$$

$$F_{mx}(x,z).\hat{x} = \frac{|\vec{m}|k}{|\vec{B}|}\left[-\frac{2x(B_0x^2 - 3B_0z^2 + k)}{(x^2+z^2)^3}\right]$$

$$F_{mx}(x,z).\hat{x} = |\vec{m}|k\frac{\left[-\frac{2x(B_0x^2 - 3B_0z^2 + k)}{(x^2+z^2)^3}\right]}{k\sqrt{\left\{\frac{x^2-z^2}{(x^2+z^2)^2} + \frac{B_0}{k}\right\}^2 + \left\{\frac{2xz}{(x^2+z^2)^2}\right\}^2}}$$

$$F_{mx}(x,z).\hat{x} = |\vec{m}|\frac{\left[-\frac{2x(B_0x^2 - 3B_0z^2 + k)}{(x^2+z^2)^3}\right]}{\sqrt{\left\{\frac{x^2-z^2}{(x^2+z^2)^2} + \frac{B_0}{k}\right\}^2 + \left\{\frac{2xz}{(x^2+z^2)^2}\right\}^2}}$$

Determining the Perpendicular Component of the Magnetic Force:

$$F_{mz}(x,z).\hat{z} = \frac{m}{|\vec{B}|}\left(\frac{\mu_0 M}{2}R_{wire}^2\right)^2\left(B_{x0}\frac{\partial B_z}{\partial x} + B_z\frac{\partial B_z}{\partial z}\right)$$

$$F_{mz}(x,z).\hat{z} = \frac{|\vec{m}|k^2}{|\vec{B}|}\left[\left(B_x + \frac{B_0}{k}\right)\left(\frac{\partial}{\partial x}B_z(x,z)\right) + (B_z)\left(\frac{\partial}{\partial z}B_z(x,z)\right)\right]$$

$$F_{mz}(x,z).\hat{z} = \frac{|\vec{m}|k^2}{|\vec{B}|}\left[\left\{\frac{x^2-z^2}{(x^2+z^2)^2} + \frac{B_0}{k}\right\}\left\{-\frac{2z(3x^2-z^2)}{(x^2+z^2)^3}\right\} + \left\{\frac{2xz}{(x^2+z^2)^2}\right\}\left\{\frac{2x(x^2-3z^2)}{(x^2+z^2)^3}\right\}\right]$$

$$F_{mz}(x,z).\hat{z} = \frac{|\vec{m}|k^2}{|\vec{B}|}\left[\left\{\frac{x^2-z^2}{(x^2+z^2)^2}\right\}\left\{-\frac{2z(3x^2-z^2)}{(x^2+z^2)^3}\right\} + \left(\frac{B_0}{k}\right)\left\{-\frac{2z(3x^2-z^2)}{(x^2+z^2)^3}\right\} + \left\{\frac{2xz}{(x^2+z^2)^2}\right\}\left\{\frac{2x(x^2-3z^2)}{(x^2+z^2)^3}\right\}\right]$$

$$F_{mz}(x,z).\hat{z} = \frac{|\vec{m}|k^2}{|\vec{B}|}\left[\left\{\frac{x^2-z^2}{(x^2+z^2)^2}\right\}\left\{\frac{-6x^2z+2z^3}{(x^2+z^2)^3}\right\} + \left(\frac{B_0}{k}\right)\left\{-\frac{2z(3x^2-z^2)}{(x^2+z^2)^3}\right\} + \left\{\frac{2xz}{(x^2+z^2)^2}\right\}\left\{\frac{2x^3-6xz^2}{(x^2+z^2)^3}\right\}\right]$$

$$F_{mz}(x,z).\hat{z} = \frac{|\vec{m}|k^2}{|\vec{B}|}\left[\left\{\frac{x^2(-6x^2z+2z^3)-z^2(-6x^2z+2z^3)}{(x^2+z^2)^5}\right\} + \left\{\frac{2xz(2x^3-6xz^2)}{(x^2+z^2)^5}\right\} + \left(\frac{B_0}{k}\right)\left\{-\frac{2z(3x^2-z^2)}{(x^2+z^2)^3}\right\}\right]$$

$$F_{mz}(x,z).\hat{z} = \frac{|\vec{m}|k^2}{|\vec{B}|}\left[\left\{\frac{-6x^4z+2x^2z^3+6x^2z^3-2z^5}{(x^2+z^2)^5}\right\} + \left\{\frac{4x^4z-12x^2z^3}{(x^2+z^2)^5}\right\} + \left(\frac{B_0}{k}\right)\left\{-\frac{2z(3x^2-z^2)}{(x^2+z^2)^3}\right\}\right]$$

$$F_{mz}(x,z).\hat{z} = \frac{|\vec{m}|k^2}{|\vec{B}|}\left[\left\{\frac{-6x^4z+2x^2z^3+6x^2z^3-2z^5+4x^4z-12x^2z^3}{(x^2+z^2)^5}\right\} + \left(\frac{B_0}{k}\right)\left\{-\frac{2z(3x^2-z^2)}{(x^2+z^2)^3}\right\}\right]$$

$$F_{mz}(x,z).\hat{z} = \frac{|\vec{m}|k^2}{|\vec{B}|}\left[\left\{\frac{-2x^4z-4x^2z^3-2z^5}{(x^2+z^2)^5}\right\} + \left(\frac{B_0}{k}\right)\left\{-\frac{2z(3x^2-z^2)}{(x^2+z^2)^3}\right\}\right]$$

$$F_{mz}(x,z).\hat{z} = \frac{|\vec{m}|k^2}{|\vec{B}|}\left[\left\{\frac{-2z(x^4+2x^2z^2+z^4)}{(x^2+z^2)^5}\right\} + \left(\frac{B_0}{k}\right)\left\{-\frac{2z(3x^2-z^2)}{(x^2+z^2)^3}\right\}\right]$$

$$F_{mz}(x,z).\hat{z} = \frac{|\vec{m}|k^2}{|\vec{B}|}\left[\left\{-\frac{2z}{(x^2+z^2)^3}\right\} + \left(\frac{B_0}{k}\right)\left\{-\frac{2z(3x^2-z^2)}{(x^2+z^2)^3}\right\}\right]$$

$$F_{mz}(x,z).\hat{z} = \frac{|\vec{m}|k^2}{|\vec{B}|}\left[\left\{-\frac{2z}{(x^2+z^2)^3}\right\}+\left(\frac{B_0}{k}\right)\left\{\frac{-6x^2z+2z^3}{(x^2+z^2)^3}\right\}\right]$$

$$F_{mz}(x,z).\hat{z} = \frac{|\vec{m}|k^2}{|\vec{B}|}\left[\left\{\frac{-2kz-6B_0x^2z+2B_0z^3}{(x^2+z^2)^3}\right\}\right]$$

$$F_{mz}(x,z).\hat{z} = \frac{|\vec{m}|k^2}{|\vec{B}|}\left[\left\{\frac{-2z(3B_0x^2-B_0z^2+k)}{(x^2+z^2)^3}\right\}\right]$$

$$F_{mz}(x,z).\hat{z} = |\vec{m}|k\frac{\left[-\frac{2z(3B_0x^2-B_0z^2+k)}{(x^2+z^2)^3}\right]}{k\sqrt{\left\{\frac{x^2-z^2}{(x^2+z^2)^2}+\frac{B_0}{k}\right\}^2+\left\{\frac{2xz}{(x^2+z^2)^2}\right\}^2}}$$

$$F_{mz}(x,z).\hat{z} = |\vec{m}|\frac{\left[-\frac{2z(3B_0x^2-B_0z^2+k)}{(x^2+z^2)^3}\right]}{\sqrt{\left\{\frac{x^2-z^2}{(x^2+z^2)^2}+\frac{B_0}{k}\right\}^2+\left\{\frac{2xz}{(x^2+z^2)^2}\right\}^2}}$$

Expression for the axial component of magnetic force:

$$F_{mx}(x,z).\hat{x} = |\vec{m}| \frac{\left[-\frac{2x(B_0x^2 - 3B_0z^2 + k)}{(x^2+z^2)^3}\right]}{\sqrt{\left\{\frac{x^2-z^2}{(x^2+z^2)^2} + \frac{B_0}{k}\right\}^2 + \left\{\frac{2xz}{(x^2+z^2)^2}\right\}^2}}$$

Expression for the axial component of magnetic force:

$$F_{mz}(x,z).\hat{z} = |\vec{m}| \frac{\left[-\frac{2z(3B_0x^2 - B_0z^2 + k)}{(x^2+z^2)^3}\right]}{\sqrt{\left\{\frac{x^2-z^2}{(x^2+z^2)^2} + \frac{B_0}{k}\right\}^2 + \left\{\frac{2xz}{(x^2+z^2)^2}\right\}^2}}$$

Appendix C.

Appendix C provides the derivation of the expression for magnetic force experienced by a malaria-infected red blood cell in the magnetic focusing design presented in chapter 3 of this dissertation.

Magnetic field of the wire magnetized perpendicular to its axis (x_w) in the z direction:

$$\vec{B} = K\left(B_{y_w}\hat{\boldsymbol{y}}_{\boldsymbol{w}} + B_z\hat{\boldsymbol{z}}\right) + B_0\hat{\boldsymbol{z}}$$

$$where, K = \frac{\mu_0 M}{2}(R_{wire})^2;\ B_{y_w} = \frac{2y_w z}{({y_w}^2 + z^2)^2}; B_z = \frac{z^2 - {y_w}^2}{({y_w}^2 + z^2)^2}$$

where, R_{wire} = radius of the magnetic wire; and M = Magnetization of the wire in kA/m.

Magnetic force acting on the RBC:

$$\vec{F}_{mag} = \frac{\Delta\chi V_{RBC}}{\mu_0}(\vec{B}.\nabla)\vec{B}$$

Now,

$$\vec{B} = K\left(B_{y_w}\hat{\boldsymbol{y}}_{\boldsymbol{w}} + B_z\hat{\boldsymbol{z}}\right) + B_0\hat{\boldsymbol{z}} = K\left(B_{y_w}\hat{\boldsymbol{y}}_{\boldsymbol{w}} + B_{z1}\hat{\boldsymbol{z}}\right), where\ B_{z1} = B_z + \frac{B_0}{K}$$

$$(\mathrm{B}.\nabla) = K\left(B_{y_w}\frac{\partial}{\partial y_w} + B_{z1}\frac{\partial}{\partial z}\right)$$

$$(\mathrm{B}.\nabla)\mathrm{B} = K^2\left(B_{y_w}\frac{\partial}{\partial y_w} + B_{z1}\frac{\partial}{\partial z}\right)\left(B_{y_w}\hat{\boldsymbol{y}}_{\boldsymbol{w}} + B_{z1}\hat{\boldsymbol{z}}\right)$$

$$(\mathrm{B}.\nabla)\mathrm{B} = K^2\left[\left(B_{y_w}\frac{\partial B_{y_w}}{\partial y_w} + B_{z1}\frac{\partial B_{y_w}}{\partial z}\right)\hat{\boldsymbol{y}}_{\boldsymbol{w}} + \left(B_{y_w}\frac{\partial B_{z1}}{\partial y_w} + B_{z1}\frac{\partial B_{z1}}{\partial z}\right)\hat{\boldsymbol{z}}\right]$$

Magnetic force in $\mathbf{y_w}$-direction:

$$F_{mag}\hat{\boldsymbol{y}}_{\boldsymbol{w}} = \frac{\Delta\chi V_{RBC}}{\mu_0} K^2 \left(B_{y_w} \frac{\partial B_{y_w}}{\partial y_w} + B_{z1} \frac{\partial B_{y_w}}{\partial z} \right)$$

Magnetic force in the x-direction:

$$F_{mag}\hat{\boldsymbol{x}} = (F_{mag}\hat{\boldsymbol{y}}_{\boldsymbol{w}})\sin\theta$$

Magnetic force in the y-direction:

$$F_{mag}\hat{\boldsymbol{y}} = (F_{mag}\hat{\boldsymbol{y}}_{\boldsymbol{w}})\cos\theta$$

Magnetic field gradients:

$$\frac{\partial B_{y_w}}{\partial y_w} = \frac{\partial}{\partial y_w}\left[\frac{2y_w z}{({y_w}^2 + z^2)^2}\right] = \frac{2z}{({y_w}^2 + z^2)^2} - \frac{8y_w^2 z}{({y_w}^2 + z^2)^3}$$

$$\frac{\partial B_{y_w}}{\partial z} = \frac{\partial}{\partial z}\left[\frac{2y_w z}{({y_w}^2 + z^2)^2}\right] = \frac{2y_w}{({y_w}^2 + z^2)^2} - \frac{8z^2 y_w}{({y_w}^2 + z^2)^3}$$

$$\frac{\partial B_z}{\partial y_w} = \frac{\partial}{\partial y_w}\left[\frac{z^2 - {y_w}^2}{({y_w}^2 + z^2)^2}\right] = \frac{4y_w({y_w}^2 - z^2)}{({y_w}^2 + z^2)^3} - \frac{2y_w}{({y_w}^2 + z^2)^2}$$

$$\frac{\partial B_z}{\partial z} = \frac{\partial}{\partial y_w}\left[\frac{z^2 - {y_w}^2}{({y_w}^2 + z^2)^2}\right] = \frac{4z({y_w}^2 - z^2)}{({y_w}^2 + z^2)^3} + \frac{2z}{({y_w}^2 + z^2)^2}$$

Magnetic force in y_w-direction:

$$F_{mag}\hat{\boldsymbol{y}}_{\boldsymbol{w}} = \frac{\Delta\chi V_{RBC}}{\mu_0} K^2 \left(B_{y_w} \frac{\partial B_{y_w}}{\partial y_w} + B_{z1} \frac{\partial B_{y_w}}{\partial z} \right), where\ B_{z1} = B_z + \frac{B_0}{K}$$

$$F_{mag}\hat{\boldsymbol{y}}_{\boldsymbol{w}} = \frac{\Delta\chi V_{RBC}}{\mu_0} K^2 \left[\frac{2y_w z}{({y_w}^2 + z^2)^2} \left(\frac{2z}{({y_w}^2 + z^2)^2} - \frac{8y_w^2 z}{({y_w}^2 + z^2)^3} \right) + \left(\frac{z^2 - {y_w}^2}{({y_w}^2 + z^2)^2} + \frac{B_0}{K} \right) \left(\frac{2y_w}{({y_w}^2 + z^2)^2} - \frac{8z^2 y_w}{({y_w}^2 + z^2)^3} \right) \right]$$

Magnetic force in z-direction:

$$F_{mag}\hat{\boldsymbol{z}} = \frac{\Delta\chi V_{RBC}}{\mu_0} K^2 \left(B_{y_w} \frac{\partial B_{z1}}{\partial y_w} + B_{z1} \frac{\partial B_{z1}}{\partial z} \right), where\ B_{z1} = B_z + \frac{B_0}{K}$$

$$F_{mag}\hat{\boldsymbol{z}} = \frac{\Delta\chi V_{RBC}}{\mu_0} K^2 \left[\frac{2y_w z}{({y_w}^2 + z^2)^2} \left(\frac{4y_w({y_w}^2 - z^2)}{({y_w}^2 + z^2)^3} - \frac{2y_w}{({y_w}^2 + z^2)^2} \right) + \left(\frac{z^2 - {y_w}^2}{({y_w}^2 + z^2)^2} + \frac{B_0}{K} \right) \left(\frac{4z({y_w}^2 - z^2)}{({y_w}^2 + z^2)^3} + \frac{2z}{({y_w}^2 + z^2)^2} \right) \right]$$

Appendix D.

Appendix D describes the coordinate system used in the magnetic focusing designs of chapter 2 and chapter 4. The perpendicular distances y_{w1} and y_{w2} determine the magnetic force that is experienced by a magnetic particle located at position (x,y) in the 2D channel space.

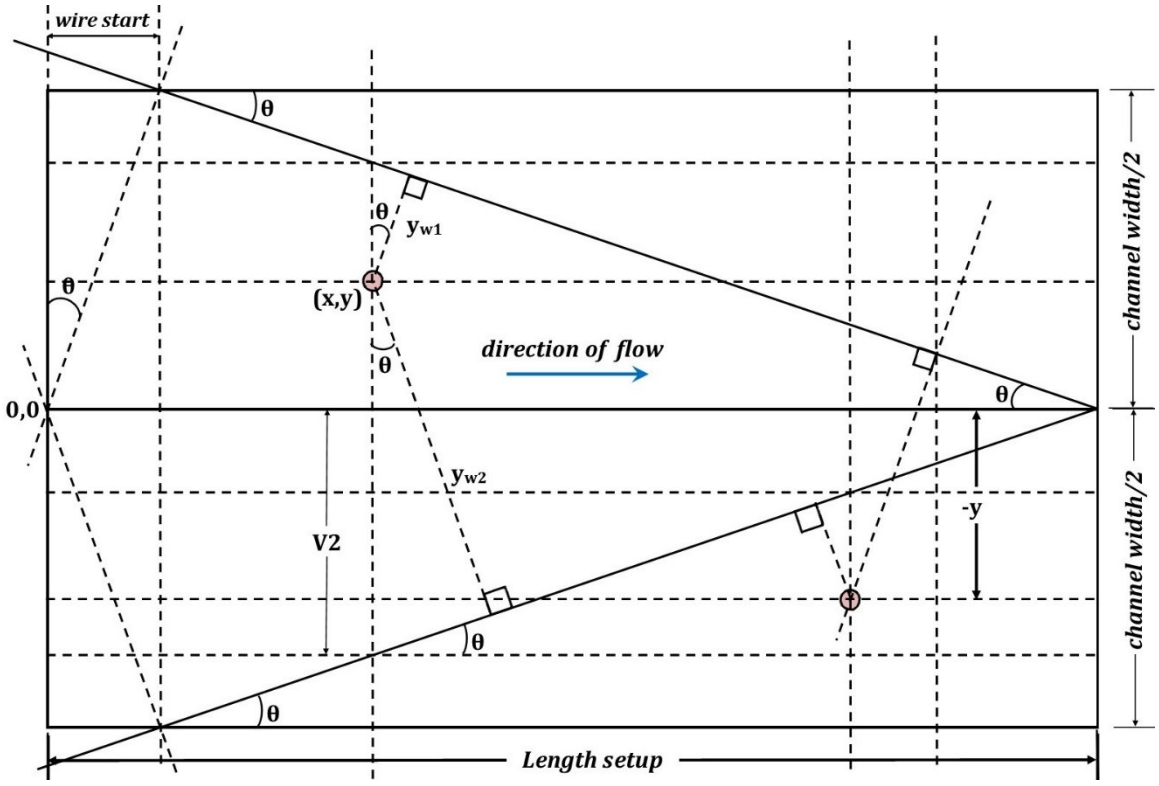

Figure D1. Coordinate system of the magnetic particle focusing design.

$$\tan\theta = \frac{wire\ start}{channel\ width/2} \Rightarrow wire\ start = \tan\theta . \frac{channel\ width}{2}$$

$$\tan\theta = \frac{channel\ width/2}{wire\ end - wire\ start} \Rightarrow\ wire\ end = \frac{channel\ width/2}{\tan\theta} + wire\ start$$

$$\sin\theta = \frac{channel\ width/2}{wire\ length} \Rightarrow\ wire\ length = \frac{channel\ width/2}{\sin\theta}$$

$$\tan\theta = \frac{y + V1}{wire\ end - x} \Rightarrow\ V1 = [\tan\theta.\ (wire\ end - x)] - y$$

$$y_w = V1.\cos\theta$$

Vita

Siddharth Vyas

Education

Drexel University, Philadelphia, Pennsylvania USA
Ph.D. (pending), Electrical Engineering, March 2017
M.S., Electrical Engineering, 2011

Rajiv Gandhi Technical University, Indore, M.P., India
B.E., Electrical Engineering, 2005

Selected Journal Publications, and Conference Presentations and Proceedings

- S. Vyas, V. Genis, and G. Friedman. Computational Study of a Magnetic Design to Improve the Diagnosis of Malaria: 2D-Model. Journal of Magnetism and Magnetic Materials, Vol. 423, pp. 301 –305, 2017.
- S. Vyas, V. Genis, and G. Friedman. Computational Study of Kinematics of Capture of Magnetic Particles by Stent: 2D-Model. IEEE Transactions on Magnetics, Vol. 52, No. 7, #5400204, 2016.
- V. Genis, S. Vyas, E. Carr, and A. Pollock. Quality Control Education - A University Course in Acoustic Emission. Proceedings of the ASEE Conference, pp. 1 – 14, 2014.
- V. Genis, S. Vyas, T. Midora, and R. Bottari. Industry-University Collaboration in Course Development and Instruction. Proceedings of the Annual CIEC Conference, pp. 1 – 10, 2010.
- V. Genis, S. Vyas, and J. Milbrandt. Traditional and Real-Time Remote NDT Instruction. Materials Evaluation. Vol. 68, No. 2, pp. 128 – 134, 2010.

Patents

A magnetic device to improve diagnosis of malaria. Siddharth Vyas, Gennady Friedman, and Vladimir Genis. U.S. Provisional Patent Application Serial Number 62/277,530.

Teaching Experience

Doctoral Teaching Fellow – Engineering Technology – Spring 2008 – Winter 2017
Engineering Design Teaching Fellow – CoE - Fall 2007 – Winter 2008
Mentor – RISE Student Summer Program at Drexel Univ. – Summer 2015

Awards

Graduate Student Award for Inspired Teaching – CoE Drexel Univ. – 2008
Outstanding Student Award – Engineering Technology – Drexel Univ. – 2014